AFFDL-TR-78-24

# THE MEASUREMENT OF CRACK TIP STRESSES BY X-RAY DIFFRACTION

*JOHN E. ALLISON*

*STRUCTURAL INTEGRITY BRANCH*
*STRUCTURAL MECHANICS DIVISION*

MARCH 1978

TECHNICAL REPORT AFFDL-TR-78-24
Final Report for Period June 1976 to December 1977



AIR FORCE FLIGHT DYNAMICS LABORATORY
AIR FORCE WRIGHT AERONAUTICAL LABORATORIES
AIR FORCE SYSTEMS COMMAND
WRIGHT-PATTERSON AIR FORCE BASE, OHIO 45433

*NOTICE*

*When Government drawings, specifications, or other data are used for any purpose other than in connection with a definitely related Government procurement operation, the United States Government thereby incurs no responsibility nor any obligation whatsoever; and the fact that the government may have formulated, furnished, or in any way supplied the said drawings, specifications, or other data, is not to be regarded by implication or otherwise as in any manner licensing the holder or any other person or corporation, or conveying any rights or permission to manufacture, use, or sell any patented invention that may in any way be related thereto.*

*This report has been reviewed by the Information Office (OI) and is releasable to the National Technical Information Service (NTIS). At NTIS, it will be available to the general public, including foreign nations.*

*This technical report has been reviewed and is approved for publication.*

JOHN E. ALLISON
Project Engineer

ROBERT M. BADER, Chief
Structural Integrity Branch
Structural Mechanics Division

*FOR THE COMMANDER*

HOLLAND B. LOWNDES, JR., Acting Chief
Structural Mechanics Division

*"If your address has changed, if you wish to be removed from our mailing list, or if the addressee is no longer employed by your organization please notify* AFFDL/FBE *,W-PAFB, OH 45433 to help us maintain a current mailing list".*

*Copies of this report should not be returned unless return is required by security considerations, contractual obligations, or notice on a specific document.*

UNCLASSIFIED

SECURITY CLASSIFICATION OF THIS PAGE *(When Data Entered)*

| REPORT DOCUMENTATION PAGE | | READ INSTRUCTIONS BEFORE COMPLETING FORM |
|---|---|---|
| 1. REPORT NUMBER<br>AFFDL-TR-78-24 | 2. GOVT ACCESSION NO. | 3. RECIPIENT'S CATALOG NUMBER |
| 4. TITLE *(and Subtitle)*<br>The Measurement of Crack Tip Stresses by X-ray Diffraction | | 5. TYPE OF REPORT & PERIOD COVERED<br>Final Report for Period July 1976 to December 1977<br>6. PERFORMING ORG. REPORT NUMBER |
| 7. AUTHOR*(s)*<br>John E. Allison | | 8. CONTRACT OR GRANT NUMBER*(s)* |
| 9. PERFORMING ORGANIZATION NAME AND ADDRESS<br>Air Force Flight Dynamics Laboratory (AFFDL/FBE)<br>Wright-Patterson AFB, Ohio 45433 | | 10. PROGRAM ELEMENT, PROJECT, TASK AREA & WORK UNIT NUMBERS<br>Project 2307<br>Task 01<br>Work Unit 01 |
| 11. CONTROLLING OFFICE NAME AND ADDRESS<br>Air Force Flight Dynamics Laboratory (AFFDL/FBE)<br>Wright-Patterson AFB, Ohio 45433 | | 12. REPORT DATE<br>March 1978<br>13. NUMBER OF PAGES<br>126 |
| 14. MONITORING AGENCY NAME & ADDRESS*(if different from Controlling Office)* | | 15. SECURITY CLASS. *(of this report)*<br>Unclassified<br>15a. DECLASSIFICATION/DOWNGRADING SCHEDULE |

16. DISTRIBUTION STATEMENT *(of this Report)*

Approved for public release; distribution unlimited.

17. DISTRIBUTION STATEMENT *(of the abstract entered in Block 20, if different from Report)*

18. SUPPLEMENTARY NOTES

19. KEY WORDS *(Continue on reverse side if necessary and identify by block number)*

stress measurement
x-ray diffraction
crack growth retardation
residual stresses
crack tip

20. ABSTRACT *(Continue on reverse side if necessary and identify by block number)*

To ensure the structural integrity of present day structures subjected to variable amplitude cyclic stress histories, a knowledge of the crack tip stress field is important. In this investigation, crack tip stresses were measured in specimens of 1020 and 1045 steel using a semi-automatic x-ray diffraction technique. Crack tip residual stresses were measured in the unloaded condition and crack tip "applied" stresses were measured under load. It was observed that, for the alloys tested and within the confines of stress analysis by x-ray diffraction, a dependence exists for the maximum crack tip residual stress on

DD FORM 1 JAN 73 1473 EDITION OF 1 NOV 65 IS OBSOLETE

UNCLASSIFIED

SECURITY CLASSIFICATION OF THIS PAGE *(When Data Entered)*

the level of the previous stress intensity factor and also for the maximum crack tip "applied" stress on the level of the applied stress intensity. This is in sharp contrast to theoretical models of the crack tip stress fields which predict an independence between crack tip stresses and stress intensity levels. Crack tip stresses were observed relative to the fatigue crack growth retardation process. Post overload crack tip stresses were greatly reduced from their pre-overload levels. Limited studies indicated that crack growth, after an overload, had little or no effect on the overload-induced crack tip residual stress distribution. Measurements taken at applied loads, indicated that portions of the material behind the tip of the extended crack were in compression while areas ahead of the extended crack were in tension. These results were considered in light of possible retardation mechanisms. Recommendations were offered for further research.

## FOREWORD

The research work reported herein was conducted with the Structural Integrity Branch, of the Structural Mechanics Division of the Air Force Flight Dynamics Laboratory, Air Force Systems Command, Wright-Patterson Air Force Base, Ohio, under project 2307 Solid Mechanics, and work unit 2307Ø101 Research in Structural Integrity. The research was conducted by J.E. Allison (AFFDL/FBE) from Jun 76 to Dec 77.

## ACKNOWLEDGEMENTS

First and foremost, I am deeply indebted to the personnel of the Structural Test Facility, Air Force Flight Dynamics Laboratory, Wright-Patterson AFB, Ohio. Without their constant assistance and advice this thesis would not have been possible. I owe special thanks to Messrs. Harold Stalnaker, Larry Bates, Jack Smith and Richard Kleismit for their aid in the experimental phases of this study.

I would like to extend my appreciation to my advisor, Professor J.W. Spretnak, for his counseling and philosophical guidance and to my friends and co-workers in both the Air Force Flight Dynamics Laboratory and Materials Laboratory for their interest and for the many discussions of technical problems encountered during this investigation. Appreciation is also extended to Mr. J. Potter for his aid in developing the initial objectives of this study. I thank the U.S. Air Force and the Air Force Flight Dynamics Laboratory for providing me with the time, facilities and funds for the completion of this study.

I owe very special thanks to Miss Constance Boesenberg and Mr. Jeff Wead for their tireless effort in preparing this thesis. My appreciation is also extended to Mr. Jim Hicks for his development of data plotting routines. A special thanks is due a very special friend, Ms. Julia Miller, for her ever-present encouragement and understanding.

TABLE OF CONTENTS

TABLE OF CONTENTS (Continued)

LIST OF ILLUSTRATIONS

LIST OF ILLUSTRATIONS (Cont'd)

LIST OF TABLES

## ABSTRACT

To insure the structural integrity of present day structures subjected to variable amplitude cyclic stress histories, a knowledge of the crack tip stress field is important. In this investigation, crack tip stresses were measured in specimens of 1020 and 1045 steel using a semi-automatic x-ray diffraction technique. Crack tip residual stresses were measured in the unloaded condition and crack tip "applied" stresses were measured under load. It was observed that, for the alloys tested and within the confines of stress analysis by x-ray diffraction, a dependence exists for the maximum crack tip residual stress on the level of the previous stress intensity factor and also for the maximum crack tip "applied" stress on the level of the applied stress intensity. This is in sharp contrast to theoretical models of the crack tip stress fields which predict an independence between crack tip stresses and stress intensity levels. Crack tip stresses were observed relative to the fatigue crack growth retardation process. Post overload crack tip stresses were greatly reduced from their pre-overload levels. Limited studies indicated that crack growth, after an overload had little or no effect on the overload-induced crack tip residual stress distribution. Measurements taken at applied loads, indicated that portions of the material behind the tip of the extended crack were in compression while areas ahead of the extended crack were in tension. These results were considered in light of possible retardation mechanisms. Recommendations were offered for further research.

# SECTION I

# INTRODUCTION

Many present day structures are subjected to cyclic stresses which are generally high enough to cause the initiation and subcritical growth of fatigue cracks leading to subsequent catastrophic failure of the structure. The growth of these fatigue cracks is largely dependent on the interaction of the magnitude and order of these cyclic stresses. The accurate prediction of this fatigue crack growth behavior, of obvious importance in ensuring structural integrity, depends on accurate modeling of non-constant amplitude load-interactions. One important phenomenon in this process is the retardation of fatigue crack growth due to the application of a high tensile stress. This beneficial retardation of fatigue crack growth has been studied from many view points; however, a completely satisfactory explanation of the retardation phenomenon is lacking.

A number of crack growth retardation mechanisms have been proposed including crack tip residual compressive stresses, crack closure and crack tip blunting. The more widely accepted and well-substantiated models are based on the inducement of compressive residual stresses either in the plastically deformed region ahead of the crack tip or in the deformed region behind the propagating crack tip.

The objective of this study is to (1) determine the feasibility of using a semi-automatic x-ray diffraction device for measuring crack tip stresses, applied and residual, and (2) use this x-ray diffraction

technique to study some of the variables affecting these crack tip stresses. This study provides unique data for evaluating current models of the crack tip stress field and current crack growth retardation models. It, therefore, provides a basis for obtaining an improved capability to predict the fatigue crack growth behavior in structures subjected to variable amplitude cyclic loadings.

## II. REVIEW OF THEORY AND PREVIOUS WORK

### A. Fatigue Crack Growth

#### 1. Fundamentals

The local stresses at the tip of a crack in an elastic medium are uniquely related to the stress intensity factor, $K$[1]. The stress intensity factor is a material independent geometric parameter which has the form

$$K = \sigma\sqrt{\pi a} \cdot \beta \qquad (1)$$

where $\sigma$ is the remote stress on a body, ksi; a is the crack length, in.; and $\beta$ is a geometrical calibration factor that accounts for specific crack geometries. K has the units ksi $\sqrt{in.}$

Constant amplitude cyclic loading, depicted in Figure 1, causes the stress to alternate between a maximum value, $\sigma_{max}$, and a minimum value, $\sigma_{min}$. The ratio of the minimum stress to the maximum stress is called the load ratio, R ($\sigma_{min}/\sigma_{max}$), and the stress range, $\Delta\sigma$, is given by $\sigma_{max} - \sigma_{min}$. The stress range can be substituted for $\sigma$ in equation 1 giving

$$\Delta K = \Delta\sigma\sqrt{\pi a} \cdot \beta \qquad (1b)$$

where $\Delta K$ is the stress intensity range.

Fatigue crack growth rate behavior under constant stress amplitude loading can be reasonably well-described[2] in terms of the stress

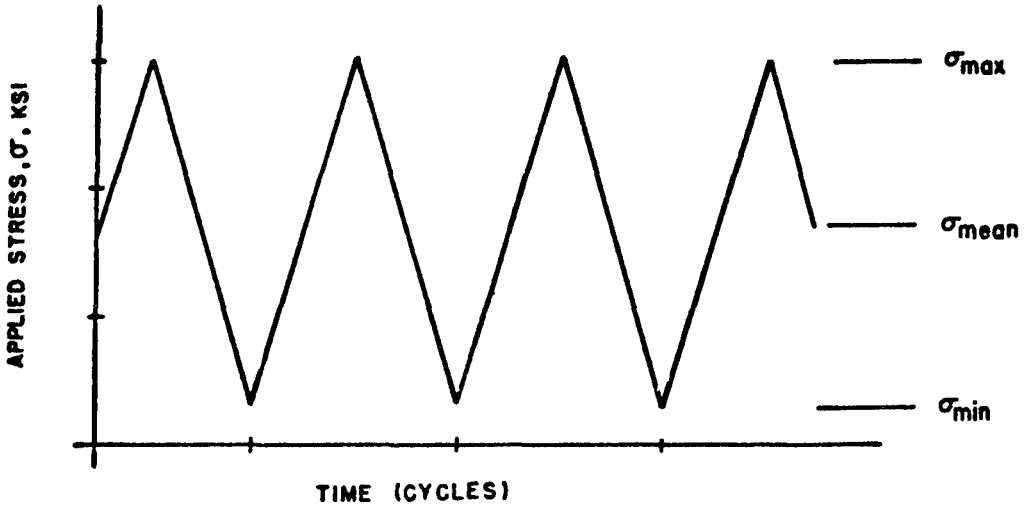


FIGURE 1. SCHEMATIC OF CYCLIC LOADING

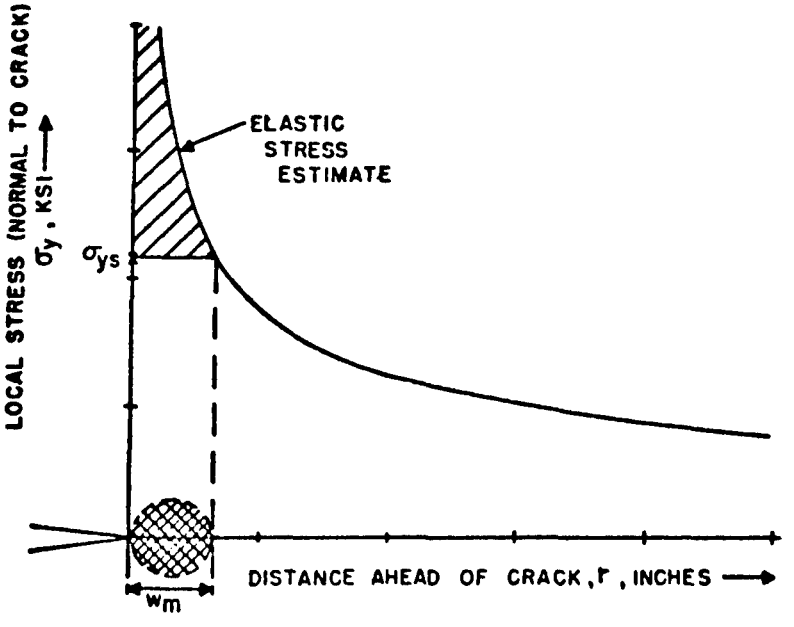


FIGURE 2. CRACK TIP STRESS FIELD

intensity factor range, by the relationship

$$\frac{da}{dN} = C(\Delta K)^n \qquad (2)$$

where a is the crack length, in.; N is the number of cycles; da/dN is the fatigue crack growth rate; $\Delta K$ is the stress intensity factor range, $K_{max} - K_{min}$; and C, n are constants for a given material. This relationship can be significantly affected by other variables such as the load ratio, R, environment and temperature, and thus many variations on equation 2 exist[3].

2. The Crack Tip Plastic Zone

According to elastic stress field solutions, the stress normal to the crack at its tip is inversely proportional to the square root of the distance, r, away from the crack tip, as shown in Figure 2[1]. Thus, as r goes to zero the normal stress goes to infinity. In reality, metals tend to exhibit a yield stress above which they deform plastically. Thus, there is always a region around the tip of a crack under load where plastic deformation occurs, limiting the stress to a finite value. The plastic region is known as the crack tip plastic zone, $W_m$ (Figure 2). Many estimates of the crack tip plastic zone size exist, most of which have the form

$$W_m = \alpha \left(\frac{K}{\sigma_{ys}}\right)^2 \qquad (3)$$

where $W_m$ is the full extent of the monotonic (underload) plastic zone size in the x direction, in.; K is the stress intensity factor, ksi $\sqrt{\text{in.}}$; and $\sigma_{ys}$ is the material yield strength. Estimates of the constant $\alpha$ are given in Table I for both plane stress and plane strain crack tip stress conditions.

Typically in thick materials, the strain in the thickness direction is constrained to zero by the surrounding elastic material and, thus, a smaller plastic zone is formed under plane strain conditions. The estimates given in Table I are for elastic-perfectly plastic materials. Corrections for strain hardening materials can be found in the literature[4]. Crack tip plastic zone shapes, both plane stress and plane strain, have also been predicted[5,6]. Figure 3[1] shows a three-dimensional schematic of the plastic zone.

Upon unloading of the crack, the plastically deformed region is constrained to its original volume by the surrounding elastic matrix, thus, exerting compressive stresses on the plastically deformed material. Because no external loading is present on the body, these stresses are called residual stresses. The resulting residual stress profile is shown schematically in Figure 4. It has been speculated[7] that the material at the crack tip will be subjected to compressive stresses greater than the compressive yield strength, thus, causing "reversed" plastic flow. A rough approximation of the size of this reversed plastic zone, $W_R$, can be made by substituting $2\sigma_{ys}$ for $\sigma_{ys}$ in equation 3[7]. For cyclic loading situations, the cyclic yield stresses could be used and the stress intensity range, $\Delta K$, substituted for the maximum stress intensity factor, K. These substitutions result in

$$W_R = \alpha \left( \frac{\Delta K}{2\sigma_{ys}} \right)^2 \qquad (4)$$

An approximation for the cross-over point from compressive stress to tensile stress, point B in Figure 4, is given by 2.5 times the reversed plastic zone[8] or

$$r_{OB} = 2.5\, \alpha \left( \frac{\Delta K}{2\sigma_{ys}} \right)^2 \qquad (5)$$

TABLE I PLASTIC ZONE CONSTANTS

| PLANE STRESS | PLANE STRAIN | REFERENCE |
|---|---|---|
| $\alpha = 1/2\pi$ | $\alpha = 1/4\sqrt{2}\pi$ | IRWIN (1) |
| $\alpha = 1/\pi$ | | RICE (7) |
| $\alpha = \pi/8$ | | DUGDALE (6) |

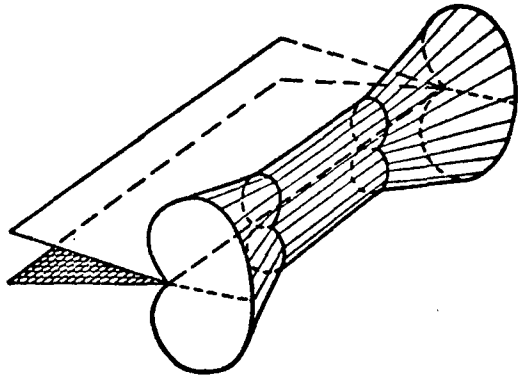

Figure 3. Three Dimensional Plastic Zone

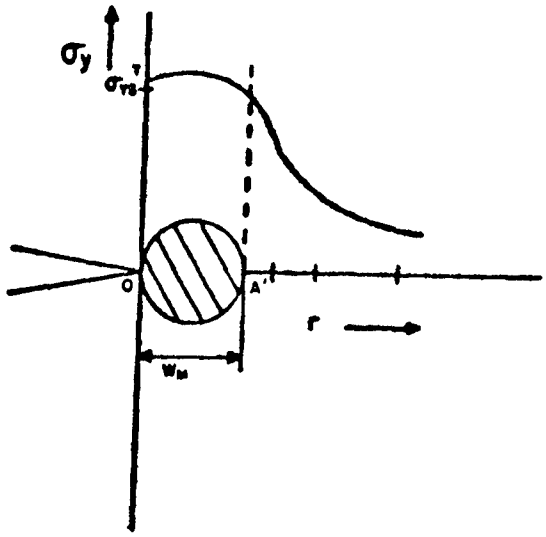


(a) AT LOAD

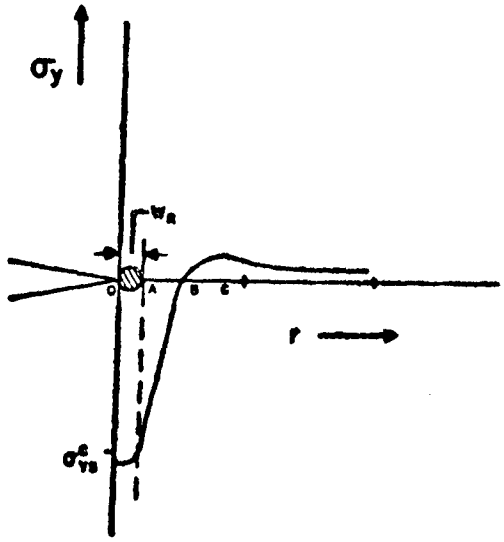


(b) AFTER LOAD

FIGURE 4: RESIDUAL COMPRESSIVE STRESSES AT CRACK TIP AFTER UNLOADING

Finite element techniques have been used to analyze the stress state ahead of "growing" cracks[9,10]. These analyses predict the existence of compressive residual stresses; however, the magnitude of these stresses is not predicted to reach or exceed the compressive yield strength. The magnitude and extent of compressive residual stresses increase with increasing stress intensity. With the exception of the reversed flow, the finite element technique is in fair agreement with Rice's estimate of the residual stress profile. It is these compressive residual stresses upon which the more widely accepted fatigue crack growth retardation models are based.

These analytical crack tip stress field models have not been subjected to previous experimental verification. As will be discussed in a later section, the only experimental technique readily available for measuring crack tip stresses is x-ray diffraction. Previous investigations using the x-ray diffraction technique[11,12,13] have indicated that these measurements are technically feasible. These studies found the crack tip residual stresses to be compressive, but not fully reversed (i.e., they did not reach the compressive yield strength). A recent study[13] also measured crack tip stresses under load. Results from these investigations will be described more fully in the next section; however, they were very limited studies. The present study has the unique opportunity of measuring these crack tip stresses in detail and, thus, may serve as a basis for verification of current analytical models of the crack tip stress field.

While crack tip stress measurements have not been generally feasible, attempts have been made to experimentally observe the crack tip plastic zone. Hahn and Rosenfield[14-16] used an acid etching

technique for highlighting the deformed microstructure in $Fe_3Si$ steel. Several thicknesses of specimens were used with observations being made directly on the outer surfaces and on the interior by sectioning. Their results qualitatively confirmed the differences between the plane stress and plane strain plastic zones, although in the thinnest specimen (.061 in.) the difference between plastic zones was not nearly as pronounced, indicating that plane stress conditions may exist entirely through thin specimens. They also noted the existence of two distinct regions of deformation. The most intense of these regions was roughly .25 the size of the overall deformed region. This is in agreement with Rice's prediction if the smaller, heavily deformed region was, in fact, due to reversed cyclic yielding. Attempts to correlate quantitatively their observations with analytic predictions were poor, their results being considerably less than the predictions.

Chanani[17] used an interference microscopy technique to outline the "dimpled" region at the crack tip caused by high loads. Using this technique, he was able to determine the monotonic plastic zone size, $W_m$. For his 0.063 inch aluminum specimens, he reported a very good correlation between his data and Rice's theoretical model ($\alpha = 1/\pi$).

Other techniques that have been applied with fair success include microhardness measurements[18], miniature strain gauges[19], plastic replication techniques[20,21] and a Selected Area-Electron Channel Pattern technique[20,21].

3. Fatigue Crack Growth Retardation

As early as 1959, researchers[22-24] began to notice that high tensile stress cycles followed by low stress cycles caused subsequent crack growth to substantially slow down or retard. From 1959 to the

present, this fatigue crack growth retardation phenomenon and its many variations have been the subject of intense investigation.

The primary observations are shown schematically in Figure 5. Under constant stress amplitude loading, the crack grows at a linearly increasing rate, segment AB in Figure 5. Upon application of an overload, if crack growth is not arrested, some investigators have observed an initial acceleration (e.g., Ref 17). This is followed by decreasing crack growth rate until a minimum is reached at point D. This is known as delayed retardation[17,25-29]. From point D, the crack growth rate will slowly begin to increase until the original or steady-state growth rate is reached at point E. The number of cycles required for the crack growth rate to return to its steady state rate is the number of delay cycles, N* in Figure 5.

A number of factors have been investigated to determine their effects on crack growth retardation in a variety of structural metal alloys. In general, these studies support a crack tip residual stress phenomenon of one form or another as the mechanism for retardation. The following is a brief summary of their findings:

(1) The number of delay cycles increases with increasing overload ratios, $K_{ol}/K_{max}$ (e.g., Ref 17, 30-32).

(2) As the number of overload cycles is increased, delay cycles also increase approaching an asymptotic value (e.g., Ref 29).

(3) Delay cycles also increase with increasing dwell times during the application of the overload[33-35].

(4) In studies of various steel alloys[27,36,37], by raising an alloy's yield strength through heat treatment, it was possible to significantly lower the number of delay cycles. This might be

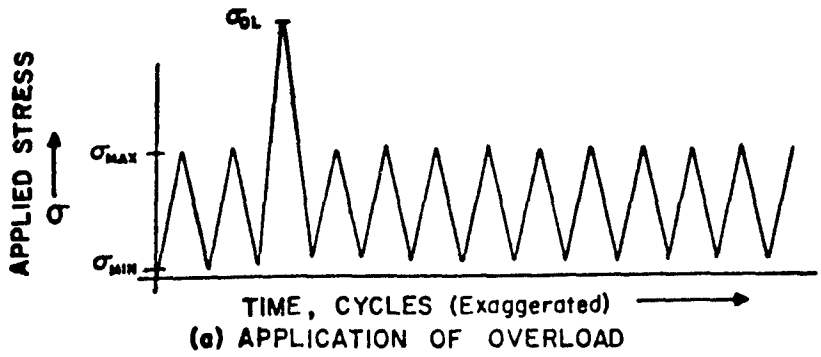

(a) APPLICATION OF OVERLOAD

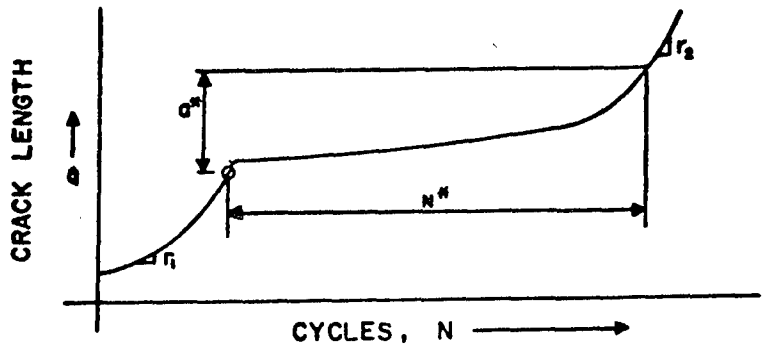

(b) CRACK GROWTH BEHAVIOR

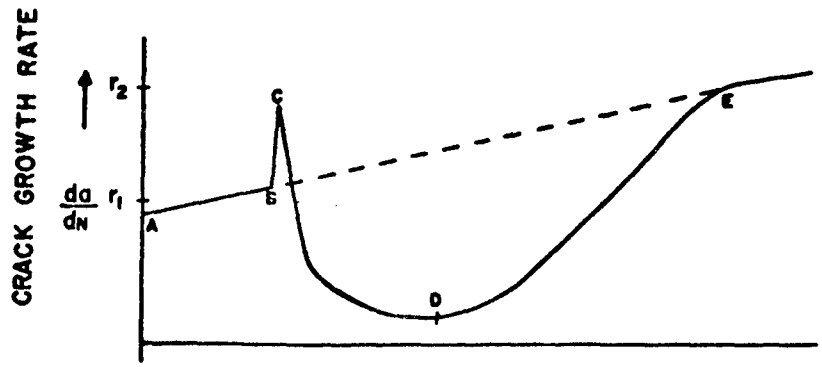

(c) CRACK GROWTH RATE BEHAVIOR

FIGURE 5. SCHEMATIC OF CRACK GROWTH RETARDATION BEHAVIOR

attributed to a decrease in plastic zone size due to an increase in yield strength and/or the increased constant amplitude crack growth rate behavior for the higher strength steels.

(5) Substantial decreases in the number of delay cycles have been reported when the overload is immediately followed by a compressive load[23,24,30,35,38,39].

(6) Pronounced decreases in delay cycles can result from annealing after the application of an overload and prior to base level cycling[17,34,37,40]. Since care was taken to ensure that the annealing did not change the metal microstructure, the implication is that any compressive residual stresses were relaxed by annealing.

(7) Corrosive environments tend to decrease the number of delay cycles[17].

(8) Testing at elevated temperature (560°F), Shih and Wei[34] noticed a marked increase in delay cycles of Ti-6Al-4V over that seen at room temperature. Macha[41] tested IN 100, a nickel-based superalloy, at temperatures up to 1350°F and saw a trend toward decreasing crack growth retardation. Shih and Wei attributed their results to a decreased yield strength at 560°F and, thus, an enlarged plastic zone (constant amplitude crack growth rate behavior being constant between room temperature and 560°F). Macha, on the other hand, reported no substantial changes in the yield strength of IN 100 at 1350°F and attributed his findings to the increased constant amplitude crack growth rate at 1350°F.

(9) Baseline load ratio, R, effects have been generally reported to be secondary[17,30,42] as have hold times at zero load after the overload and prior to baseline cycling[35,43].

(10) The effect of specimen thickness has not been studied in great detail; however, some results may be gleaned from the literature. Sharpe et al.[43] reported that for 2024-T851 aluminum ranging in thickness from 0.25 - 1.0 inch, no changes in delay cycles were observed. Chanani[17] investigated both 2000 and 7000 series aluminums in thicknesses of 0.063, 0.250 and 0.50 inches and found a moderate decrease in delay cycles as specimen thickness increased. Closer scrutiny of Chanani's results indicate a more pronounced thickness effect on the overload affected crack length, a*. For the 0.063 inch thickness, a* is roughly equal to Rice's estimate of the plane stress plastic zone ($\alpha = 1/\pi$). However, as thickness was increased to 0.5 inch, a* was better approximated by Irwin's plane stress plastic zone ($\alpha = 1/2\pi$).

Other attempts to correlate a* with a form of calculated overload plastic zone size, $W_m^{ol}$, have been made. Von Euw et al.[42] studied 0.126 inch thick 2024-T3 aluminum and found a good correlation between a* and $\alpha = 1/\pi$. Testing in thicker material, Matsuoka[8] in an extensive study of 0.80 inch thick HY80 Steel found a remarkably good correlation between a* and a factor developed in his investigations of $1.5\ (\pi/8)\ (\Delta K/2\sigma_{ys})^2$. This was developed from his assumption that the steady state crack growth rate should be reached when the current crack length reaches the point in the compressive residual stress zone where the stress passed through zero (Point B, Figure 3). According to Rice, equation 5, the distance $r_{OB}$ is 2.5 times the reversed plastic zone; however, Matsuoka used Dugdale's[6] expression for plane stress plastic zone size ($\alpha = \pi/8$). This equates very closely to Irwin's $\alpha = 1/2\pi$. Results by McGee[35] indicate a fair correlation between a* and $\alpha = 1/2\pi$ for 0.25 inch thick 2219-T851 aluminum at R equal 0.1. Gallagher[27] found a strong

correlation between a* and $\alpha = 1/2\pi$ for two heat treatments (120 and 220 ksi) of 4340 steel in 0.5 inch thick specimens. It should be noted that for the thicker sections, retardation behavior, much like fracture toughness[1], is almost assuredly affected by the dominant plane strain plastic zone size. Thus, even though in the thicker specimens good correlations are found with Matsuoka's analysis ($\alpha = 1.5\pi/8$) and with plane stress plastic zone sizes due to Irwin ($\alpha = 1/2\pi$), these may be fortuitous. The correlations might more correctly be drawn with a combined plane stress/plane strain factor being somewhere between $\alpha = 1/2\pi$ (Irwin - plane stress) and $\alpha = 1/4\ \sqrt{2\pi}$ (Irwin - plane strain)[1]. The importance of these a* vs $W_m^{ol}$ correlations is not only in acquiring an understanding of the retardation phenomenon, but also in understanding how the plastic zone size is used in fatigue crack growth retardation models. In the majority of the commonly used models, the plastic zone correction factor, $\alpha$, can be a significant variable.

4. Load-Interaction Models

A number of analytical models have been developed to predict load-interaction (i.e., retardation) effects for structures subjected to variable amplitude loading. They basically fall into three categories: empirical models, residual stress intensity models, and closure models. All three model types are based on alterations of the basic constant amplitude crack growth rate behavior described by equation 2 as the crack grows into and through the overload-induced plastic zone, $W_m^{ol}$. Figure 6 offers a basic schematic of these models. After an overload application, the baseline crack tip plastic zone, $W_m^i$, propagates through the overload zone at some reduced rate until it reaches point $a_p$, the original crack length plus $W_m^{ol}$ (Figure 6). None of the models currently available

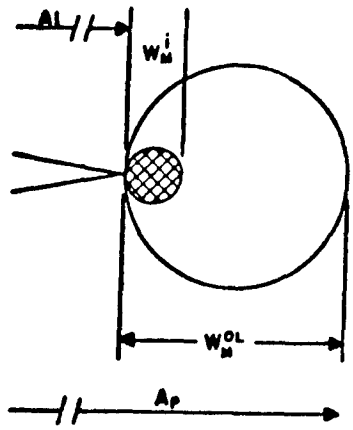


(a) IMMEDIATELY AFTER OVERLOAD

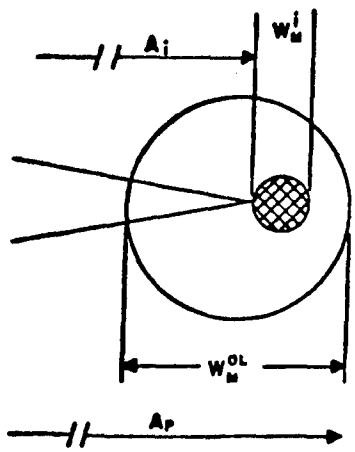


(b) LATER TIME AFTER OVERLOAD

FIGURE 6. LOAD-INTERACTION MODEL OF RETARDATION

predicts all of the effects observed during load-interaction studies. Most of these models attempt to account for unexplained effects by the incorporation of empirical constants. Generally, load-interaction predictions have been accurate to within a factor of plus or minus 2[44] or 3[45] depending on the investigator. These models have been varied by many investigators to suit particular applications and they are described in a broad sense in the following discussion.

a. Empirical Models

In 1970, Wheeler[46] developed a load-interaction model based on an empirical alteration of the Paris pre-exponential constant, c, from equation 2. The Wheeler model has the form

$$\frac{da}{dN} = C_w \cdot f(\Delta K) \qquad (6)$$

where $f(\Delta K)$ is defined in equation (1) and

$$C_w = \left( \frac{W_m^i}{a_p - a_i} \right)^m \qquad \text{for } a_i + W_m < a_p$$

All variables used to calculate $C_w$ are defined in Figure 6, except m. The m factor is an empirically derived shaping parameter which was originally suggested to be material and spectrum dependent. Because of its empirical nature a large amount of latitude exists for obtaining predictions. It cannot account for the previously discussed delayed retardation phenomenon.

b. Residual Stress Intensity Models

Although no load-interaction models are based on crack tip compressive residual stresses due to the application of an overload, the residual stress intensity factor models are analogous in that as the crack grows through $W_m^{ol}$, the maximum and minimum stress used in equation 1 are reduced. The seminal work for these models was a development by

Willenborg et al.[47] in 1971. Willenborg et al. suggested that the stress term in equation 1 be replaced by an effective stress, $\sigma^{eff}$, reduced by an amount given by

$$\sigma_{red} = \sigma_{ap} - \sigma^{i}_{max} \tag{7}$$

where $\sigma_{ap}$ is the stress required to propagate a crack to the elastic-plastic boundary, $W_m^{ol}$, formed by the overload. The new stresses are given by

$$\sigma^{eff}_{max} = \sigma_{max} - \sigma_{red} \tag{8a}$$

$$\sigma^{eff}_{min} = \sigma_{min} - \sigma_{red} \tag{8b}$$

From these, an effective load ratio, $R_{eff}$, is calculated, which is then used in conjunction with one of the many variations of equation 2 to account for R effects. For residual stress intensity models $\Delta\sigma_{eff} = \Delta\sigma$ and, thus, $\Delta K_{eff} = \Delta K$. When $\sigma^{eff}_{min}$ is negative, $K^{eff}_{min}$ is undefined and is, therefore, truncated to zero, making $K^{eff}_{max} = \Delta K_{eff} \neq \Delta K$. Thus, the Willenborg model can be called an effective stress intensity model. Effective stresses are calculated for each successive load level until the crack reaches length $a_p$. The Willenborg model cannot adequately predict crack growth behavior for structures subjected to certain types of ordered load spectra[48]. The overload induced plastic zone, $W_m^{ol}$, is sometimes used as a variable to alter prediction[35,45]. In improved versions[27,49] some experimentally determined material constants are required to account for crack arrest and the effect of compressive loads subsequent to an overload. The Willenborg model and

its derivatives do not account for delayed retardation. Despite the need for empirical factors and some arbitrary decision making, it has been effectively used by investigators[27,35,45,48] to predict load-interaction effects.

c. Closure Models

It has been observed[50-52] that under constant amplitude loading, fatigue cracks tend to close before all tensile load is removed. It has been postulated by Elber[50] that this is due to the residual tensile deformation left in the wake of a moving crack tip. These residual displacements clamp the crack tip closed until a sufficient crack opening load is applied. This is the suggested physical basis for the closure models, which extend these earlier observations of constant amplitude behavior to account for load-interaction effects. Basically, closure models modify the stress range by subtracting the ineffective portion of the stress cycle from the overall stress cycle or

$$\Delta\sigma_{eff} = \sigma_{max} - \sigma_{op} \tag{9}$$

where $\Delta\sigma_{eff}$ is the effective stress range and $\sigma_{op}$ the crack opening stress. In its original conception, $\Delta\sigma_{eff}$ is used with equation 1b to determine an effective stress intensity factor which is then applied to equation 2 which becomes

$$\frac{da}{dN} = C(\Delta K_{eff})^n \tag{10}$$

Using this model, good correlations have been found[50,53]; however, some inadequacies have been noted. In its original form the

closure model does not predict effects due to compression loads[53] nor does it predict delayed retardation. It has also been noted that in some cases[54] it predicts excessive retardation and in others[53] is not sufficient to account for the amount of retardation observed. Several improvements have been attempted on Elber's original closure model. These improved models sometimes use empirically determined relationships for the opening stress; however, difficulties have been encountered in pinpointing this crack opening stress. It has been observed that measurements at different locations along the crack result in different opening stresses[51,55]. Other empirically based derivatives of the closure model have been considered including a residual force model developed by Bell et al.[54] which uses an assumed crack tip compressive residual stress magnitude and profile. This assumed residual stress profile is used primarily as a prediction fitting parameter. Its assumed shape and magnitude have not been experimentally verified. Finite element models have been developed[9,10] which predict crack opening and closing loads as well as crack tip residual stress fields; however, these models have also not been experimentally verified. Both the residual force model and finite element techniques predict delayed retardation and the finite element method predicts effects due to compressive spikes after an overload as well.

d. Closing Remarks

No single load-interaction model completely describes all the retardation effects observed to date. Some subtle effects such as delayed retardation may not have a significant effect on crack growth predictions for variable amplitude load histories. However, the inadequacy of current models to accurately predict such effects (without

the use of empirically based "correction" factors) reveals their lack of a physical basis. This lack of a physical basis leads to an inevitable situation in which a "new" phenomenon occurs which negates or reduces crack growth retardation (e.g., hold times, aggressive environments, etc.) and which could eventually cause premature catastrophic failure. This is not to mention the great deal of time and effort required to develop meaningful empirical factors for different loading conditions and different materials. Improvements in the ability to make reliable life predictions for variable amplitude loading situations, with little or no arbitrary decision making, requires a load-interaction model which has a strong physical basis. It is the intention of this thesis to reveal information which might one day lead to such a model. This investigation goes about this goal in two ways. The first is to measure crack tip stresses and compare them with the theories commonly used in retardation models. Hopefully, this will lead to a non-arbitrary value for the overload-affected zone size, $a_0^*$, in load-interaction models. The second path to the objective is by observing crack tip stress phenomena related to the overload process which might reveal something of the physical phenomena associated with crack growth retardation.

B. Measurement of Applied and Residual Stresses by X-Ray Diffraction

There are two categories of crack tip stresses, applied and residual. The term crack tip applied stresses will be used to indicate those crack tip stresses which are induced by an external load. Crack tip residual stresses are those which exist at the crack tip after all external load has been removed. Crack tip residual stresses are presumably due to local plastic deformation which has been constrained by the surrounding elastic matrix. There are a limited number of methods of measuring residual stresses and an even more limited number for measuring applied stresses[56]. Those acceptable for measuring residual stresses include ultrasonic critical angle reflectometry[57], mechanical relaxation (dissection) methods[58,59], miniature strain gauges[19] and x-ray diffraction[58]. For measuring applied stresses, x-ray diffraction and strain gauges are applicable and in some cases ultrasonic critical angle reflectometry may be used. In general, local strain is the measured quantity and stress is calculated by assuming linear elasticity[60]. Of the above mentioned techniques, x-ray diffraction is the only non-destructive method which is readily applicable for measuring applied and residual stress in very small areas (.0002 - .0008 $in^2$). Recent developments in x-ray diffraction equipment[61] have made it a very versatile metallurgical instrument for use in measuring stresses on a variety of different specimen geometries and loading configurations. For these reasons and because of the availability of a semi-automated x-ray

diffraction device, this study centered on the use of x-ray diffraction for measuring crack tip stresses.

1. Theoretical Background of X-Ray Diffraction Stress Measurements

When a beam of x-rays impinges on the surface of a crystalline object, x-rays are scattered by each atom. If a large number of x-rays are scattered such that they mutually reinforce one another, that is, they are in phase, then a diffracted beam has been produced[60]. In the early twentieth century, Bragg observed that this diffraction phenomena occurred when the x-ray wavelength, $\lambda$, the crystal lattice spacing, d, and the x-ray incidence angle, $\theta$, all meet certain conditions. These conditions are given in what is now called Bragg's Law, which is

$$n\lambda = d \sin \theta \tag{11}$$

where n is an integer greater than 1.
When these conditions are met, an x-ray beam will be diffracted at an angle, $\theta$, equal to the incidence angle.

In standard x-ray diffractometry, the x-ray wavelength is fixed and the lattice spacing is calculated after experimentally determining the angle at which x-rays are diffracted (generally this angle is given as the angle between the incident x-ray and the diffracted x-ray which is equal to twice the incident angle or $2\theta$).

When a polycrystalline material is strained, the lattice spacing, d, changes and, thus, the diffraction angle, $2\theta$, shifts proportionally. From this diffraction angle shift the local strain can be calculated. Knowing the strain, certain assumptions can be made and the stress can be calculated[60]. The important assumptions are (1) that stress can be related to lattice strain by conventional elasticity theory and (2) over

the measurement region the material is subject to plane stress conditions, that is, the stress normal to the surface is zero. The first assumption is generally acceptable because of the small gauge section being measured by x-ray diffraction, that is, the spacing of lattice planes which is only altered by the elastic stress and not by plastic flow[60]. Because of the shallow depth of penetration of the x-rays, 95% of which are from a depth of 0.0005 inch, it is generally acceptable to assume plane stress conditions.

Using linear elasticity theory and assuming plane stress conditions, the stress in an arbitrary direction, $\phi$, can be related to two strains, one normal to the surface and another at an arbitrary angle, $\psi$, (see Figure 7). This relationship is given by[i.e., 60]

$$\sigma_\phi = (\varepsilon_{\phi\psi} - \varepsilon_\perp) \left( \frac{E}{1+\nu} \right) \frac{1}{\sin^2\psi} \tag{12}$$

where $\sigma_\phi$ is stress in the $\phi$ direction; $\varepsilon_{\phi\psi}$ is the strain in the direction of measurement, $\phi$, at an arbitrary angle, $\psi$, to the surface; $\varepsilon_\perp$ is the strain in the $\phi$ direction normal to the surface; E is the bulk modulus of elasticity; and $\nu$ is Poisson's ratio for the bulk material.

The strain differential $(\varepsilon_{\phi\psi} - \varepsilon_\perp)$ can be approximated[62] in terms of the strained lattice spacings as

$$\varepsilon_{\phi\psi} - \varepsilon_\perp = \frac{d\psi - d_\perp}{d_\perp} \tag{13}$$

Equation 13 can be substituted into equation 12 to get stress in terms of the lattice spacings. Since the lattice spacings are related to a measurable quantity, the diffraction angle, $2\theta$, by Bragg's Law, it is more convenient to write equation 12 in terms of $2\theta$. This can be done

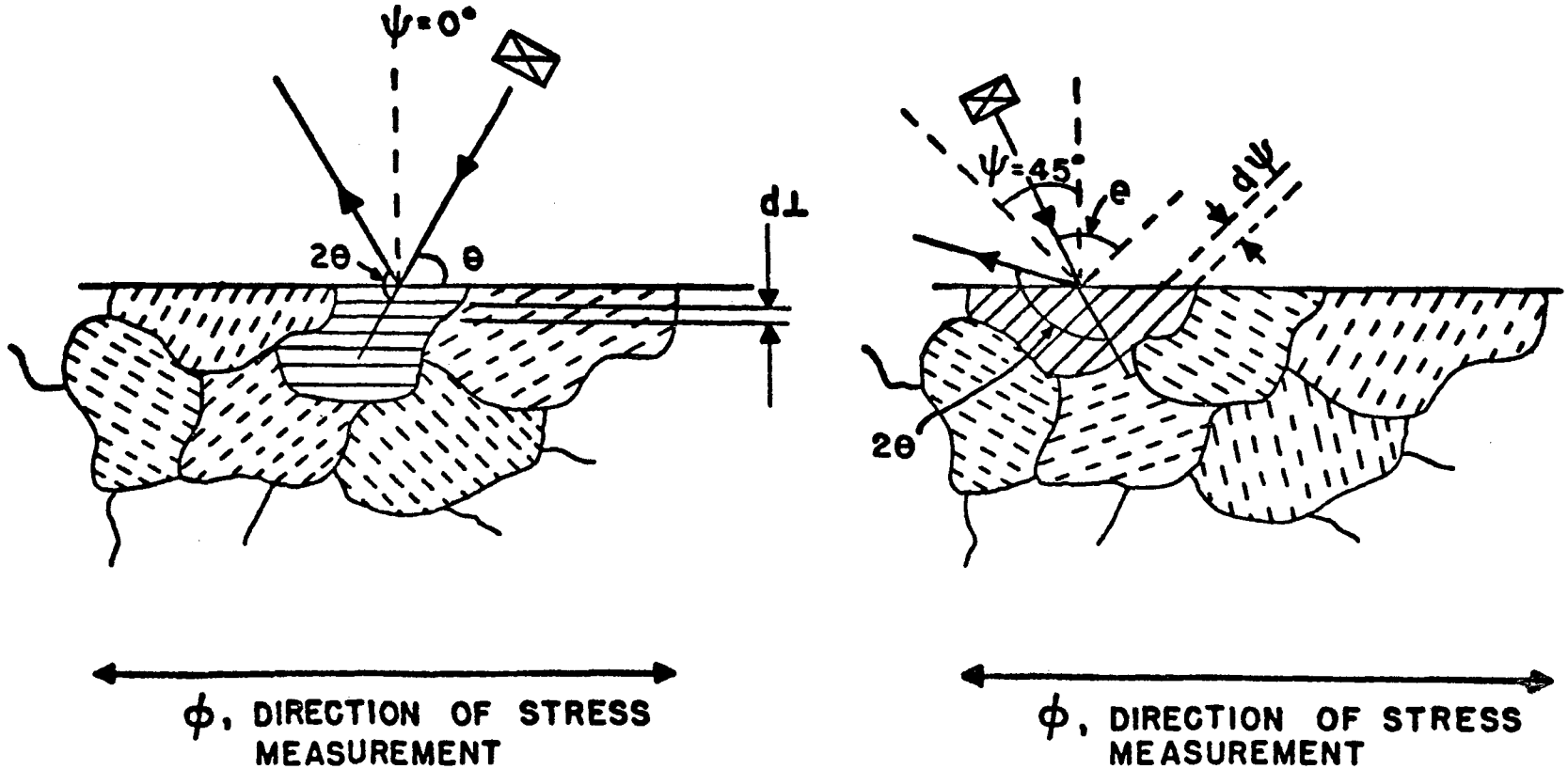


(a) $\psi = 0°$ (b) $\psi = 45°$

FIGURE 7. DIAGRAM OF STRESS ANALYSIS BY XRAY DIFFRACTION
REF. 73

by differentiating equation 11 and combining it with equations 13 and 12 to yield

$$\sigma_\phi = S\ (2\theta_\perp - 2\theta_\psi) \tag{14}$$

or

$$\sigma_\phi = S \cdot \Delta 2\theta \tag{14b}$$

where

$$S = \frac{\cot\ \theta}{2} \cdot \frac{E}{1+\nu} \cdot \frac{1}{\sin^2\psi} \tag{15}$$

$2\theta_\perp$ is the diffraction angle from planes parallel to the surface and $2\theta_\psi$ is the diffraction angle from planes inclined to the surface. The stress factor, S, can be determined either by calculation involving the mechanically measured bulk elasticity properties, E and $\nu$, or by a calibration procedure involving the measurement of the stress produced by known loads[62]. In general, the two methods give equivalent stress factors; however, deviations have been observed[58] for some alloys and, thus, the latter is preferred. There are, of course, certain limitations on the x-ray diffraction technique. One involves the stress factor which is normally considered a constant. In equation (15) , the stress factor is assumed to be a linear function of $1/\sin^2\psi$. Experimentation[58,63-65] has shown that for certain alloys this function is not linear and, thus, anomolous stress calculations can ensue. Marion and Cohen[64] have developed a technique for correcting for this phenomenon; however, it entails the measurement of $\Delta 2\theta$ at various values of $\psi$. Another important consideration is the grain size of the object being studied. If the grain size is large relative to the x-ray beam size, it can lead to major

error, in that the results will depend on the particular grains making a large contribution to the diffraction peak[62]. If these grains are aligned such that the crystallographic planes of interest are not parallel to the measurement axis, the stress measured will not be indicative of the bulk stress. In general, these limitations can be overcome; however, care must be taken to ensure that they have not affected experimental results in a manner unknown to the investigator.

2. Previous Experimental Measurements

a. General Experimental Observations

It is a well-established experimental fact[i.e., 58,63,66,67] that when an alloy is subjected to uniaxial loading within the elastic region, the differential x-ray diffraction angle, $\Delta 2\theta$ is a linear function of the applied stress given by equation 14. These measurements have been demonstrated in numerous metal alloys. Upon plastic deformation, the relationship between $\Delta 2\theta$ and stress is still valid as the lattice spacing is not affected by plastic flow. In practice, some anamolies have been observed for the case of uniaxial plastic deformation[63,65-69]. These anamolies take the form of either tensile or compressive residual stresses after removal of the load. The origin of these residual stresses is not completely known[65]; however, they have been shown to be true residual stresses for some materials. The observation has been attributed either to a hardening effect or a surface effect[13]. Dietrich[70] used x-ray diffraction to measure both radial and tangential stresses around a hole which had been severely plastically deformed by mandrelization. His measurements, made on a 1045 steel, indicate that this pseudo-residual stress is not apparent for non-uniaxial deformation in plain carbon steels.

Because of its small beam size, x-ray diffraction is well-suited to measuring stress gradients. One example of this is recent work by Chrenko[71] in which residual stresses were mapped across a weld in 304 stainless steel. In a distance of 0.25 inch, the stress was observed to change smoothly from -80 ksi to +60 ksi. Dietrich[70] observed residual stress changes from -60 ksi to +20 ksi within a 0.2 inch region around a cold-worked fastener hole. Prevey[72] has extensively investigated gradients in surface residual stresses due to grinding.

Residual stresses have been shown to have dramatic effects on the life of specimens subjected to cyclic loading[73]. Several investigators[74,75] have observed that residual surface stresses produced by shot peening tend to relax to a lower stress with repeated cyclic loading. Other investigators[11,76,77] have studied the substructure at the tip of a fatigue crack, relating dislocation density as measured by x-ray diffraction line broadening to the crack growth rate, da/dN.

b. Crack Tip Stress Measurement

Three studies have attempted to measure crack tip residual stresses. Taira[11] observed that the residual stress distribution in a cracked specimen of .33% carbon steel followed the general shape of previous analytical predictions but had a lower maximum stress and did not extend away from the crack as far as had been predicted.

Similar results were observed in an unpublished Society of Automotive Engineer's study[12]. Two ferritic steels containing roughly .20% carbon were studied, one heat-treated to a yield strength of 47 ksi and the other 112 ksi. Residual stress measurements were made by four different laboratories, with beam sizes varying from .0003in$^2$ to .004in$^2$. A pronounced effect of beam size (or laboratory) was seen.

Measurements produced using the largest beam size did not observe any crack tip residual stresses. In general, the shape of the residual stress profile followed that previously predicted by Rice's analysis; however, the maximum stress was much smaller and the crossover point (point B in Figure 4) was much closer to the crack tip than would be predicted by Rice. Having been conducted prior to the advent of the semi-automated x-ray diffraction stress analyzer, these investigations typically required thirty to sixty minutes per datum point and were thus quite limited in their extent.

In a recent study, Macherauch and Wolfstieg[13] measured both crack tip applied and residual stresses in an unspecified alloy. The observed cross-over point for the crack tip residual stresses agreed very well with Rice's prediction; however, the maximum measured compressive residual stress was roughly 40% of the yield strength. Because of insufficient information regarding the material and specimen geometry, the crack-tip-applied stress profile could not be directly compared with observations from the present study. However, in a qualitative sense the results of the present study appeared to be in agreement with Macherauch's results.

c. Closing remarks

In the past, x-ray diffraction measurements have required long exposure time per measurement (one to 24 hours) and therefore measurements of the type investigated in this study have been either too tedious or too costly to consider. In the 1960's, researchers developed various prototypes of semi-automatic x-ray diffraction equipment, which provided a rapid means (one to three minutes) of making residual stress measurements. One such device was developed by Weinman[61].

This device, specifically developed for ferritic steel alloys, differs from conventional diffraction equipment in several major ways. It has two x-ray sources at fixed angles to the specimen surface versus conventional systems which have only one. The system has two sets of x-ray detectors (Geiger-Mueller tubes) which are automatically positioned at the center of the diffracted x-ray beam. In addition, the system electronically compares the diffraction angles of the two x-ray sources and automatically computes the stress using manually set stress factor. This system, known as FASTRESS, is currently marketed by the American Analytical Company and was used in this investigation. These devices were developed for use in production quality control[78]; however, they are capable of efficiently producing precise data and are, therefore, gaining limited acceptance[70,71,79] as a general purpose research tool.

# III. EXPERIMENTAL TEST PROGRAM

## PROCEDURES AND APPARATUS

### A. General Plan

In order to measure crack tip stresses by x-ray diffraction, a two part investigation was planned. In the first phase, a low yield strength, low carbon steel was used to determine the general feasibility of the intended measurement. Upon successful completion of this phase, a higher yield strength, low carbon steel was investigated for more definitive measurements of crack tip stresses and to study phenomena related to crack growth retardation. Material selection and surface preparation were considered very important to the success of this study as was calibration and standardization of the x-ray diffraction stress analyzer.

### B. Material Selection

The primary constraints governing material selection were suitability for use with the x-ray diffraction device available to this study and the yield strength of the material. The x-ray diffraction device is limited to diffraction angles $2\theta$ between 152 degrees and 159 degrees and is equipped with chromium x-ray tubes. These two factors were considered fixed and, thus, limited the study to alloys possessing crystallographic planes which diffract chromium produced x-rays ($\lambda$ = 2.2909A°) at a $2\theta$ angle close to 156.0 degrees. Essentially, this limited selection to aluminums, which have a diffraction peak at 156.9 degrees from the 222 plane and body-centered cubic steels (ferritic steels) which diffracts chromium radiation

at 156.2° from the 211 plane[62]. Experience has shown that the aluminum peak at 156.9° is generally a low intensity peak which is poorly suited to stress measurements by x-ray diffraction[80]. Thus, aluminum alloys were excluded from further consideration.

Because of the small x-ray beam (0.025 inch diameter) used in this investigation, it was necessary to use an alloy with a very fine microstructure. This ensured that the stress measurements were averaged across many grains rather than across one or few grains. Low carbon steels can be heat-treated to produce a fine grain size and were considered as the primary alloys for consideration.

A 1020 steel was selected to determine the feasibility of the intended measurements. Properly heat-treated, this alloy has an ASTM grain size of 10 to 11 and a yield strength of approximately 55 ksi. This low value for yield strength ensured that the "plastic-zone" would be large (0.2 inch) for normal loads. The material was acquired from ARMCO Steel, Inc., in a hot-rolled, sheet condition. This sheet had been rolled at temperatures from 1700°F to 2400°F, quenched to 1200-1300°F, coiled and finally air cooled to room temperature. For the second part of this study, a 1045 steel was selected. This alloy had been used in quenched state in a previous study[70] which had determined the yield strength to be about 100 ksi and the grain size to be ASTM 11 to 12. For the present study, a three foot by eight inch by 0.25 inch sheet was subjected to a grain refining heat-treatment in which the specimen was heated to 1475°F and quenched a number of times. The final heat treatment consisted of heating to 1475°F and then quenching in a sodium choloride bath at 400°F.

C. Surface Preparation and Specimen Fabrication

X-ray diffraction is a surface phenomena and, thus, surface preparation is very important. Early in the investigation, this topic was given considerable attention. The 1020 steel was acquired in a hot-rolled condition to minimize surface stresses. Stress measurements on the as-received sheets revealed a high residual compressive stress (30-50 ksi). (Subsequent inquiry revealed that in the surface oxide removal and straightening process, significant stress-inducing cold-working occurred). Several techniques were studied for removing this surface stress including annealing, grinding, electropolishing and acid etching. Initially, the specimens were straightened and vacuum annealed at 1400°F for 1 hour before furnace cooling. Next, a low stress grinding procedure was used to remove a 0.010 inch decarburized region and to flatten the specimens. The low stress grinding process involved removing 0.001 inch per pass for five passes, 0.0005 inch per pass for six passes, and 0.0002 inch per pass for ten passes. This left a small tensile stress typical of a conventional grinding process[67]. Attempts to remove this stress by deep acid etching were unsuccessful, in that large variations in measured stress were observed after etching. The origin of this scatter was not identified; however it was thought to be either a surface roughness effect due to aggressive etching[60] or a texturing effect due to a severe microstructural banding which was present from the hot rolling. At this point, a decision was made to proceed with the as-ground surface for the initial experimentation.

Smaller crack growth specimens were manufactured from the 1045 steel. This allowed the use of a small, high-vacuum annealing furnace. Specimen blanks were ground using the previously described low stress grinding procedure, annealed in a high-vacuum (10 micron of $H_g$) for thirty-five minutes at 1000°F and furnace cooled. This provided an acceptable specimen surface with a $\pm$5 ksi residual stress.

Four different specimen geometries were used in this study. A large (3' x 8") center cracked tension panel was used in the feasibility demonstration, while wedge opening load (modified compact) crack growth specimens were used for measurements on the 1045 steel. Subscale tensile specimens and a large tensile specimen for stress calibration were also used. The nominal thickness of both alloys was 0.232 inch. Complete specimen drawings are given in Appendix I.

D. Material Characterization

Both the 1020 and 1045 steels were fully characterized. Metallographic and x-ray diffraction characterization were performed to ensure suitability for use with the x-ray diffraction stress analyzer. Chemical compositions were determined as were tensile properties and constant amplitude crack growth rates.

Optical and transmission (replication) microscopy revealed the 1020 steel to have the coarse ferrite-pearlite structure shown in Figure 8. The average grain diameter was approximately 500 microinches. The 1045 steel had very fine spherodized carbides ($Fe_3C$) in a ferrite matrix with scattered proeutectic ferrite grains. This structure is shown in Figure 9. The average grain diameter was estimated to be 63 microinches.

X-ray film cassettes were used to examine portions of the diffraction cones from both the 1020 and 1045 steels. The 1045 steel showed a uniform, well-defined diffraction pattern. The 1020 steel had a slightly spotty but well-defined diffraction ring. A standard diffractometer was used to determine the diffraction peak width and its general characteristics. An example diffraction peak for the 1020 steel is shown in Figure 10. Diffraction peaks for both alloys were narrow (less than one degree wide) and had pronounced $K\alpha_1$ and $K\alpha_2$ doublets. They were both centered at a diffraction angle, $2\theta$, of 156.5°.

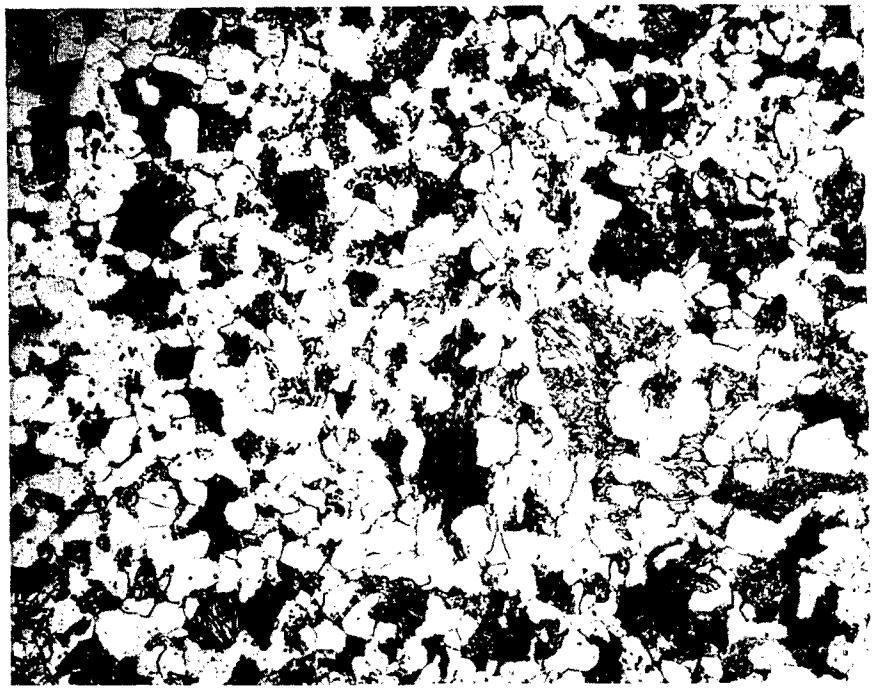

(a) Surface View (400X)

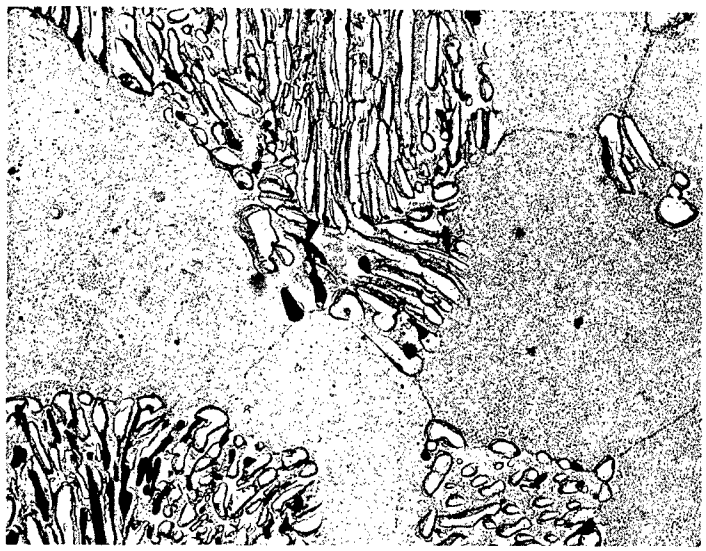

(b) Surface View (10,000X)

Figure 8. Microstructure of 1020 Steel (Picral Etch)

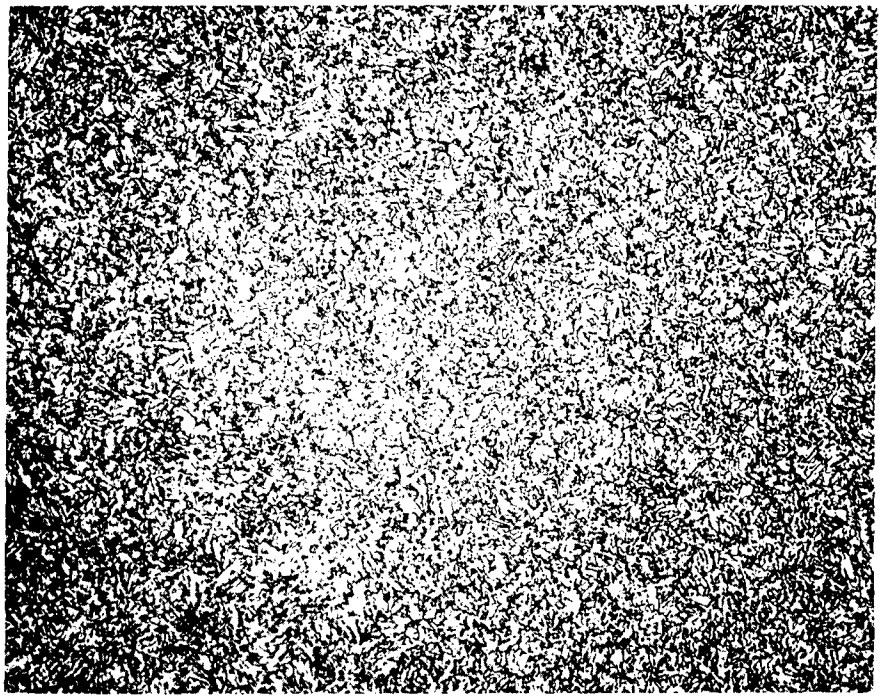

(a) Surface View (400X)

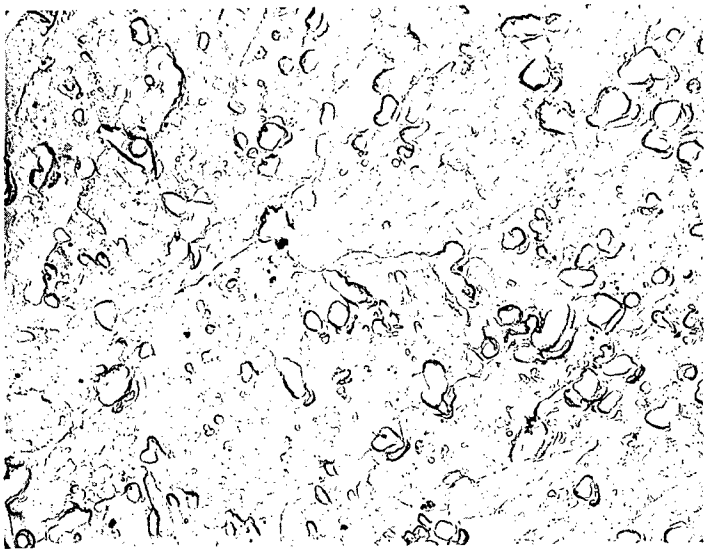

(b) Surface View (10,000X)

Figure 9. Microstructure of 1045 Steel (Picral Etch)

Chemical analysis was performed by the Analytical Services Branch, Air Force Materials Laboratory. Their findings, listed in Table II, sured that the alloys were within the specifications of 1020 and 1045 steel alloys.

TABLE II CHEMICAL COMPOSITIONS

| Alloy/Constituents | Mn | Si | Cu | Cr | C | S | Fe |
|---|---|---|---|---|---|---|---|
| 1020 | 1.0 | 0.09 | 0.32 | <0.05 | 0.22 | 0.021 | Balance |
| 1045 | 0.63 | 0.21 | 0.02 | 0.07 | 0.5 | 0.013 | Balance |

Subscale tensile specimens were used to ascertain the yield strength and ultimate strength of both alloys. Average properties for seven specimens of 1020 steel were: a proportional limit of 59.8 ksi, an 0.2 percent offset monotonic yield strength of 70.1 ksi, an ultimate strength of 77.2 ksi and an elongation of 39.5 percent. The 1020 steel had a hardness (Rockwell B) of 80. Six 1045 steel specimens were averaged to get a proportional limit of 104.8 ksi, an 0.2 percent offset monotonic yield strength of 112.1, an ultimate strength of 114.1 ksi and an elongation of 22.5 percent. The 1045 steel had a hardness (Rockwell C) of 23 in both the quenched and the quenched and annealed state. Tensile testing was conducted in a displacement controlled Instron test machine at a displacement rate of 0.1 inch per minute. Typical load-displacement curves are included in Appendix II.

Compact specimens were used to determine the constant amplitude crack growth rate behavior of the two alloys. The stress intensity calibration for this specimen is given in Appendix IV. Test results are shown in Figure 11 along with visually estimated trend lines. Testing was conducted in a 20,000 pound capacity hydraulic test system. Specimens were tested cyclically at room temperature in lab air at a frequency of 2.5 cycles per second and a load ratio

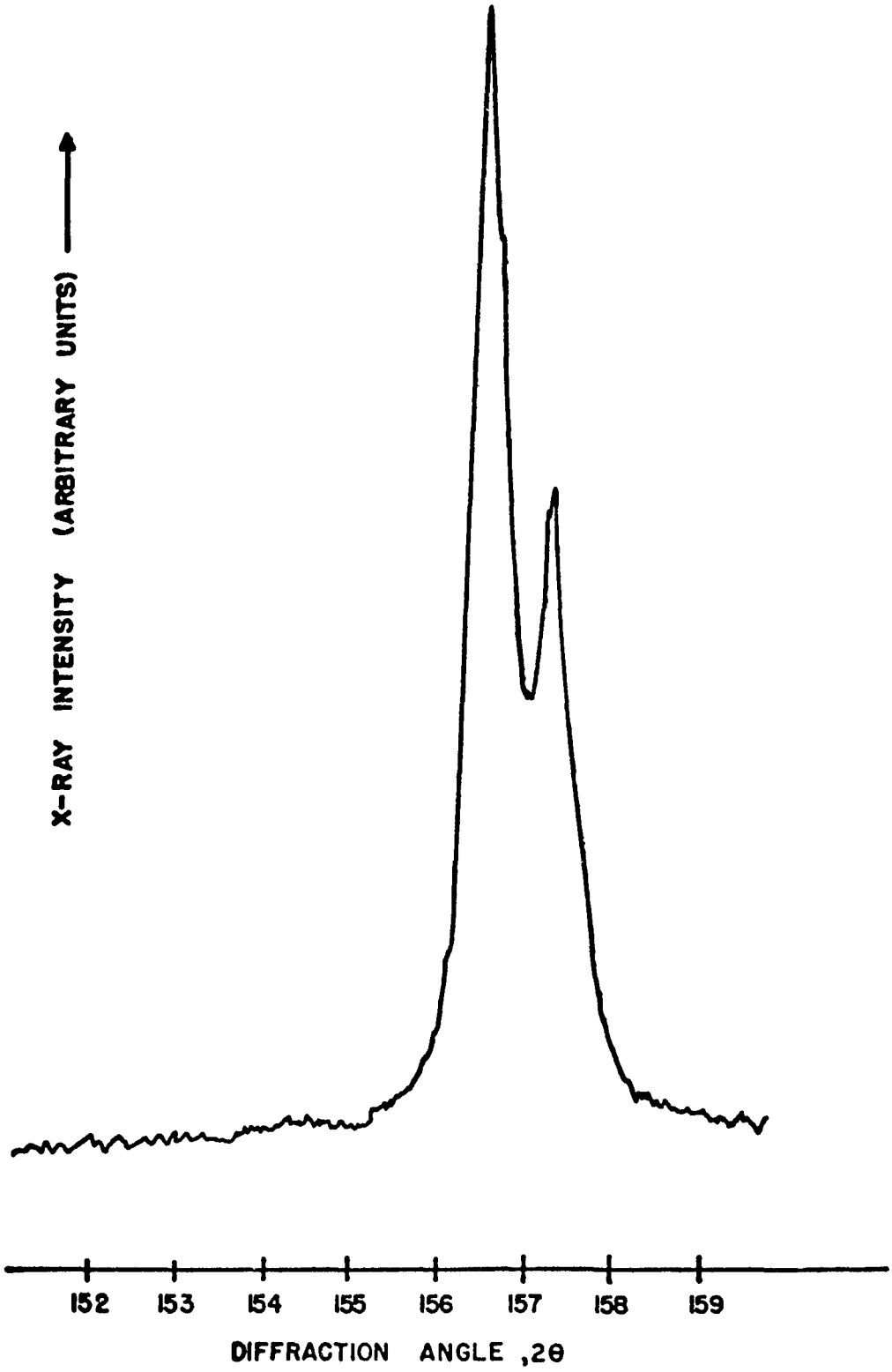


FIGURE 10: X-RAY DIFFRACTION PEAK FOR 1020 STEEL

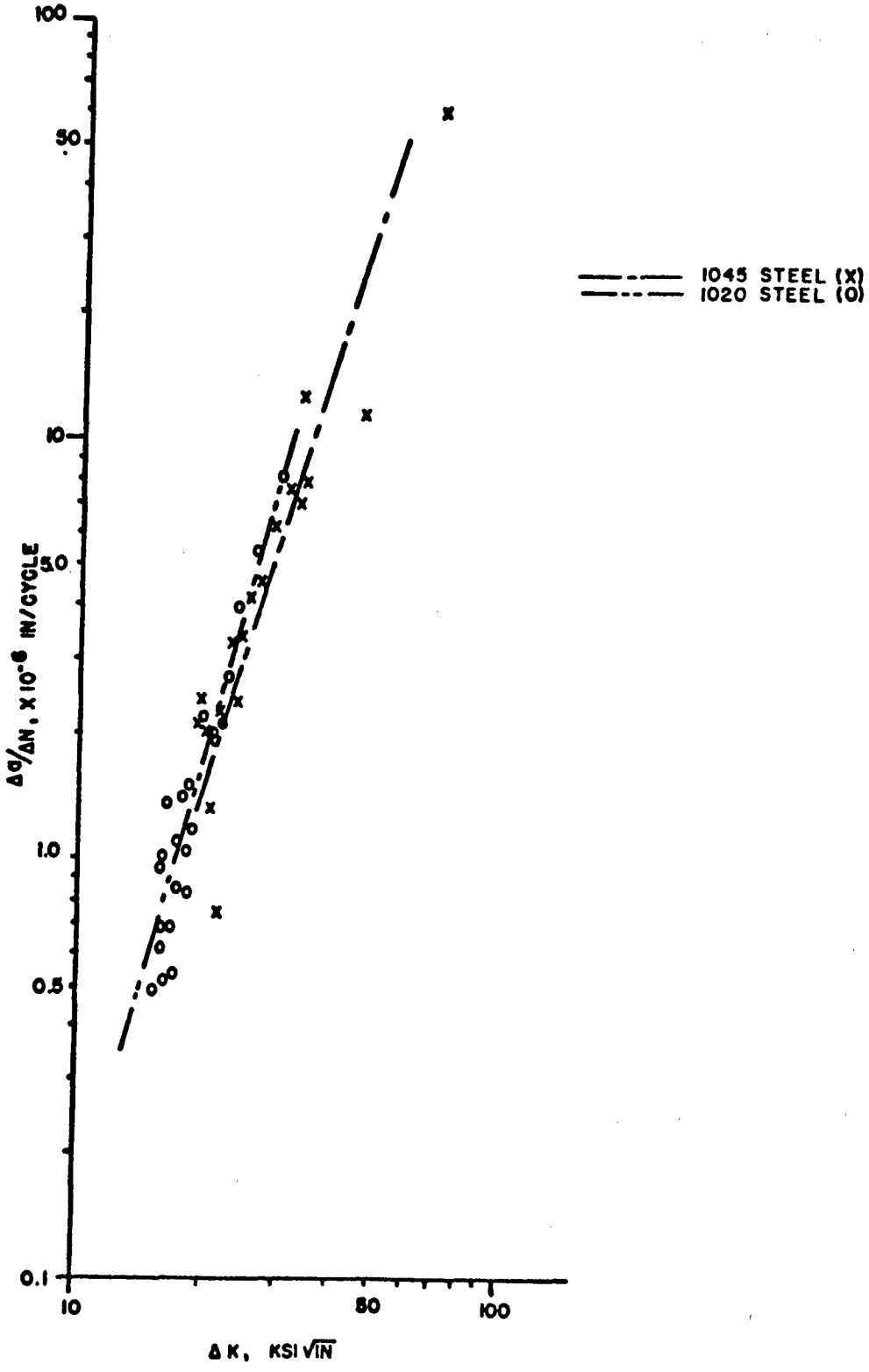


FIGURE II: CONSTANT AMPLITUDE CRACK GROWTH RATE BEHAVIOR

of 0.1. Crack lengths were recorded on acetate replicas and measured at a magnification of 70X.

E. Semi-Automatic X-Ray Diffraction Stress Analyzer

A semi-automatic x-ray diffraction stress analyzer, FASTRESS, was used in this investigation. This analyzer was primarily developed for use on low carbon steels and so was well-suited to this study. It is composed of an x-ray head (Figure 12) and an electronic console (Figure 13). The x-ray head is mounted on a travelling stage capable of accurately indexing 0.001 inch in the x, y and z directions.

The FASTRESS unit is equipped with two complete x-ray diffraction goniometers, one which measures lattice spacings normal to the surface ($\psi = 0°$) and one which measures lattice spacings oriented at 45° to the surface ($\psi = 45°$). Each goniometer has a chromium x-ray tube and a two Geiger tube x-ray detection device. The x-ray beam size is variable. A special collimator was used for this study which produced an 0.025 inch diameter x-ray spot on the specimen. The x-ray excitation voltage was 35 KV and the current was nominally 10 ma. The x-ray detectors automatically scan the range of $2\theta$ values (limited to 152 degrees to 159 degrees) and search for the diffraction peak using a servo-mechanism. The separation distance between the detectors is variable. Care was taken in establishing this separation distance to ensure that anamolous results did not occur due to interference of the $K_\alpha$ doublet.

The difference between the diffraction angles, $\Delta 2\theta$, is registered in the electronics console and electronically multiplied by the preset stress factor, S, before being plotted on the chart recorder. A stress factor of 86.6 ksi/degree was calculated from equation 15 using the bulk

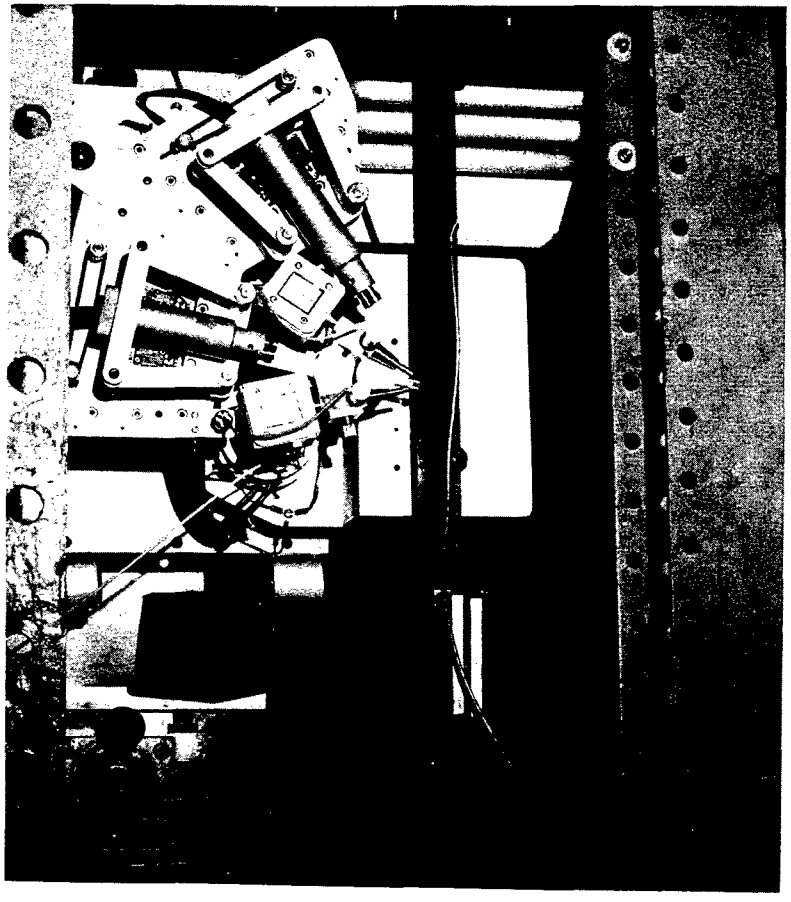

Figure 12. X-Ray Apparatus

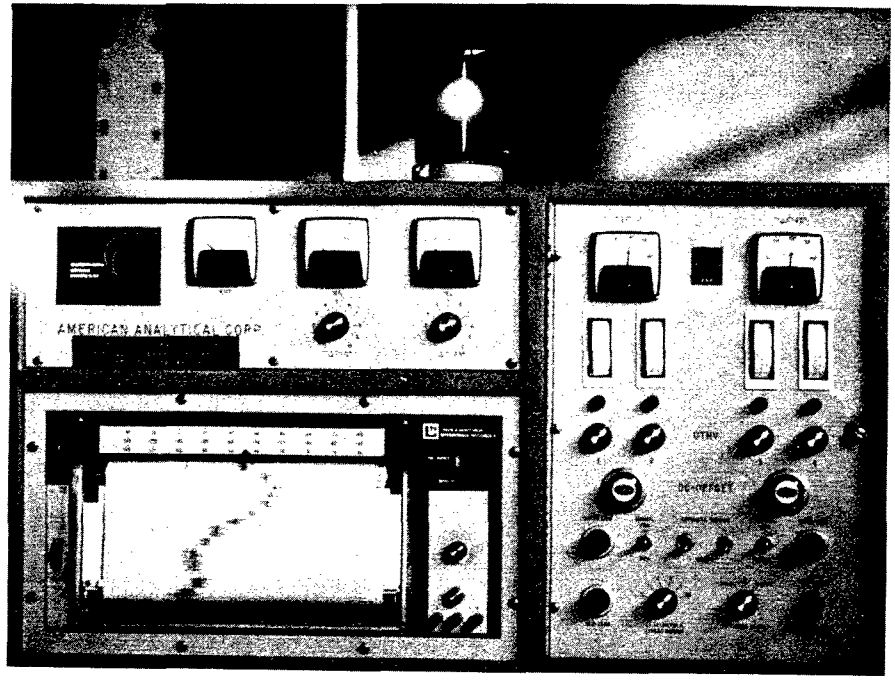

Figure 13. Electronic Console

elastic constant E = 30 x $10^6$ psi and $\nu$ = 0.3.

The FASTRESS was calibrated both by using previously measured standards and by measuring applied stress on a tensile specimen of 1020 steel. Residual stresses in two standard steel specimens were measured on three different diffractometers, two of which are dedicated to residual stress measurements. These standards were measured daily on the FASTRESS to ensure that the system was operating correctly and that its results were repeatable. This measurement proved to be very stable over the course of the investigation. A second calibration procedure was developed to check the accuracy and linearity of the stress factor. This involved loading a 1020 tensile specimen with a given load below the proportional limit and measuring the applied stress with the FASTRESS. Various load levels were applied to the specimen. A plot of the x-ray determined stress values versus applied stress is shown in Figure 14. Due to the extremely good correlation it was assumed that the calculated stress factor of 86.6 ksi/degree was accurate. After determining the stress factor, the specimen was loaded well past the proportional limit, thus, causing uniaxial plastic deformation. Upon unloading, a 44 ksi tensile residual stress remained. This is in agreement with previously reported results[13]. The 1045 steel used in this study was also used in a study by Dietrich and Potter[70]. Using an identical calibration procedure that study determined that a stress factor of 86.6 ksi/degree was accurate for the 1045 steel.

For use in making crack tip stress distribution measurements, the x-ray head was located next to a 200,000 pound load frame (Figure 15). This load frame was used to precrack and overload the initial center cracked panel of 1020 steel. For use with the small compact specimens,

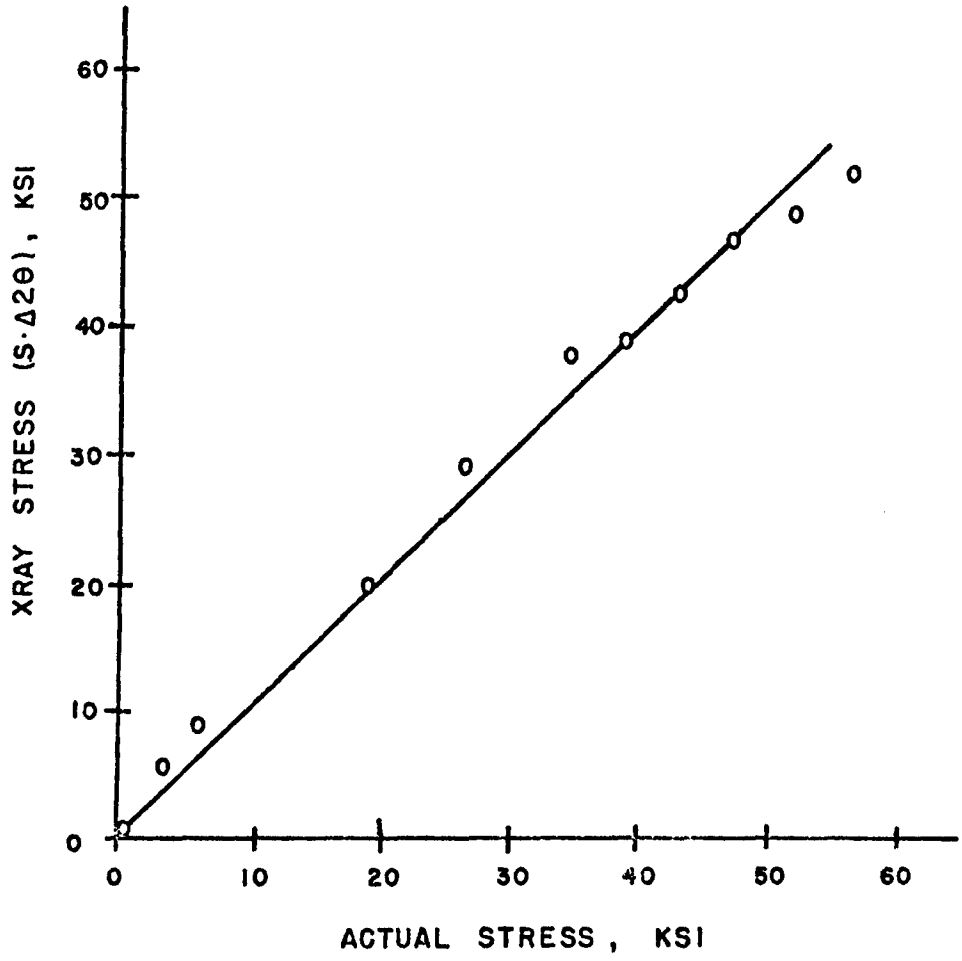


FIGURE 14: CALIBRATION CURVE FOR X-RAY DIFFRACTION STRESS FACTOR, S, FOR 1020 STEEL

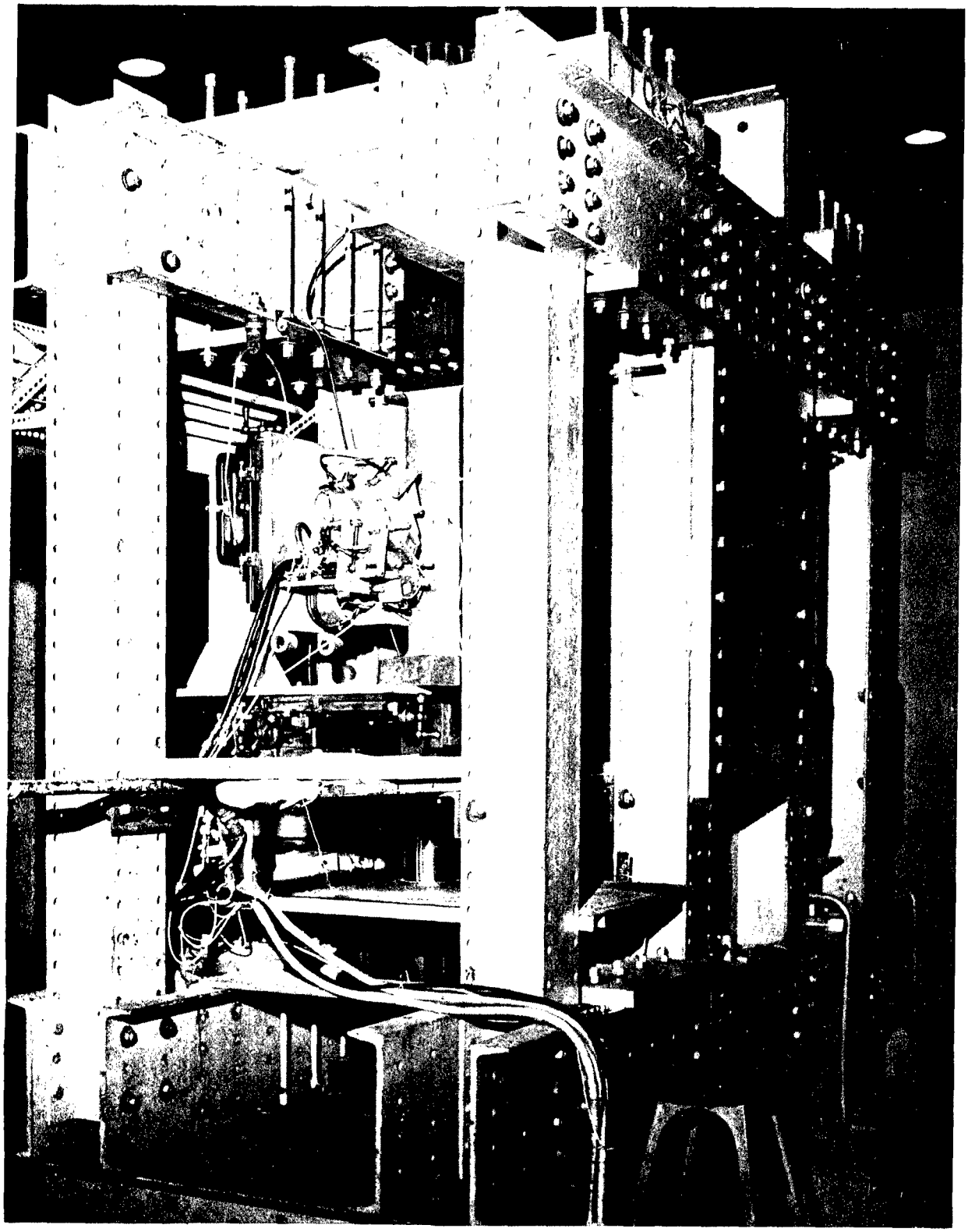

Figure 15. X-Ray Head with 200,000 Pound Load Frame

the 200,000 pound system was modified by placing a small hydraulic actuator and a 10,000 pound capacity load cell in line. This allowed the application of low level loads with much greater accuracy. The compact specimens were precracked on a 20,000 pound cyclic loading frame and then placed in the 10,000 pound frame for stress measurements with load and without load. A fiducial mark was placed on each specimen. This fiducial was visually centered under a dial gauge mounted to the x-ray head. The crack tip location had been previously measured relative to this fiducial and, thus, the x-ray beam location could be readily centered at the crack tip. In actuality, because alignment was visual some error was involved. Therefore, the crack tip stresses were measured in the crack tip area to find a maximum stress. This point was assumed to be the crack tip. Generally, this point was only 0.025 inch from the location identified by the fiducial mark. Each stress measurement took approximately two minutes; measurement of an entire stress profile required one to two hours. Thus, when measuring applied stresses the load was held on the specimen for one to two hours. After the applications of an overload, the compact specimens were again placed in the 20,000 pound cyclic test frame to extend the crack. After small amounts of crack extension, the specimens were again transferred to the 10,000 pound load frame for applied and residual stress measurement.

# IV. EXPERIMENTAL RESULTS AND DISCUSSION

## A. Experimental Results

### 1. 1020 Steel Results

To assess the general feasibility of using the semi-automatic x-ray diffraction device, FASTRESS, to measure crack tip stress distributions, measurements were attempted on the as-ground surface of a center-cracked tension specimen 1020 steel. The specimen was precracked at a constant maximum stress of 18.8 ksi and a load ratio of 0.1 to a length of 0.559 inches. At this point the stress intensity was equal to 15.4 ksi $\sqrt{in}$. Crack tip residual stress distributions were measured prior to and after a tensile load which produced a stress intensity of 41.2 ksi $\sqrt{in}$, hereafter referred to as the overload. The resulting distributions are shown in Figure 16. No residual compressive stresses due to the precracking stress intensity conditions were observed; however, this was expected since the predicted plastic zone diameter (from equation 4, $\alpha = 1/\pi$) was only 0.004 inch, substantially lower than the x-ray beam diameter of 0.025 inch. After applying the 41.2 ksi $\sqrt{in}$ overload, x-ray stress measurements revealed significant compressive residual stresses. The profile of the residual stress distribution was qualitatively in agreement with theoretical estimates; however, quantitatively the agreement was not as good. The maximum compressive stress was only 44 ksi compared with a theoretical prediction of 70 ksi (the material yield strength). Additionally, the extent of the compressive stress, $r_{OB}$ in Figure 4, went well beyond that predicted by equation 5 ($\alpha = 1/\pi$). To insure the reproducibility

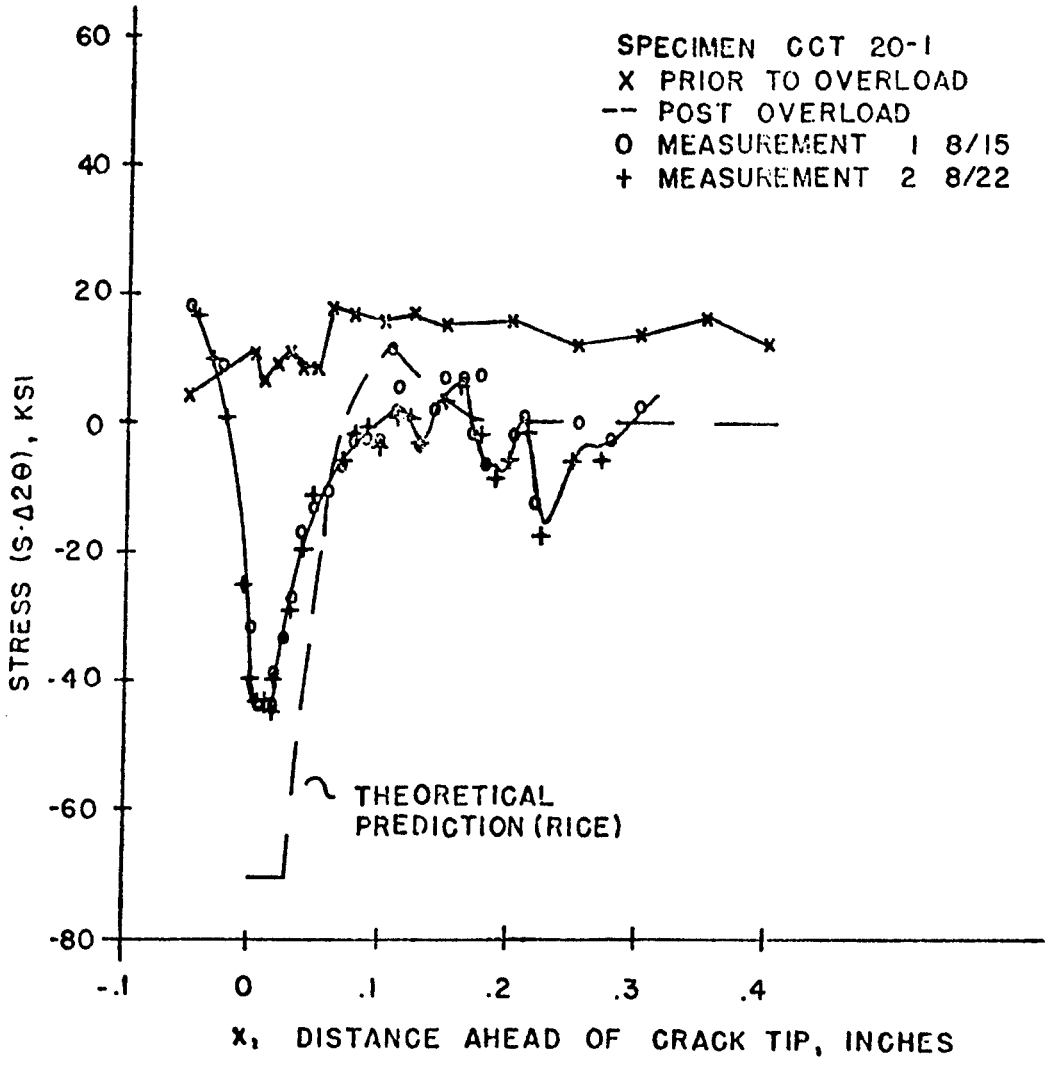


FIGURE 16: RESIDUAL STRESS PROFILE BEFORE AND AFTER 41.2 KSI $\sqrt{IN}$ OVERLOAD

of the x-ray stress measurement technique, measurements were taken again, several days after the initial measurement. These repeat measurements were extremely close to the original measurements as indicated in Figure 16*. Stress measurements were made at a number of locations on a two-dimensional grid to depict the two-dimensional profile of the residual stress distribution. The results are shown in Figure 17. Generally, the stress distribution returned smoothly to a zero stress level away from crack line. Compressive stresses extended to a distance of 0.2 inches above and 0.15 inches below the crack line.

Upon successful measurement of the crack tip residual stress distribution, the specimen was loaded to various levels while the crack tip applied stress distributions were measured. A family of curves for various applied stresses is shown in Figure 18. These measurements demonstrated the feasibility of making x-ray stress measurements while the specimen was under load. These measurements also indicated the effect of the compressive stresses on subsequent tensile loading, resulting in tensile stresses which were negated or diminished in the crack tip region.

2. 1045 Steel Results

a. Measurement of Crack Tip Residual Stress Distributions

Crack tip residual stress profiles were measured in two 1045 steel, wedge-opening-load (WOL) specimens after the application of tensile loads, hereafter called overloads. A typical crack tip residual

*The repeatability of crack tip stress measurements by x-ray diffraction was demonstrated throughout the investigation by multiple measurements. In the interest of clarity, the figures throughout this section are drawn with the data points omitted. Lines have been drawn to show the stress distributions. Actual test data are presented in Appendix III.

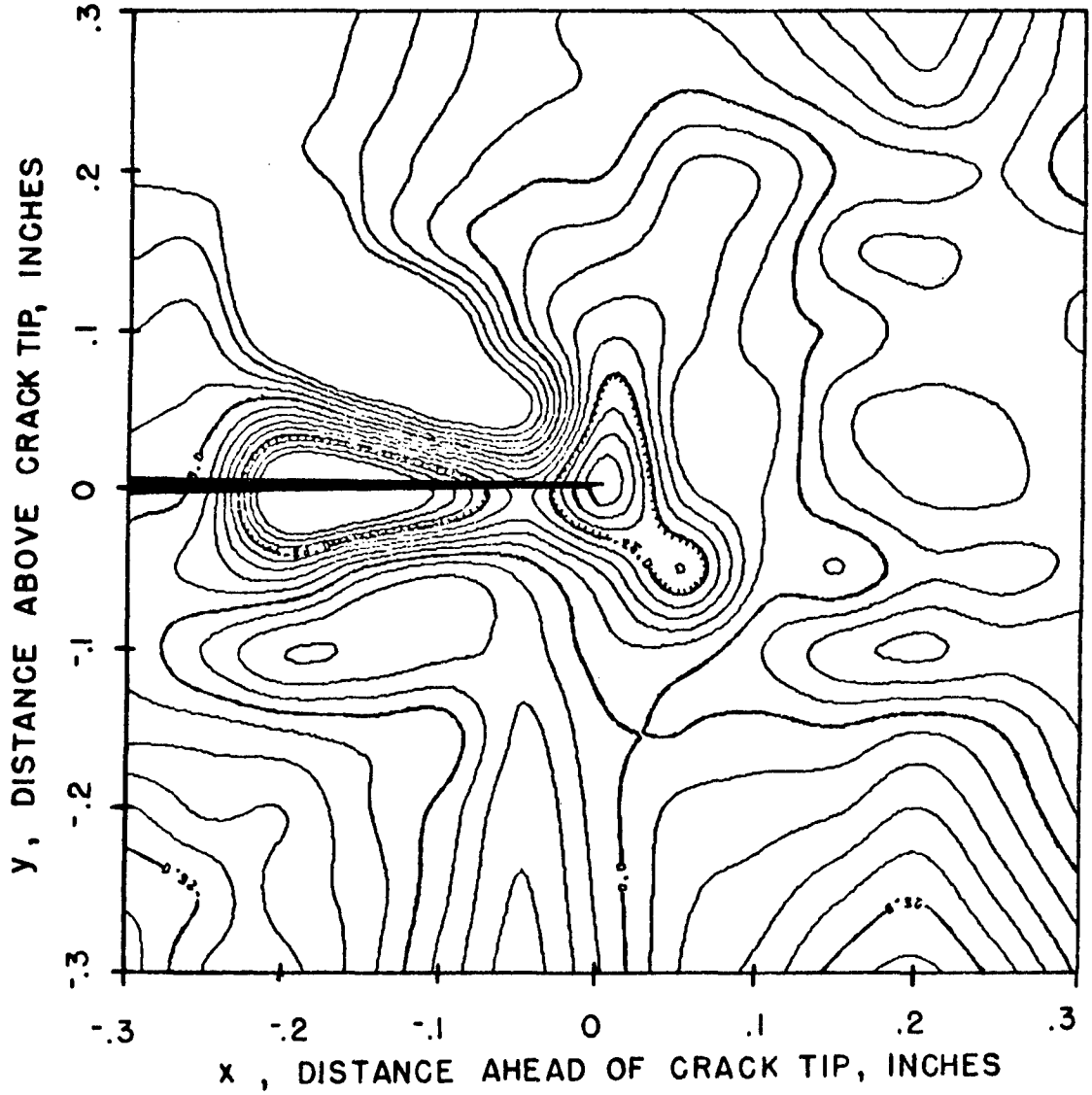


FIGURE 17: CONTOUR PLOT - RESIDUAL STRESSES ON 1020 STEEL SPECIMEN

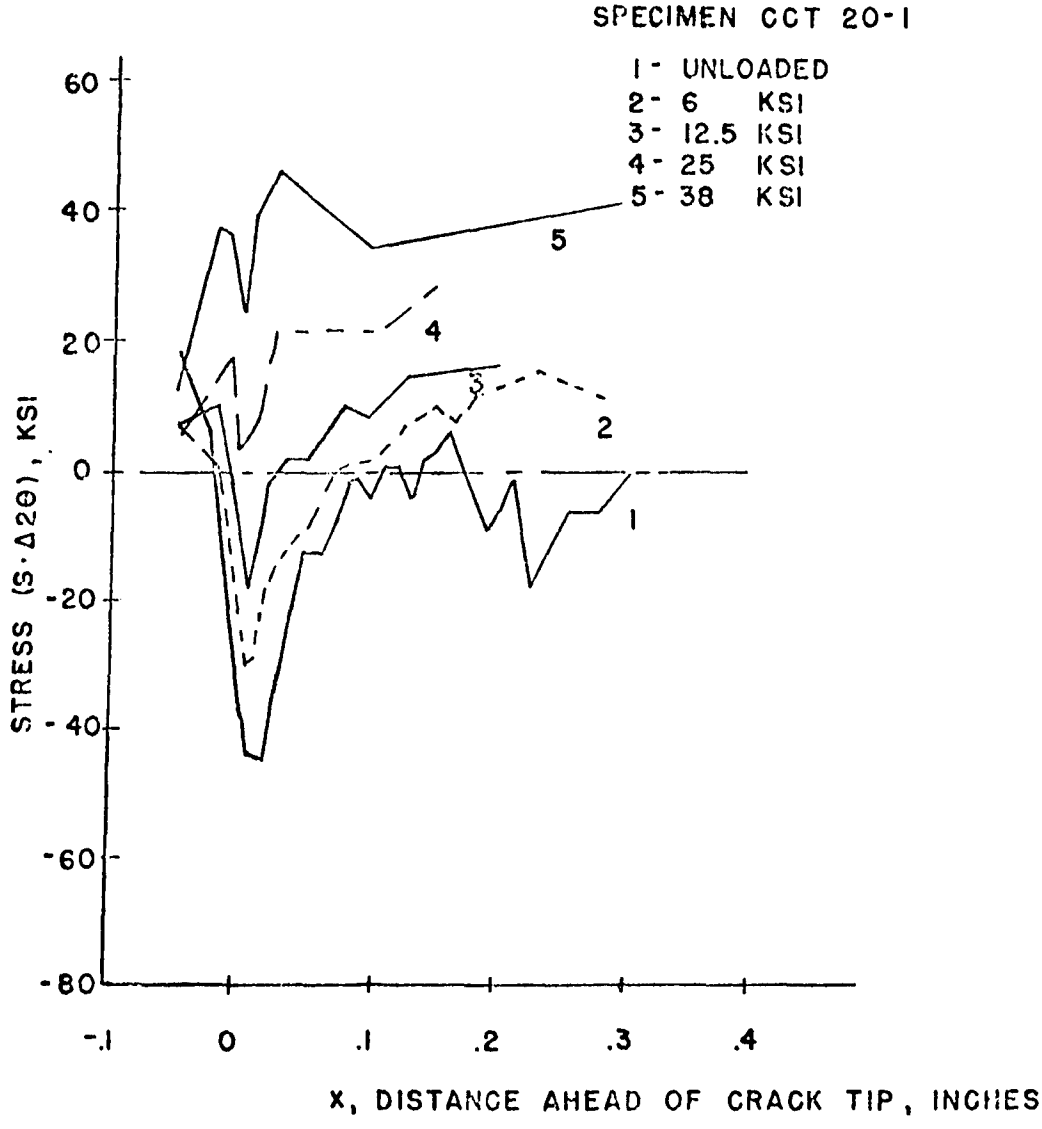


FIGURE 18: STRESS PROFILES AFTER OVERLOAD FOR VARIOUS APPLIED STRESSES

stress profile before and after an overload is shown in Figure 19. The compressive stress distribution was very evident; however, the pronounced tensile region predicted by Rice and others[1] was not observed ahead of the compressive region. A region of tensile stress was noted, however, behind the crack tip. On one specimen, stress measurements were made at many locations to depict the crack tip stress distribution above and below the crack. Figure 20 shows the stress distribution along a line in the y direction at a location of 0.005 inch ahead of the crack tip. (The stresses measured were normal to the crack line, as were all other measurements in this study). The compressive stresses smoothly decayed to 0 ksi at 0.185 inch above the crack and 0.185 inch below the crack. A two-dimensional depiction of the crack tip residual stress data is given in Figure 21. The maximum compressive stress from each residual stress profile was plotted versus the overload stress intensity in Figure 22. Contrary to theory, a strong dependence of the crack tip residual stress on the overload stress intensity was evident. No appreciable residual stress was observed for the 16.4 ksi $\sqrt{in}$ overload. Because of the low stress levels involved with the 16.4 ksi $\sqrt{in}$ overload, some uncertainty exists as to the crack tip location. It was, however, included in Figure 22 along with a scatter band, to indicate that for low overload stress intensities no measurable compressive residual stresses were observed.

The cross-over point, $r_{OB}$, between the compression and tension regions was plotted versus the overload stress intensity as shown in Figure 23. As predicted by equation 5, $r_{OB}$ has a strong dependence on the level of the overload stress intensity.

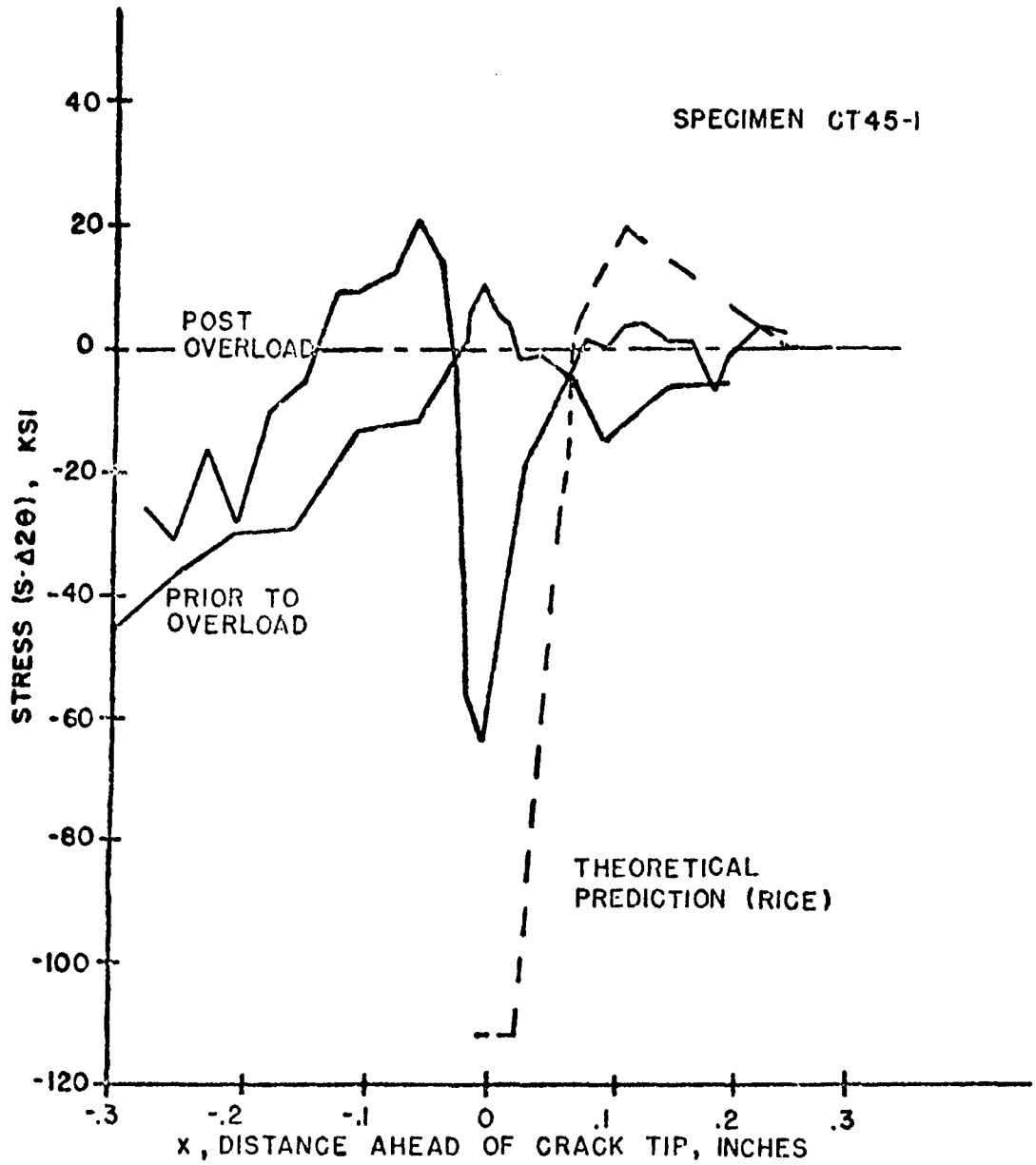


FIGURE 19: RESIDUAL STRESS PROFILE BEFORE AND AFTER 69.0 KSI IN OVERLOAD

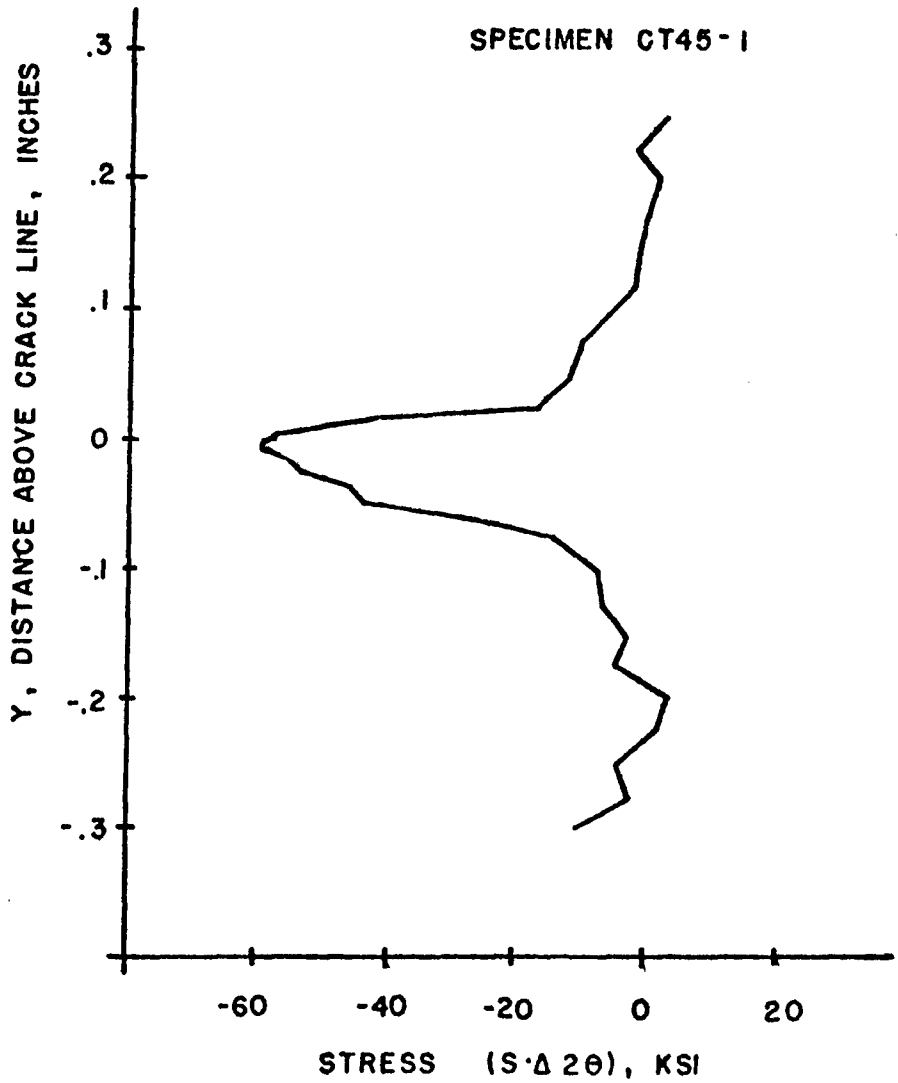


FIGURE 20: RESIDUAL STRESS PROFILE ABOVE AND BELOW CRACK TIP (X= 0.005 INCH)

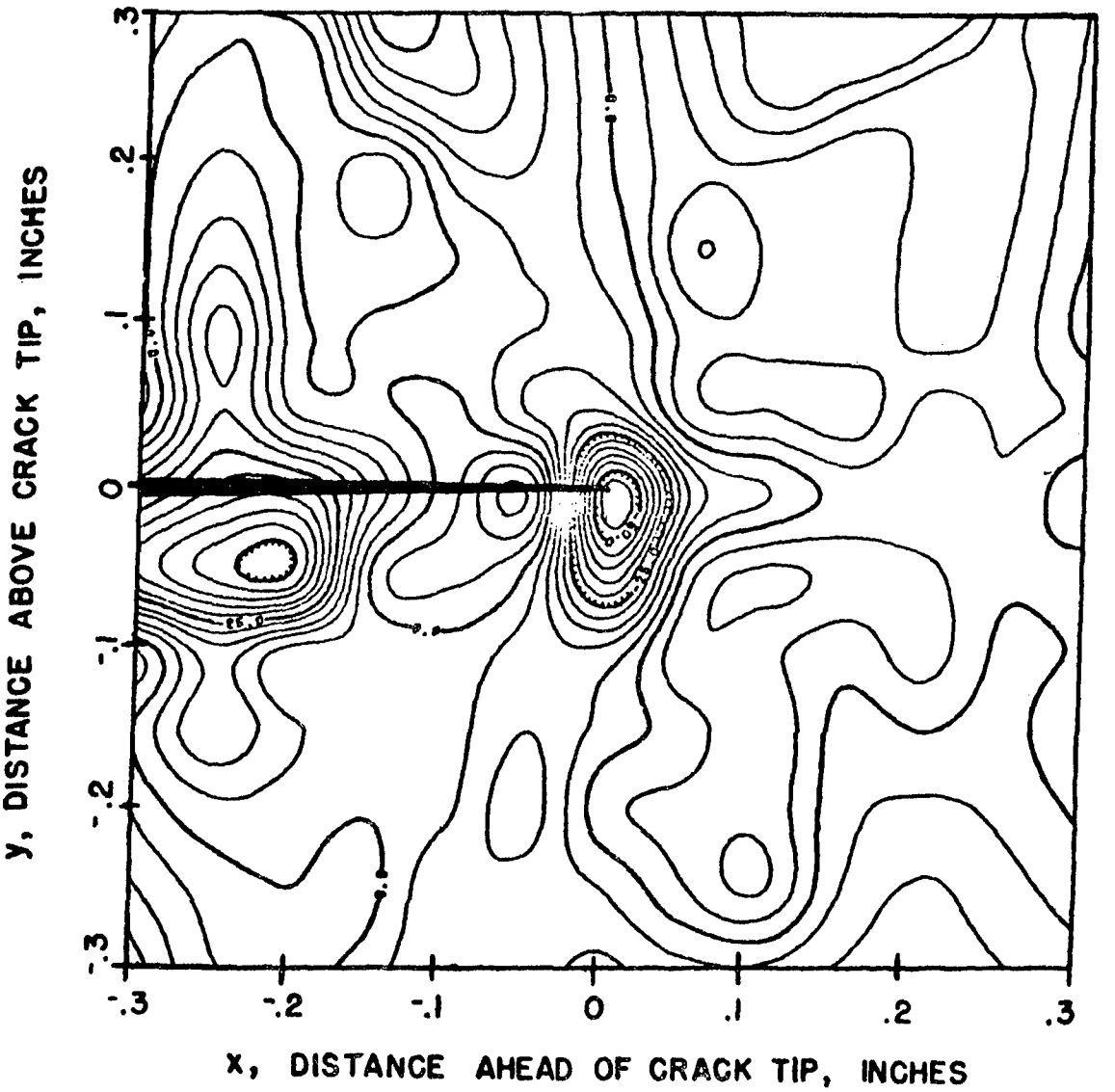


FIGURE 21: CONTOUR PLOT - RESIDUAL STRESSES ON 1045 STEEL SPECIMEN

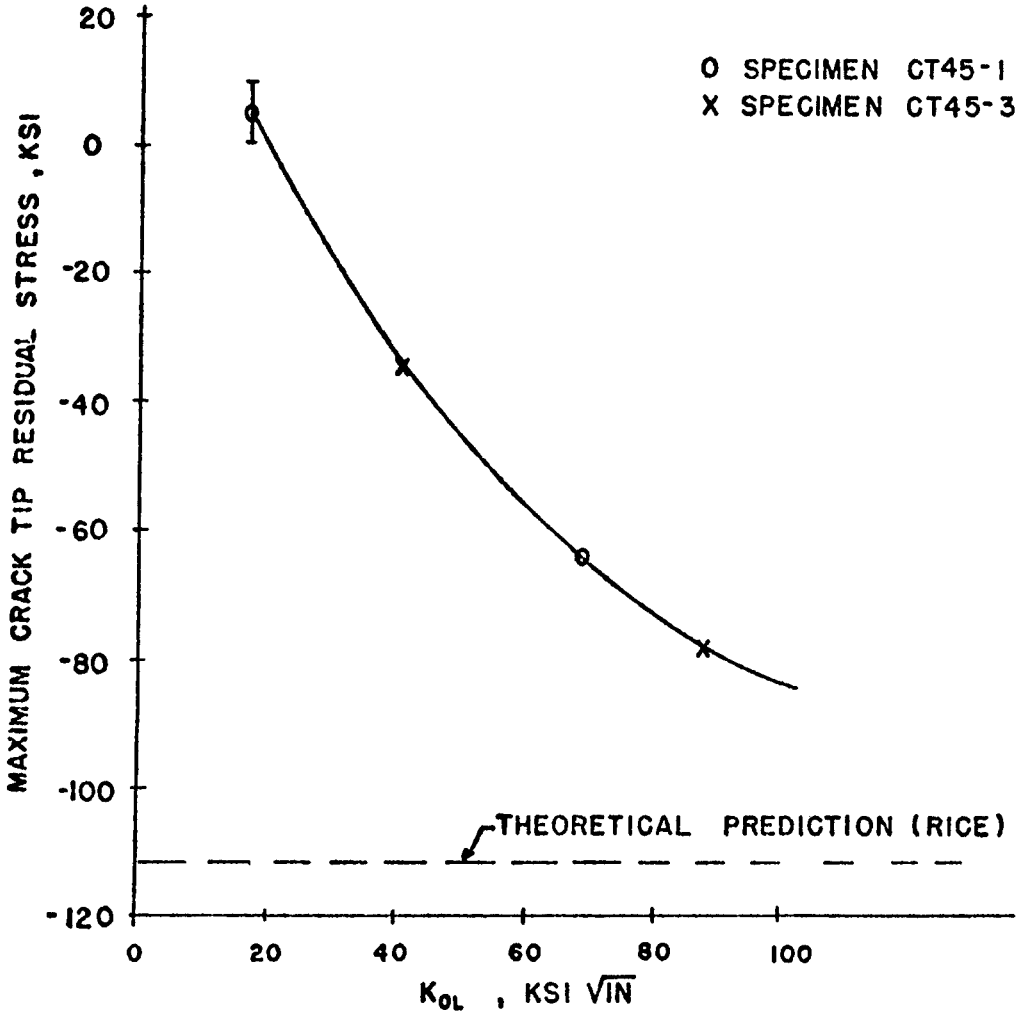


FIGURE 22: MAXIMUM MEASURED COMPRESSIVE RESIDUAL STRESS VS. OVERLOAD STRESS INTENSITY

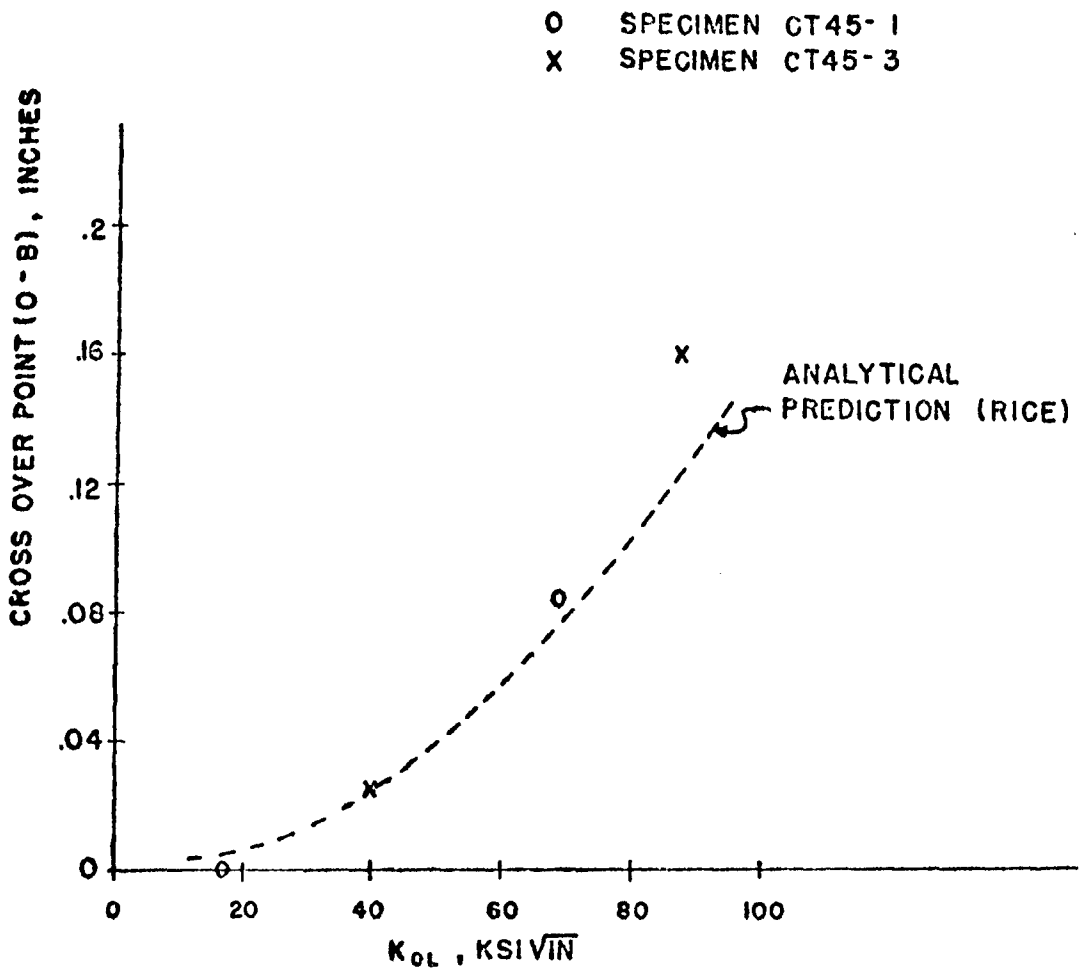


FIGURE 23: RESIDUAL STRESS CROSS OVER POINT VS. OVERLOAD STRESS INTENSITY

b. Measurement of Crack Tip Applied Stress Distributions

Crack tip applied stresses were measured in both 1045 steel specimens at various applied stress intensities. Figure 24 shows a typical crack tip applied stress profile along with the theoretical prediction according to equation 4. Qualitatively, the crack tip applied stress distributions agreed with analytical predictions; however, the stress profiles were not as pronounced as theoretical predictions. This can be seen further in Figures 25 and 26, where families of measurement curves are shown for various applied stress intensities. It was observed that the measured stress increased sharply at the crack tip irrespective of the applied stress intensity level but the "rate" at which the stress returned to a zero stress level, that is, the extent of the tensile region, was dependent on the applied stress intensity. An interesting feature was noted on specimen CT45-3 (Figure 26), in which the measured stress dropped rapidly to a low level at approximately 0.1 inch past the crack tip and then increased beyond 0.1 inch prior to finally decreasing to zero. This behavior was not seen in specimen CT45-1 (Figure 25). A possibly related observation was the crack tip deformation pattern shown in Figure 27. This photo was taken in the unloaded condition after an overload of 87.6 ksi $\sqrt{in}$ and shows bands of deformation related to the overload. These bands are possibly due to a gross slip mechanism and, thus, may relax the stress as shown in Figure 26. The origin of these bands and/or the origin of the bimodal stress profile might also be due to the geometry of the WOL specimen[1].

It can be seen in Figures 25 and 26 that the maximum measured stress increases with increasing stress intensity. This dependence on the applied stress intensity is depicted in Figure 28. It is in

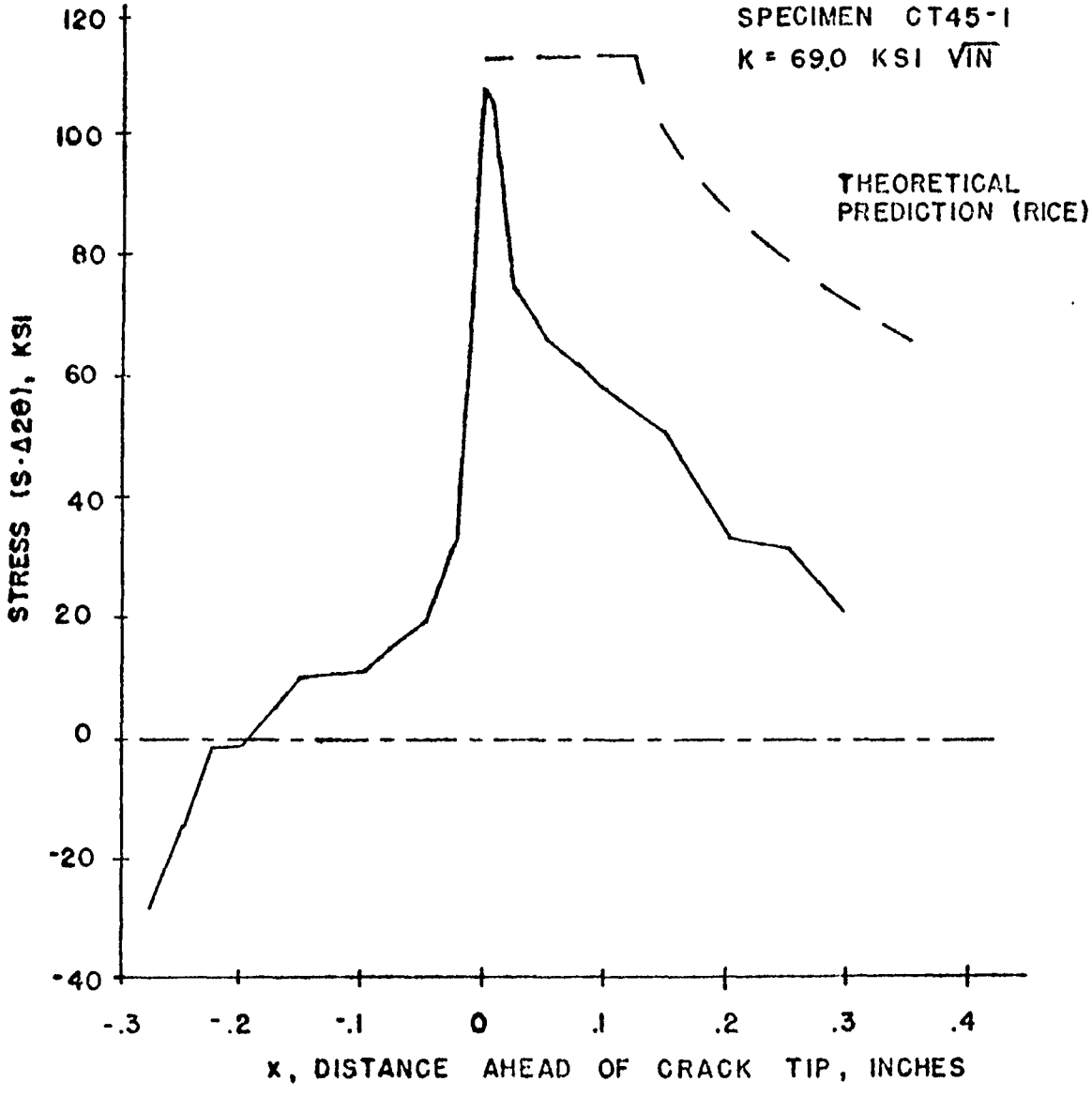


FIGURE 24: CRACK TIP APPLIED STRESS PROFILE

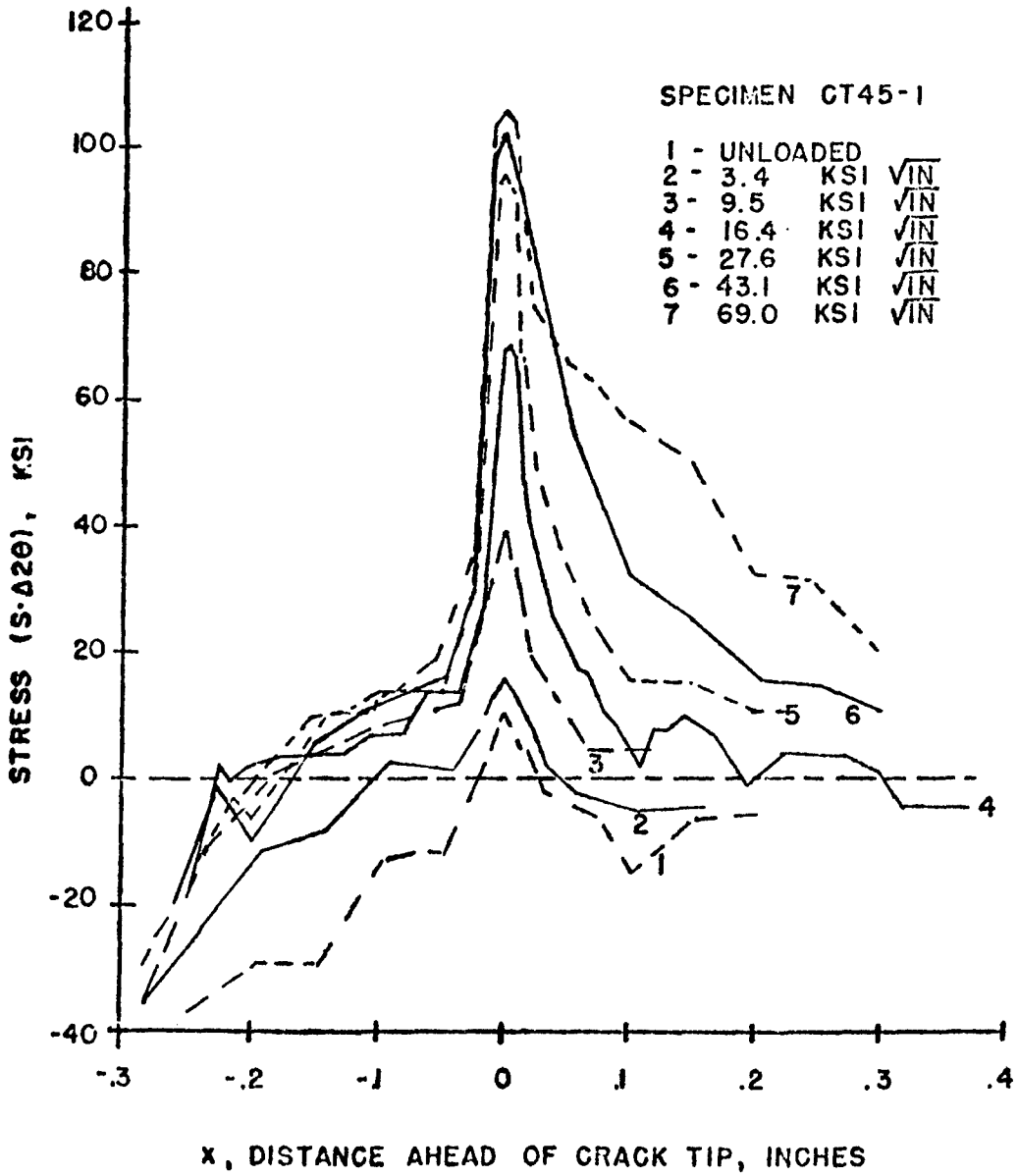


FIGURE 25: CRACK TIP APPLIED STRESS PROFILES FOR VARIOUS APPLIED STRESS INTENSITY FACTORS

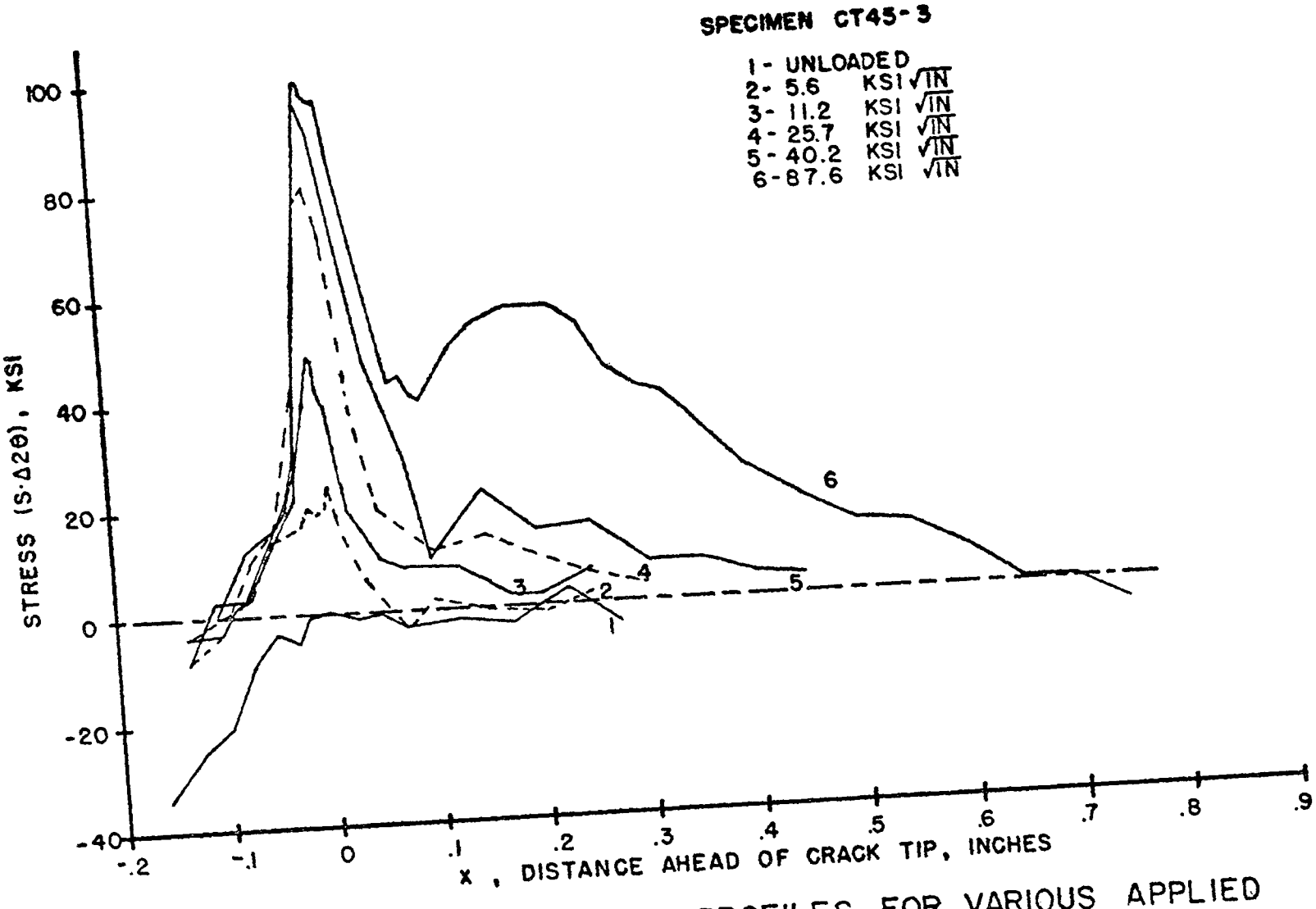


FIGURE 26: CRACK TIP STRESS PROFILES FOR VARIOUS APPLIED STRESS INTENSITY FACTORS

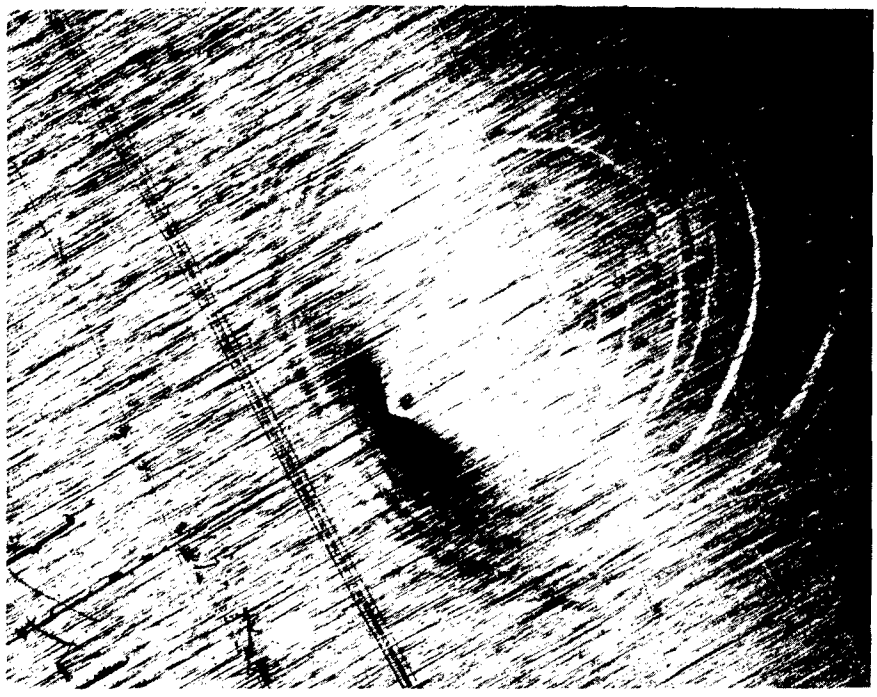

Figure 27. Post Overload Crack Tip Deformation Pattern (150X)

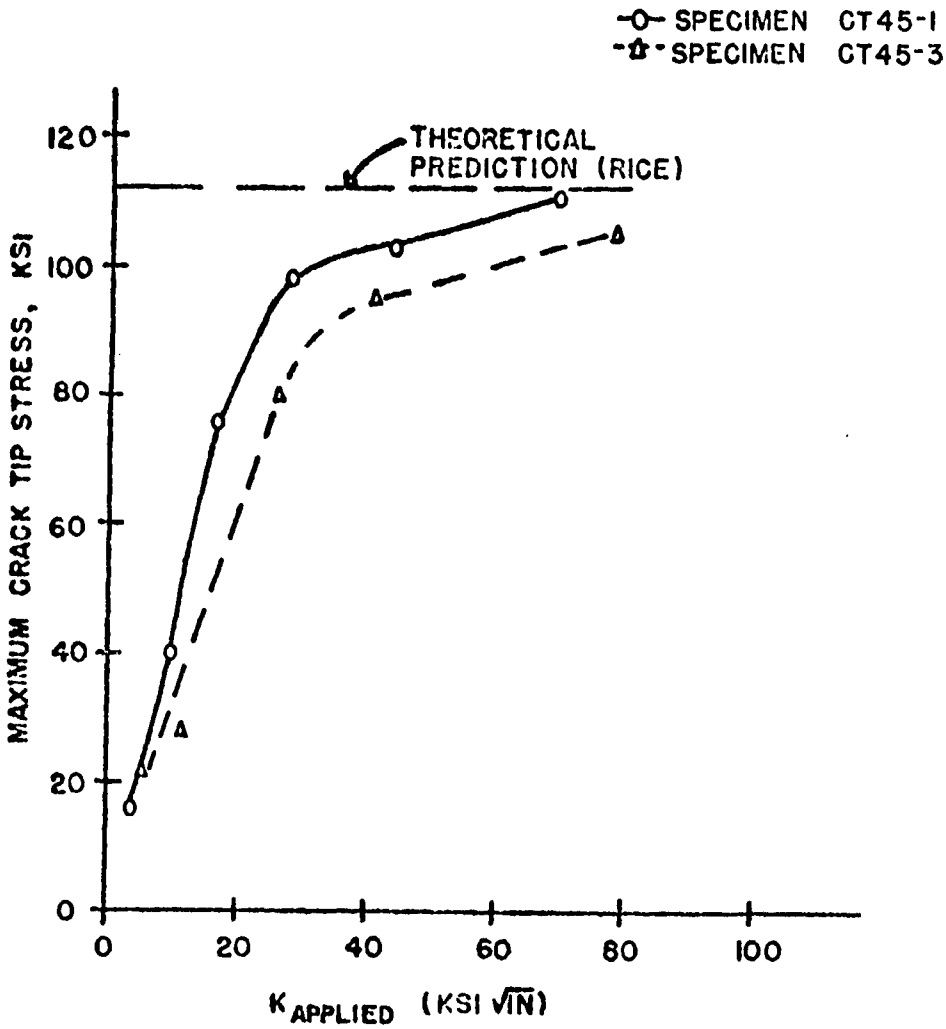


FIGURE 28: MAXIMUM MEASURED APPLIED STRESS VS. APPLIED STRESS INTENSITY

sharp contrast to theory which predicts a constant crack tip stress equal to the yield strength regardless of the level of applied stress intensity.

c. Crack Tip Stress Measurements Related to Crack Growth Retardation

An attempt was made to gain a qualitative understanding of the crack growth retardation phenomena by measuring crack tip stresses before and after an overload. Comparing figures 29 and 30, and 31 and 32, it can be seen that for both specimens the crack tip stresses subsequent to the overload are significantly reduced from those prior to the overload. For specimen CT45-1, which was subjected to an overload of 69.0 ksi $\sqrt{in}$, the difference between the maximum crack tip applied stress before (Figure 29) and after the overload (Figure 30) is close to the value of the post-overload maximum compressive stress, indicative of a simple superposition of the compressive residual stress on the pre-overload crack tip applied stress. It is significant to note that for the lower stress intensity of 16.4 ksi $\sqrt{in}$, the post overload applied stress distribution is compressive in nature. This implies that the crack tip is closed at this stress intensity level.

For specimen CT45-3, the baseline applied stress intensity of 40.2 ksi $\sqrt{in}$ induced a measureable compressive residual stress (Figure 31). After an 87.6 ksi $\sqrt{in}$ overload, the crack tip applied stress distribution was significantly reduced (Figure 32). However, the stress reduction could not be attributed to a simple superposition of the post-overload compressive crack tip residual stress on the pre-overload crack tip applied stress. It is interesting to note that if the pre-overload maximum residual stress is subtracted from the post-overload maximum

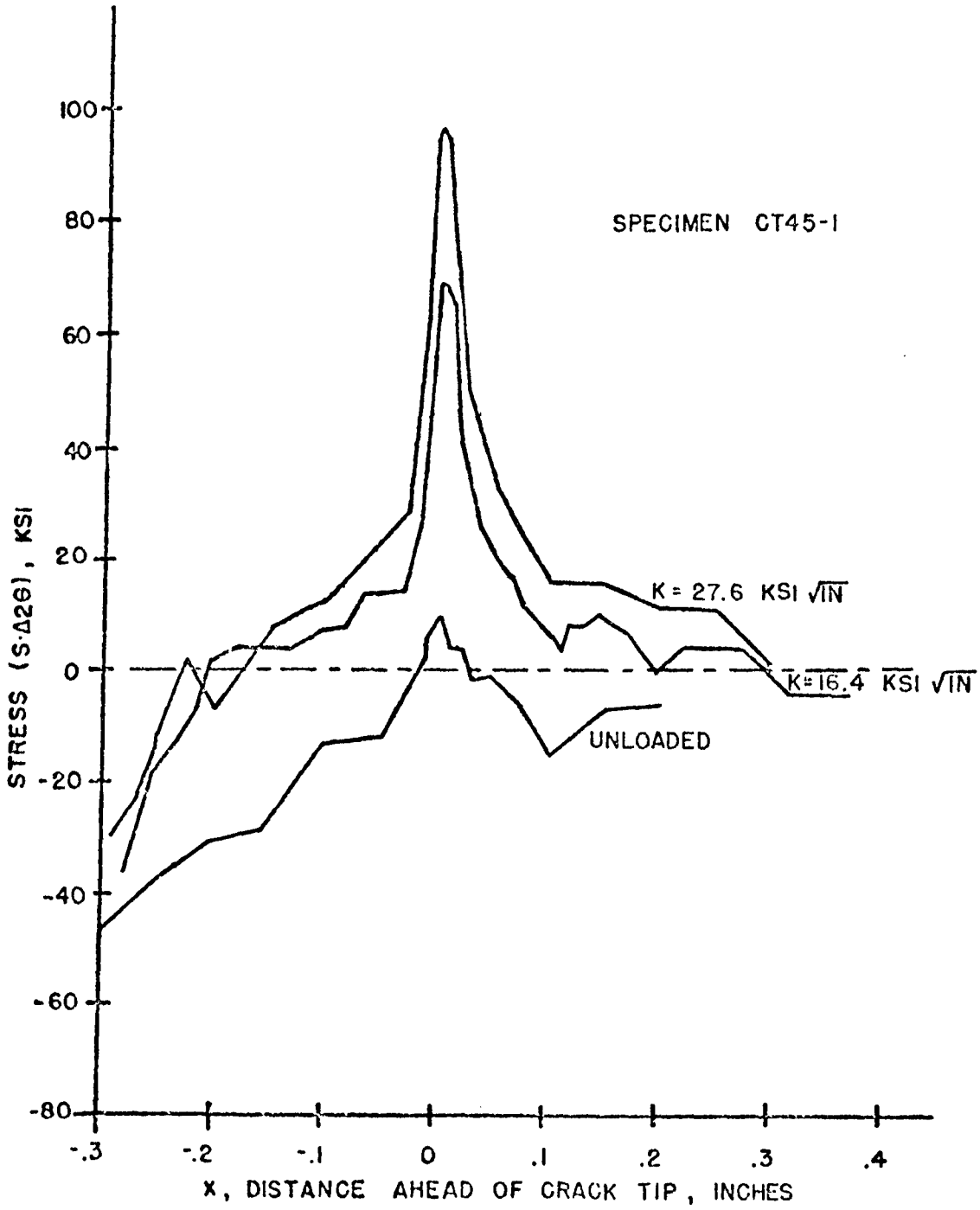


FIGURE 29. CRACK TIP STRESS PROFILES BEFORE OVERLOAD

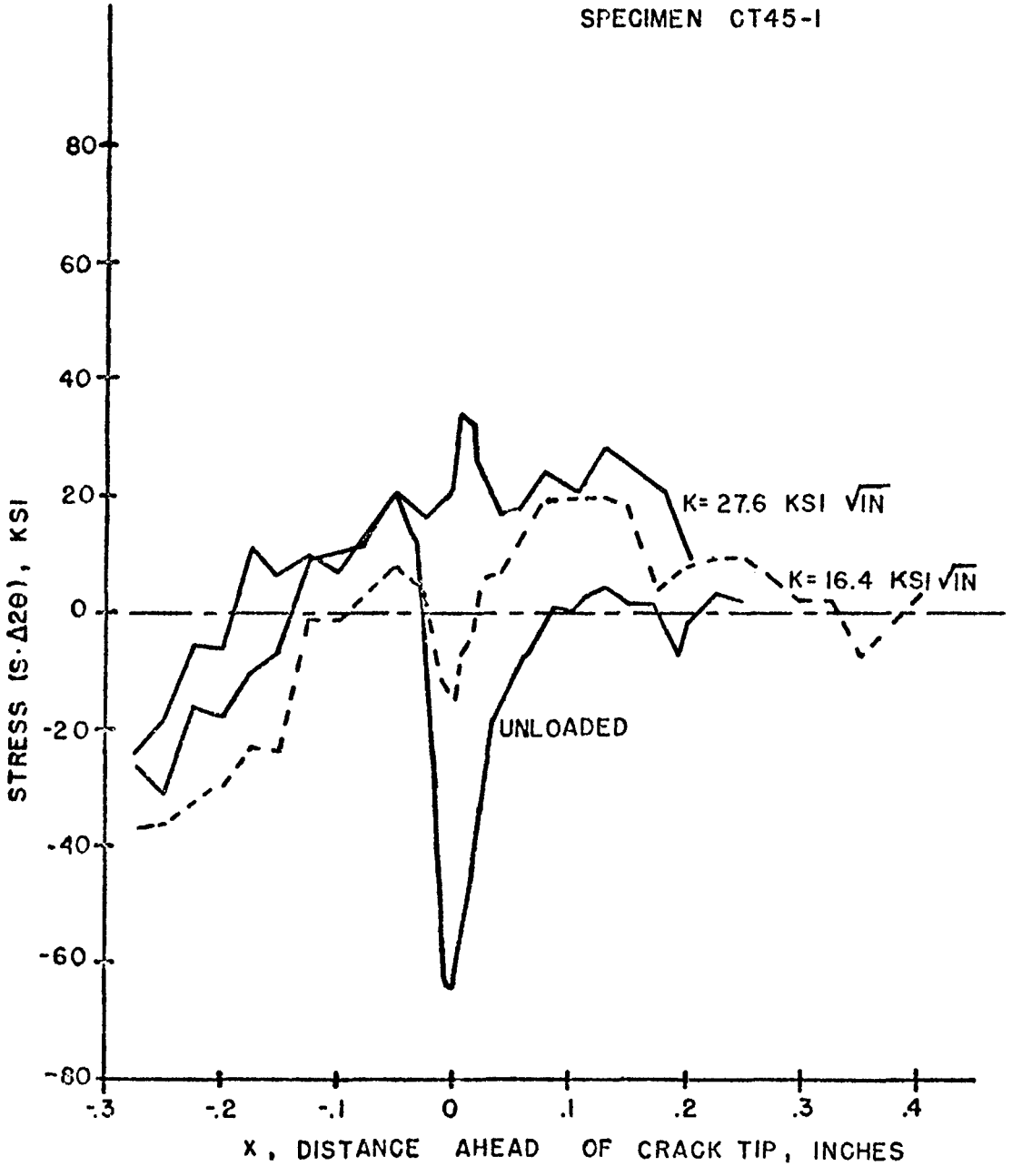


FIGURE 30: CRACK TIP STRESS PROFILES AFTER 69.0 KSI $\sqrt{IN}$ OVERLOAD

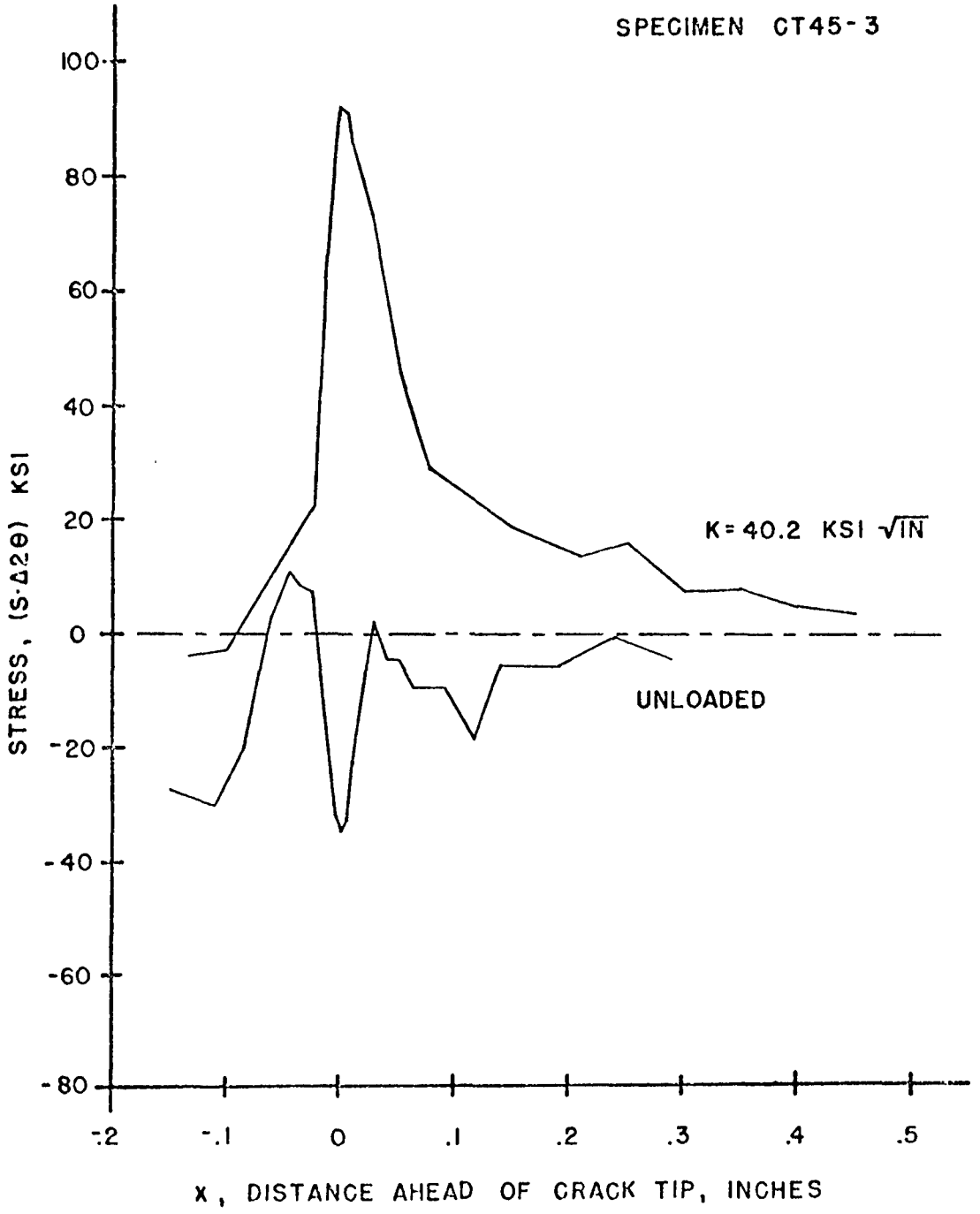


FIGURE 31: CRACK TIP STRESS PROFILES BEFORE OVERLOAD

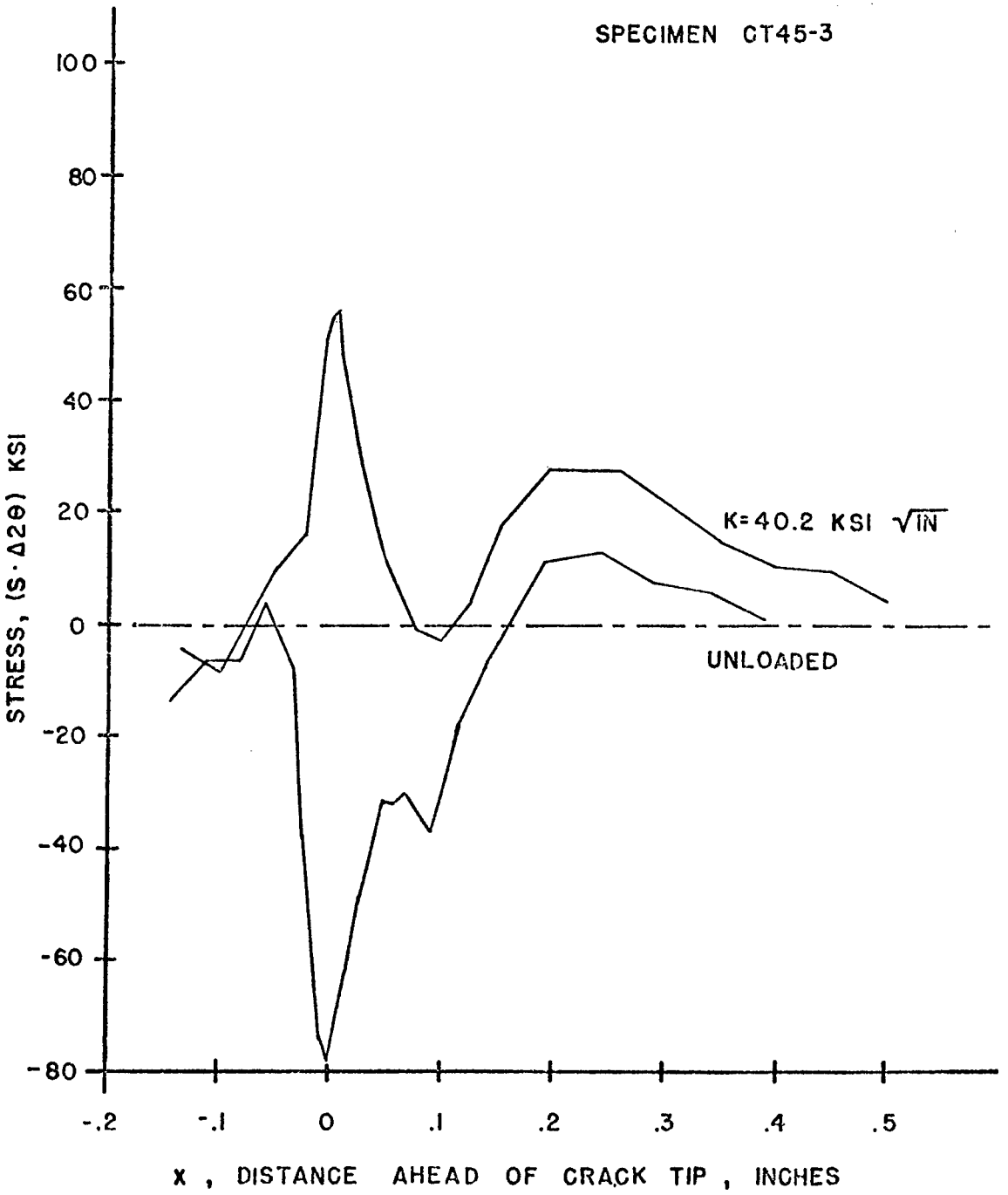


FIGURE 32: CRACK TIP STRESS PROFILES AFTER 87.6 KSI $\sqrt{IN}$

residual stress, the difference (-40 ksi) is very close to the reduction of the baseline crack tip applied stress.

Further insight into the retardation process was attempted by measuring crack tip stress profiles after the crack was propagated into the overload-affected region. Both specimens were cyclic loaded to extend the crack 0.041 inch into the overload-affected region. The specimens were loaded under constant stress amplitude conditions at a load ratio of 0.1. At a baseline stress intensity of 31.0 ksi $\sqrt{in}$* specimen CT45-1 took 5000 cycles to advance the crack 0.041 inch, while in specimen CT45-3 at a baseline stress intensity of 43.2 ksi $\sqrt{in}$, 26,000 cycles were required. After the crack was advanced into the overload-affected region, crack tip stress measurements were conducted. The results are shown in Figure 33 and Figure 34. Comparing the crack tip residual stress distribution with those measured prior to crack extension, it was observed that in specimen CT45-3 the crack tip residual stress profile was undisturbed by crack extension (Figure 34). The smaller compressive stress region in specimen CT45-1 showed a slight extension of the compressive stress profile at the tip of the extended crack (Figure 33). Upon application of a stress intensity close to the baseline stress intensity, the crack tip stress profiles in both specimens showed portions of the material behind the extended crack tip to be in compression, whereas the material immediately ahead of the crack tip was in tension.

---

*Because of an erroneous load cell calibration in the 10,000 pound load system used for x-ray diffraction measurements, the crack tip applied stress distributions were measured at loads slightly lower than those cyclic loads used to advance the crack in the 20,000 pound system. Thus, the crack tip applied stress measurements were made at a slightly lower stress intensity than the crack was subjected to in cyclic loading.

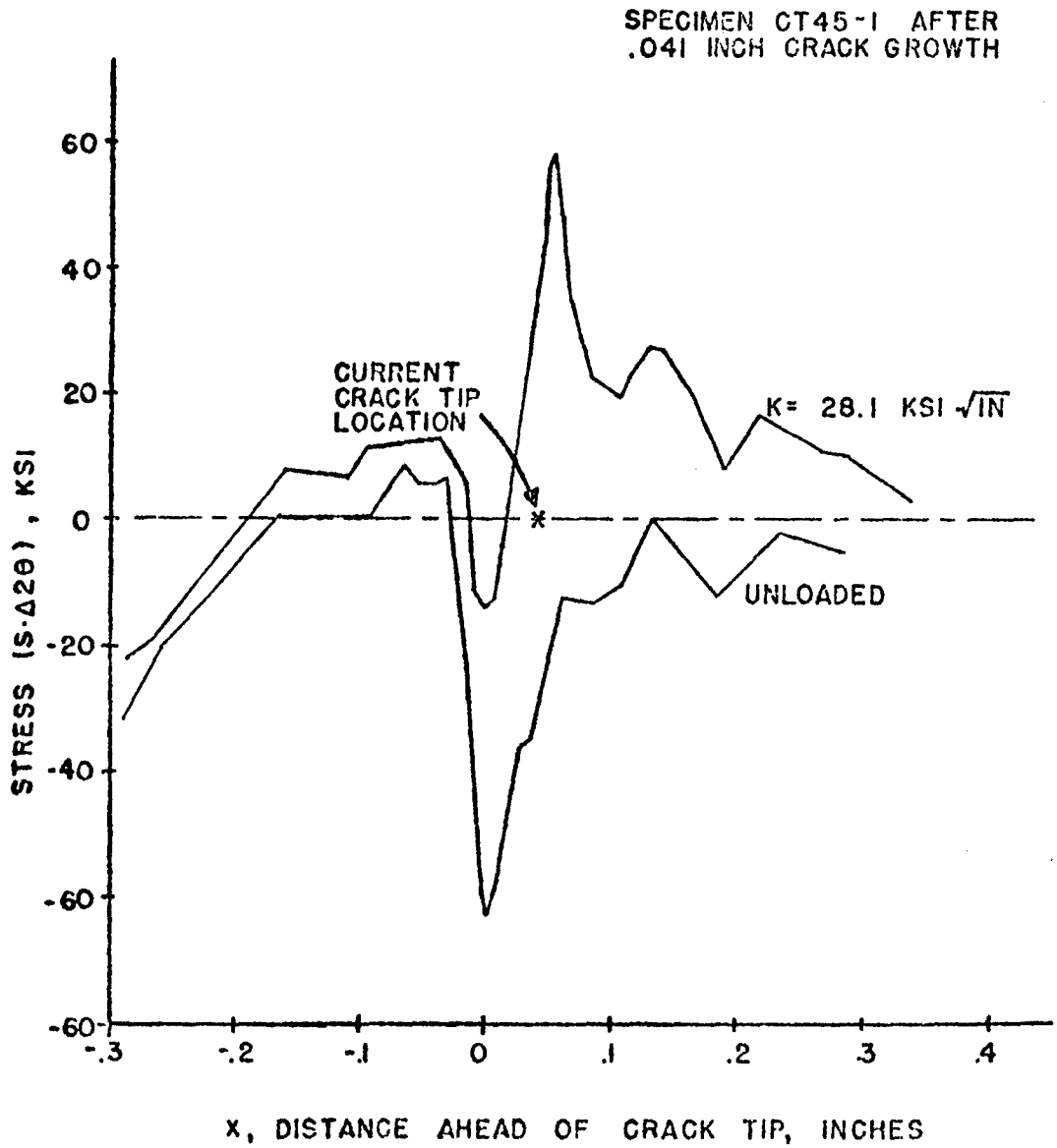


FIGURE 33. POST OVERLOAD STRESS PROFILES

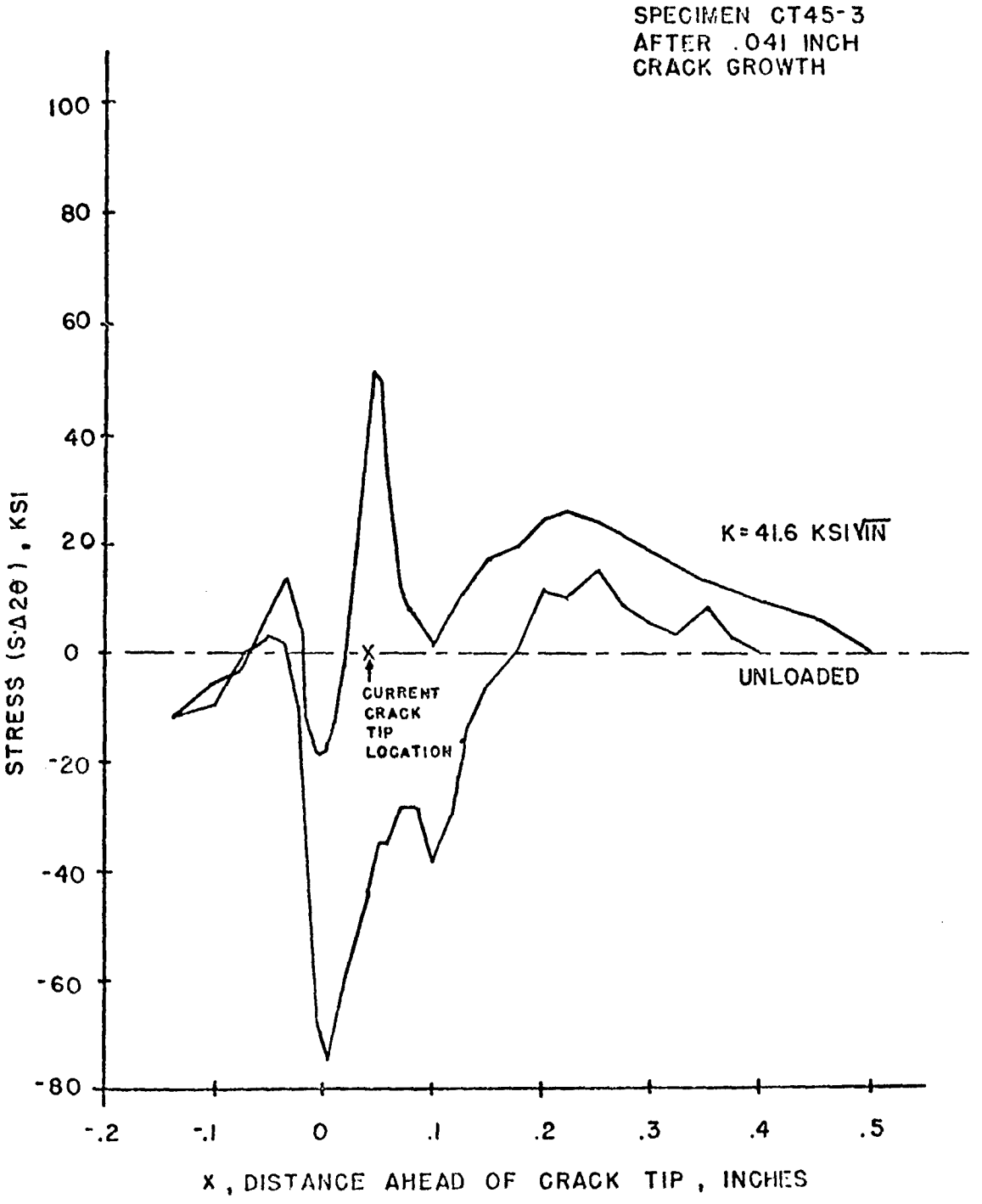


FIGURE 34: POST OVERLOAD CRACK TIP STRESS PROFILES

As in the case of the crack tip applied stress profiles measured immediately after an overload, stress measurements taken after crack extension showed the crack-tip-applied stress profiles to be significantly lower than the preoverload-crack-tip-applied stress profiles.

B. Discussion of Results

1. Feasibility, Repeatability, and Limitations of Measurements

As results throughout this investigation have demonstrated, x-ray diffraction is a viable technique for measuring sharp stress gradients such as those found at the tip of a fatigue crack. The limited number of investigators conducting crack tip stress measurements[11-13], have not reported detailed studies such as those conducted during the course of this investigation. While the feasibility of the measurement concept has been shown by these investigators, at the outset of this investigation it was not certain that these measurements would be possible with the semi-automatic x-ray diffraction equipment available. This study has shown that this device is, in fact, capable of making crack tip stress measurements to a high degree of precision and within a reasonable length of time.

These measurements were also shown to be very repeatable. In general, the accuracy of this semi-automatic x-ray diffraction device is reported to be $\pm$10 ksi for plain carbon steels[61-62]. However, this is more of an estimate of the accuracy of an absolute measurement, from one investigator to another, from one x-ray diffraction unit to another. For the equipment used for this study, the measurement accuracy from day-to-day and from specimen-to-specimen was approximately $\pm$2 ksi. Examples of the repeatability of these measurements are presented in Appendix III, along with other experimental data. Great care is required,

however, to ensure that stress measurements of this type are not affected by improper experimental procedures. A material was selected which was ideally suited to the x-ray diffraction instrument available to this investigation, both in terms of diffraction planes available and in terms of the ratio of grain size to x-ray beam size. Previous work[63] has shown that for these low carbon steels, the stress factor, S, exhibited a linear dependence on the term, $\sin^2\psi$, from equation 15. Thus, the stress could be calculated directly from equation 14. "Anamolous" residual stresses have been measured by x-ray diffraction after a specimen was subjected to uniaxial plastic deformation[e.g. 66]. Whether this is a consideration has not been completely resolved for the case of crack tip residual stresses. Experimentation in an alloy similar to those used in this study has shown that the residual stress profiles at fastener holes subject to local, constrained plastic deformation are in at least qualitative agreement with theory[70]. Additionally, in this investigation a uniaxial calibration test run was taken past the yield point. The resulting residual stress was tensile rather than compressive, the inference being that any anamolies in the crack tip residual stress profiles would be tensile in nature. As no tensile residual stresses were observed, this is not believed to be a problem.

Another factor which could affect these results is the averaging effect due to the finite x-ray beam size. Because of equipment and grain size constraints, a 0.025 inch diameter spot was selected. In the presence of a steep stress gradient this might tend to obscure sharp stress spikes. In general, a beam size effect could not account for the lack of correlation between theory and the data generated in this investigation. In the case of crack tip applied stresses, for stress intensities

above 30 ksi $\sqrt{in.}$ a plastic zone greater than 0.025 inch is predicted by equation 4 ($\alpha = 1/\pi$). In Figure 28, an inflection was observed at about 30 ksi $\sqrt{in.}$ which might be explained by this beam size effect. For stress intensities above 30 ksi $\sqrt{in.}$, no stress plateau region (plastic zone) was observed, even for predicted plastic zone of up to 0.120 inch. As concerns the crack tip residual stress measurements, plastic zones greater than 0.025 inch are predicted for overload stress intensities greater than 62 ksi $\sqrt{in.}$ In Figure 22, no inflection points are seen, nor do data for overloads greater than 62 ksi $\sqrt{in.}$ reveal a stress plateau. It was, therefore, reasoned that the beam size effect, if present, did not obscure the basic features of the crack tip stress profiles.

2. Measurement versus Theory

The results of this investigation indicate a marked deviation between the measured crack tip stresses and those predicted by theory[1]. This deviation primarily takes the form of a measured dependence of the maximum crack tip stress on either the applied stress intensity (Figure 28) or the overload stress intensity (Figure 22). The information in Figure 22 has been normalized with respect to yield strength and replotted in Figure 35. Data for both 1045 steel and 1020 steel are shown as are predictions by conventional analysis (equation 4) and finite element analysis[10]. For the results published, the finite element technique predicts a limited dependence of maximum residual stress on the overload stress intensity; however, this predicted dependence is far short of the trend observed in this thesis. Conventional analysis predicts that the maximum crack tip residual stress will always equal the material yield strength regardless of the overload stress intensity factor. In contrast to these theoretical predictions, the data from this study shows a pronounced dependence on the overload stress intensity. A similar dependence was observed for crack-tip-applied stresses on the applied stress

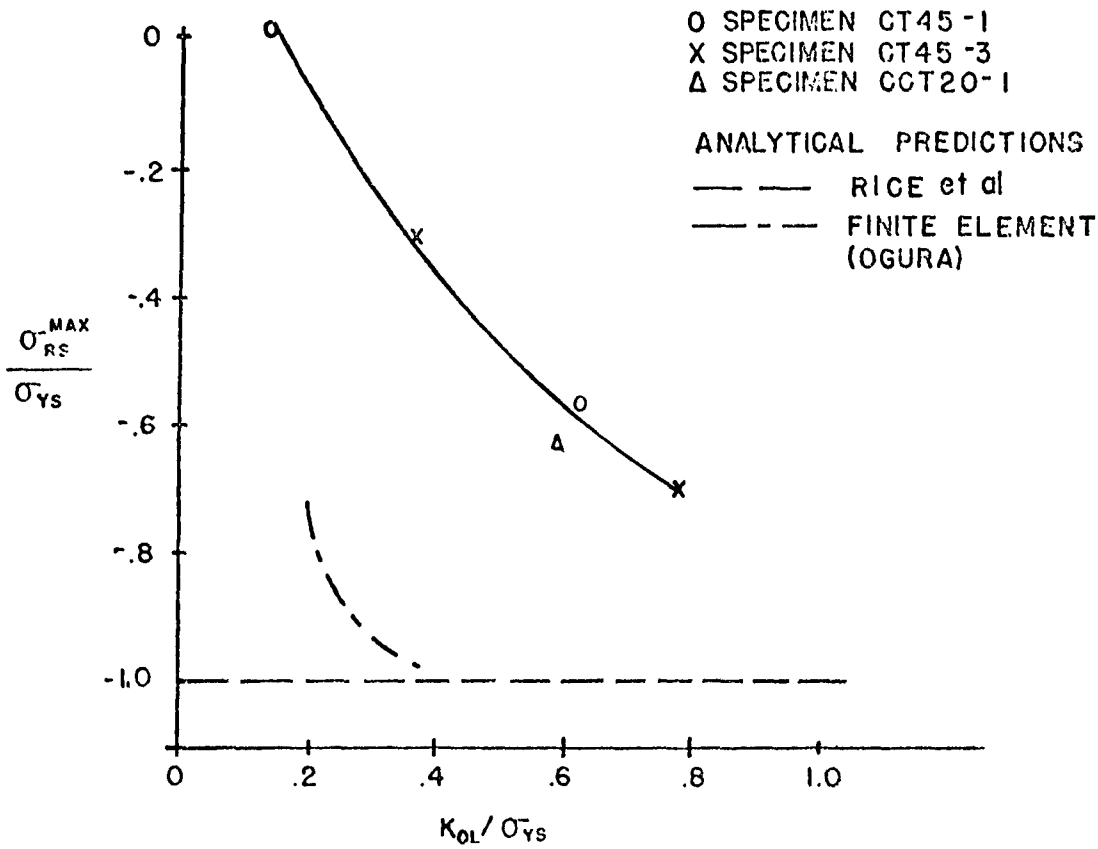


FIGURE 35: COMPARISON OF MAXIMUM MEASURED RESIDUAL STRESS TO ANALYSIS

intensity. This again is in sharp contrast to theory, which predicts an independence of the maximum crack tip applied stress on the applied stress intensity.

The results of this investigation are in general agreement with the observations of the three other crack tip stress measurement investigations[11-13]. All three investigations measured crack tip residual stress profiles and found them to be appreciably lower in value than theoretical estimates by equation 4. One investigator[13] also reported measuring crack-tip-applied stress profiles. These results were in qualitative agreement with the results of this study. These three studies were limited and only one overload or applied stress intensity was reported for each investigation.

Figure 36 is a plot of the cross-over point versus the overload stress intensity normalized with respect to yield strength. Shown in this plot are four different analytical predictions for the extent of the compressive residual stress region. There are variations of equation 5 after Dugdale ($\alpha = \pi/8$), Rice ($\alpha = 1/\pi$), and Irwin ($\alpha = 1/2\pi$). A very good correlation is observed between data from this study and the prediction by the Dugdale model. This cross-over point is of importance when considering crack growth retardation phenomenon in that, for a pure crack tip residual stress load-interaction model, this cross-over point should denote the point at which the crack growth rate returns to its steady state value[8].

The importance of the assumed crack tip stress profile was discussed in Section 2 of this report. A knowledge of this stress profile is important for a general understanding of crack tip deformation processes. Additionally, it is important for use in currently used

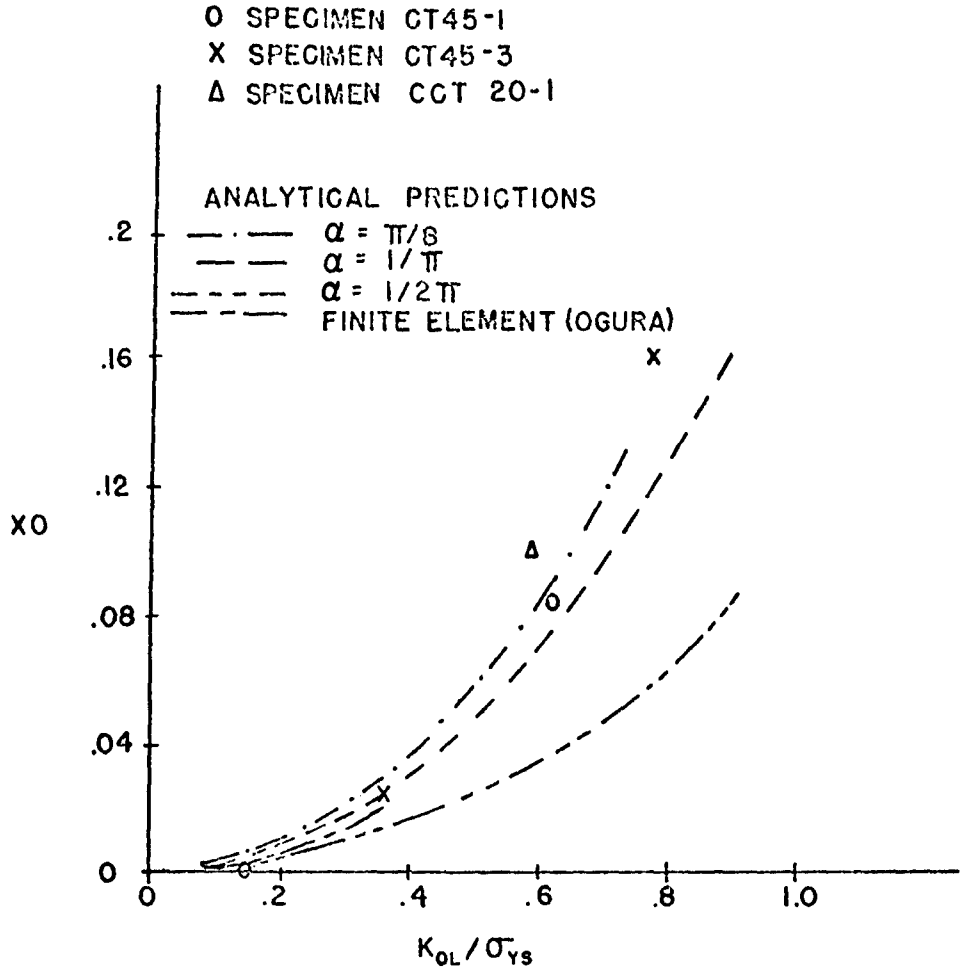


FIGURE 36 COMPARISON OF MEASURED CROSS OVER POINT TO ANALYSIS

load-interaction models. In these models, the plastic zone size and the crack tip residual stress profile can be major variables. This report is by no means criticizing the complex theoretical developments required to arrive at the current plastic zone models. However, because of the widespread use of these plastic zone models, it is suggested that further studies should be pursued to determine the source of the deviations between this study's findings and these theoretical models.

3. Observations Related to Crack Growth Retardation

After the application of an overload, the crack-tip-applied stress was observed to be significantly reduced. This reduction in stress is presumably due to the superposition of the high compressive stresses caused by the overload. For the case shown in Figure 30, at a stress intensity of 16.4 ksi $\sqrt{in}$, the diminished stress is compressive. When considering a crack tip residual stress retardation model, cycling at this baseline stress intensity would be predicted to cause no crack extension. Additionally, in considering a crack closure model, the crack might be assumed to be closed. All other crack-tip-applied stresses were tensile, although reduced significantly from their preoverload values. For baseline cycling at these stress intensities, varying amounts of retardation would be predicted. In specimen CT45-1, the crack tip stress reduction can be accounted for by a simple superposition of the compressive residual stresses and the preoverload crack tip stresses. In specimen CT45-3, it was necessary to take into account the residual stress profile prior to the overload before the superposition principal could be used to calculate the stress reduction. These observations lend credence to a retardation model based on crack tip residual stresses. In such a model the diminished stress would be calculated and related to an effective

stress intensity from a graph such as Figure 28. A crack tip residual stress mechanism for retardation could be inferred from observations by several investigators. These investigators have noted reduced retardation due to the application of a compressive spike after the overload spike or due to careful annealing after the application of an overload. Both of these observations could be attributed to the relaxation of the high compressive residual stresses formed by the overload.

Crack extension prior to the application of an overload was observed to have little or no effect on the crack tip residual stress profile. This is in constrast to results from shot-peened samples in which the surface residual stress was dissipated as cyclic loading continued[74]. Perhaps because the deformed region is constrained by the surrounding elastic matrix, dissipation of the residual stress is not possible. Upon application of a load causing a stress intensity nearly equal to the baseline stress intensity, it is observed that immediately behind the extended crack tip the material remained in compression, whereas, at the tip of the extended crack tensile stresses were apparent. In both cases the crack had extended beyond the maximum compressive stress region and into an area of lower compressive stress. The stress diminution could not be attributed to a superposition of the lower compressive stress. It can be seen that in specimen CT45-3 the maximum crack tip stress is equal to or slightly lower than the original post overload crack tip stress. This may be a basis for the delayed retardation process. These results are supportive of a closure model in which as the crack advances through the compressive stress region, it is clamped shut by these residual stresses. These results also explain the dependence of crack opening load measurements on their location behind the crack tip[51,55] in that, if a crack opening measurement device is at the

point of maximum compression it will measure a maximum opening stress, while other locations along the crack would tend to open at lower applied stresses.

# V. SUMMARY AND RECOMMENDATIONS

## A. Summary

To reliably predict the growth behavior of fatigue cracks subjected to typical cyclic stresses, of importance in ensuring the structural integrity of present day structures, a thorough knowledge of fatigue crack deformation processes is required. This report was directed toward adding to the ever-growing body of knowledge of crack tip phenomenon by experimentally studying crack tip stresses. The objectives of this investigation were to (1) determine the feasibility of using a semi-automatic x-ray diffraction stress analysis device for measuring crack tip stresses and (2) use this x-ray diffraction technique to study some of the variables affecting crack tip stresses with special regard to the fatigue crack growth retardation phenomenon.

A survey of the literature was conducted to acquire an understanding of the crack tip stress field, fatigue crack growth retardation and the models available for predicting the retardation behavior. From this survey, it was determined that two primary physical explanations exist for the retardation phenomenon, crack tip compressive residual stresses and crack closure. It was determined that three basic load-interaction models exist for predicting crack growth retardation effects: an empirical model, a residual stress intensity model and a crack closure model. None of these models completely describes all the retardation effects which have been experimentally observed; however, when applied by experienced

users, they predict crack growth lives with a scatter band of $\pm 2$ to $\pm 3$.

A second literature survey was conducted to explore the feasibility of using x-ray diffraction techniques for measuring crack tip stresses. In addition to acquiring a basic knowledge of stress analysis by x-ray diffraction, it was determined that three limited investigations had preceded this study and had succeeded in measuring crack tip stresses.

For the experimentation conducted in this investigation, a semi-automatic x-ray diffraction device was used to measure crack tip stress distributions. This device measures stresses on the surface of a crystalline object much more rapidly than the standard x-ray diffraction techniques used in previous studies. Crack tip stress distributions were measured in precracked specimens of 1020 and 1045 steel. The results were compared with current theoretical models for crack tip stress fields. The results were also considered with respect to their physical significance for use in modeling the fatigue crack growth retardation process. The main conclusions of this investigation are, for the alloys tested and within the limitations of x-ray stress analysis:

(1) Crack tip stresses can be effectively and efficiently measured by semi-automatic x-ray diffraction techniques.

(2) Crack tip residual stress distributions were measured after a tensile load (overload) had been applied. The maximum crack tip residual stress was observed to be dependent on the level of the overload stress intensity.

(3) The cross-over point at which the crack tip residual stress profile changed from compression to tension was in good agreement with the Dugdale crack tip plastic zone model.

(4) Crack tip "applied" stress distributions were measured while the specimens were under remotely applied loads. The maximum crack tip "applied" stress was observed to be dependent on the level of the applied stress intensity.

(5) Qualitatively, the crack tip stress distributions measured in this investigation are in agreement with current crack tip stress models. In a quantitative sense, however, the measured stress distributions differ significantly from theoretical predictions.

(6) It was observed that crack tip "applied" stress distributions were greatly reduced after an overload was applied. This observation is supportive of a crack tip residual stress model for crack growth retardation.

(7) It was observed that crack growth subsequent to an overload had little or no effect on the overload induced compressive residual stresses. It was further observed that upon loading, the material behind the extended crack remained in compression while the tip of the extended crack produced tensile stresses. These tensile stresses were significantly reduced compared to preoverload conditions. This observation supports both a crack closure retardation model and a residual stress model.

## B. Recommendations

The following are offered as recommended areas for further research.

1. Two questions arose in this investigation concerning the meaning of the x-ray diffraction stress measurements. The first involved the averaging effect caused when measuring a steep stress gradient with a finite sized x-ray beam. Although the discussion points to why it was not considered a serious factor in this study, work should be undertaken

to verify this conclusion. The use of very small x-ray beam diameters and extremely fine grain sizes is suggested. A second area of concern is the "anamolous" residual stresses observed by many investigators after specimens have been uniaxially plastically deformed. The mechanism for this effect is only speculated at in these previous works. It was not considered a significant factor in this study, however, that assumption was not conclusively proven. A high magnification (SEM/TEM) investigation coupled with a careful x-ray diffraction study is suggested to reveal the nature of these "anamolous" residual stresses.

2. This work revealed substantial differences between the measured crack tip stress distributions and those predicted by theory. As this work was by no means definitive, it is suggested that this deviation receive additional attention. This is especially important in view of the fact that the theories describing the crack tip stress distribution are widely used in fatigue crack growth retardation prediction. It is also suggested that a specimen such as the center-cracked tension specimen be used. This type specimen is not affected by the geometry-related problems which can be experienced in the compact specimen.

3. Crack tip stress analysis by x-ray diffraction should be further exploited for its usefulness in observing the load-interaction process. Many retardation-related observations could be studied, a few of which are: a detailed study of the crack tip residual and "applied" stress distribution as a crack advances into the overload-affected zone; the effect of compressive loads on crack tip stress distributions; the effect of multiple overload cycles and load ratio effects.

4. The x-ray diffraction device used in this study limited the

range of materials and was somewhat tedious in application. Recent developments in x-ray detection[64] and computerization of data analysis should be combined to develop an efficient x-ray diffraction stress analyzer for a wide variety of metals. Such a device could be used to measure crack tip stress distributions in other alloys, such as aluminums and austenitic steels.

## REFERENCES


1. D. Broek, Elementary Engineering Fracture Mechanics, Noordhoff International Publishing, Leyden, 1974.

2. P.C. Paris, M.P. Gomez, and W.E. Anderson, "A Rational Analytical Theory of Fatigue," The Trend in Engineering, 13 (1961), pp 9-14.

3. W.J. Plumbridge, "Review: Fatigue Crack Propagation in Metallic and Polymeric Materials," Journal of Material Science, 7(1972), pp 939-962.

4. K.M. Lal and S.B.L. Garg, "On the Evaluation of Monotonic and Cyclic Plastic Zones," Engineering Fracture Mechanics, 9 (1974) pp 433-442.

5. J.R. Rice and G.F. Rosengren, "Plane Strain Deformation Near a Crack Tip in a Power Law Hardening Material," J. Mech. Phys. Solids, 16 (1968), pp 1-12.

6. D.S. Dugdale, "Yielding of Steel Sheets Containing Slits," J. Mech. Phys. Solids, 8 (1960) pp 100-108.

7. J.R. Rice, "Mechanics of Crack Tip Deformation," Fatigue Crack Propagation, ASTM 415, Am. Soc. for Testing and Materials, 1967, pp 247-309.

8. S. Matsuoka and K. Tanaka, "The Retardation Phenomenon of Fatigue Crack Growth in HT80 Steel," Engineering Fracture Mechanics, 8 (1976), pp 507-523.

9. J.C. Newman, "A Finite Element Analysis of Fatigue Crack Closure," Mechanics of Crack Growth, ASTM STP 590, American Soc. for Testing and Materials, 1976, pp 281-301.

10. K. Ogura and K. Ohji, "FEM Analysis of Crack Closure and Delay Effects in FCG under Variable Amplitude Loading," Engr'g Frac. Mech., 9 (1977), pp 471-480.

11. S. Taira and K. Tanaka, "Study of FCP by X-Ray Diffraction Approach," Engr'g Frac. Mech., 4 (1972), pp 925-938.

12. W.P. Evans, unpublished, Minutes of Meeting of the X-Ray Fatigue Division of the Society of Automotive Engineers Fatigue Design and Evaluation Committee, University of Iowa, Iowa City, Iowa, SAE, September 1973.

13. E. Macherauch and U. Wolfstieg, "Recent German Activities in the Field of X-Ray Analysis," Materials Science and Engineering, 30 (1977) pp 1-13. (also in Z. Metallkde., 65 (1974) pp 496-500).

14. G.T. Hahn and A.R. Rosenfield, "Local Yielding and Extension of a Crack under Plane Stress," Acta. Met., 13 (1965), pp 293-306.

15. G.T. Hahn, R.G. Hoagland and A.R. Rosenfield, "Local Yielding Attending FCG," Met. Trans, 3 (1972), pp 1189-1202.

16. G.T. Hahn, M. Sarrate and A.R. Rosenfield, "Experiments on the Nature of the Fatigue Crack Plastic Zone," AFFDL-TR-70-144, Air Force Flight Dynamics Laboratory, Wright-Patterson AFB, OH, June 1970, p 425.

17. G. Chanani, Fundamental Investigation of FCG Retardation in Aluminum Alloys, AFML-TR-76-156, Air Force Materials Laboratory, Wright-Patterson AFB, OH, September 1976.

18. C. Bathias and R.M. Pelloux, "FCP in Martensitic and Austenitic Steels," Met. Trans., 4 (1973), pp 1265-1273.

19. S. Ikeda, Y. Izumi and M. Fine, "Plastic Work During FCP in a High Strength Low Alloy Steel and in 7075 Aluminum Alloys," Engr'g Frac. Mech., 9 (1977), pp 123-136.

20. J. Lankford and D.L. Davidson, "Fatigue Crack Plasticity Associated with Overloads and Subsequent Cycling," Trans. ASME, Series H., January 1976, pp 17-23.

21. D.L. Davidson and J. Lankford, "Plastic Strain Distribution at the Tips of Propagating Fatigue Cracks," Trans ASME, Series H., Jan 76, pp 24-29.

22. R.H. Christiansen, "Fatigue Cracking, Fatigue Damage and Their Detection," Metal Fatigue, Ed. by G. Sines and J.L. Waisman, McGraw-Hill, New York, 1959, pp 376-412.

23. J. Schijve, "FCP in Light Alloy Sheet Materials and Structures," Advances in Aeronautical Sciences, Vol 3, Proc. of the 2nd I.C.A.S. Congress, Zurich, Pergammon Press, 1960, p 387.

24. C.M. Hudson and H.F. Hardrath, Effects of Changing Stress Amplitude on the Rate of FCP in Two Aluminum Alloys, NASA-TN-D-960, National Aeronautics and Space Administration, September 1961.

25. J. Schijve and D. Broek, "The Results of a Test Programme Based on Gust Spectrum with Variable Amplitude Loading," Aircraft Engineering, 34 (1962), pp 314-316.

26. G.H. Jacoby, H. Nowack, H.T.M. Vau Lipzig, "Experimental Results and a Hypothesis for FCP under Variable-Amplitude Loading," Fatigue Crack Growth Under Spectrum Loads, ASTM STP 595, Am. Soc. for Testing and Materials, 1976, pp 172-183.

27. J.P. Gallagher and T.F. Hughes, Influence of Yield Strength on Overload Affected Fatigue Crack Growth Behavior in 4340 Steel, AFFDL-TR-74-27, Air Force Flight Dynamics Laboratory, July 1974.

28. W.J. Mills and R.W. Hertzberg, "Load Interaction Effects on FCP in 2024-T3 Aluminum Alloys," Engr'g Frac. Mech., 8 (1976) pp 657-667.

29. D.M. Corbly and P.F. Packman, "On the Influence of Single and Multiple Peak Overloads on FCP in 7075-T6511 Aluminum," Engr'g Frac. Mech., 5 (1973), pp 479-497.

30. W.X. Alzos, A.C. Skat, and B.M. Hillberry, "Effect of Single Overload/ Underload Cycles on FCP," Fatigue Crack Growth Under Spectrum Loads, ASTM STP 595, American Soc.for Testing and Materials, 1976, pp 41-60.

31. T.D. Gray, Fatigue Crack Retardation Following a Single Overload, AFFDL-TM-73-137 FBR, Air Force Flight Dynamics Laboratory, October 1973.

32. R.C. Rice and R.I. Stephens, "Overload Effects on Subcritical Crack Growth in Austenitic Manganese Steel," Flaw Growth and Fracture Toughness Testing, ASTM STP 536, Am. Soc. for Testing and Materials, 1973, pp 95-114.

33. O. Jonas and R.P. Wei, "An Exploratory Study of Delay in FCG" Int. J. Frac. Mech., 7 (1971) pp 116-118.

34. T.T. Shih and R.P. Wei, "Influences of Chemical and Thermal Environments on Delay in a Ti-6Al-4V Alloy," Fatigue Crack Growth Under Spectrum Loads, ASTM STP 595, Am. Soc.for Testing and Mat'ls, 1976 pp 113-124.

35. W.M. McGee and T.M. Hsu, Effects of Underloads on FCG, Vol I, AFFDL-TR-77-2, Vol I, Air Force Flight Dynamics Laboratory, Mar 77.

36. G.J. Petrak, "Strength Level Effects on FCG and Retardation," Engr'g Frac. Mech., 6 (1974), pp 725-733.

37. P.J. Bernard, T.C. Lindley and C.E. Richards, "Mechanisms of Overload Retardation during FCP," Fatigue Crack Growth under Spectrum Loads, ASTM STP 595, Am. Soc. for Testing and Materials, pp 78-96.

38. C.M. Hudson and K.N. Raju, Investigation of FCG under Simple Variable Amplitude Loading, NASA-TN-D-5702, National Aeronautics and Space Administration, March 1970.

39. V.W. Trebules, R. Roberts, and R.W. Hertzberg, "Effect of Multiple Overloads on FCP in 2024-T3 Aluminum Alloy," Flaw Growth and Fracture Toughness Testing, ASTM STP 536, Am. Soc. for Testing and Materials, 1973, p 115.

40. K.N. Raju, V. Ningiah, B.V.S. Rao, "Effect of Exposure to Elevated Temperature on Delay on Crack Growth Due to a High Stress Cycle," Int. J. of Frac. Mech., 8 (1972), p 99.

41. D.M. Macha, "FCG Retardation Behavior of IN-100 at Elevated Temperatures," 1977 SESA Spring Meeting, Dallas, TX, Soc. of Exp. Stress Analysis, May 1977.

42. E.F.J. Von Euw, R.W. Hertzberg, R. Roberts, "Delay Effects in FCP," Stress Analysis and Growth of Cracks, ASTM STP 513, Am. Soc. for Testing and Materials, 1972, pp 230-259.

43. W.N. Sharpe, D.M. Corbly and A.F. Grandt, Jr., "Effects of Rest Time on Fatigue Crack Retardation and Observations of Crack Closure," Fatigue Crack Growth Under Spectrum Loads, ASTM STP 595, Am. Soc. for Testing and Mat'ls, 1976, pp 41-60.

44. T.D. Gray and J.P. Gallagher, "Fatigue Crack Retardation following a Single Overload Using a Modified Wheeler Model," Mechanics of Crack Growth, ASTM STP 590, Am. Soc. for Testing and Materials, 1976, pp 331-344.

45. J.P. Gallagher and R.M. Engle, Jr., "Advances in Modeling Variable Amplitude Fatigue Crack Growth Behavior, Recent Advances in Engr'g Science, Proceedings of the Society of Engineering Science, Inc., November 1976, pp 433-438.

46. O.E. Wheeler, "Spectrum Loading and Crack Growth," Trans ASME Journal of Basic Engineering (D), 94 (1972), p 181.

47. J.D. Willenborg, R.M. Engle, Jr., and H.A. Wood, A Crack Growth Retardation Model Using an Effective Stress Concept, AFFDL-TM-71-1 FBR, Air Force Flight Dynamics Laboratory, January 1971.

48. R.M. Engle and J.L. Rudd, "Analysis of Crack Propagation under Variable Amplitude Loading using the Willenborg Retardation Model," AIAA/ASME/SAE 15th Structures, Structural Dynamics and Materials Conference, Las Vegas, Nevada, April 17-19 1974.

49. J.P. Gallagher, A Generalized Development of Yield Zone Models, AFFDL-TM-74-28-FBR, Air Force Flight Dynamics Laboratory, Jan 74.

50. W. Elber, "The Significance of Fatigue Crack Closure," Damage Tolerance in Aircraft Structures, ASTM STP 486, Am. Soc. for Testing and Materials, 1971, pp 230-242.

51. J.E. Rueping and B.M. Hillberry, Fatigue Crack Closure Behavior: A Comparative Study, AFOSR-TR-76-1090, Air Force Office of Scientific Research, Aug 1976.

52. O. Buck, J.D. Frandsen and H.L. Marcus, "Spike Overload and Humidity Effects on Fatigue Crack Delay in Al 7075-T651, Fatigue Crack Growth under Spectrum Loads, ASTM STP 595, Am. Soc. for Testing and Mat'ls, 1976, pp 101-111.

53. T.T. Shih and R.P. Wei, "A Study of Crack Closure in Fatigue," Engr'g Frac. Mech., 6 (1974), pp 19-32.

54. P.D. Bell and A. Wolfman, "Mathematical Modeling of Crack Growth Interaction Effects," Fatigue Crack Growth under Spectrum Loads, ASTM STP 595, Am. Soc. for Testing and Materials, 1976, pp 157-171.

55. V.E. Kearney, Crack Retardation Studies with Crack Arrest Experiments, M.S. Thesis, The Ohio State University, Columbus, OH, 1972.

56. D.M. Forney, Proceedings of a workshop on NDE of Residual Stress, Air Force Materials Lab, San Antonio, TX, Aug 1975.

57. G.A. Alers, "Ultrasonic Methods - Overview," Ibid, pp 155-162.

58. P.S. Prevey, "X-ray Diffraction Residual Stress Measurement on Machined Surfaces," Ibid, pp 62-72.

59. S.L. Cole, The Effect of Mean Stress and R Ratio on the Fatigue Behavior of Turbine Alloys, M.S. Thesis, University of Missouri, Columbis, MO, May 1976.

60. B.D. Cullity, Elements of X-Ray Diffraction, Addison-Wesley Publishing Co., Inc., Reading, Mass., 1967.

61. E.W. Weinman, J.E. Hunter, and D.D. McCormack, "Determining Residual Stresses Rapidly," Metal Progress, 96 (1969), pp 88-90.

62. M.E. Hilley, ed., Residual Stress Measurement by X-Ray Diffraction, SAE J784a, Soc. of Automotive Engrs, 1971.

63. E. Macherauch, "Lattice Strain Measurements on Deformed FCC Metals," Adv. in X-Ray Analysis, 9 (1965), pp 103-114.

64. R.H. Marion and J.B. Cohen, "The Need for Experimentally Determined X-Ray Constants," Adv. in X-Ray Anal., 20 (1976), pp 355-367.

65. B.D. Cullity, "Some Problems in X-Ray Stress Measurements," Adv. in X-Ray Anal., 20 (1976), pp 259-271.

66. A.L. Esquival, "X-Ray Diffraction Study of the Effects of Uniaxial Plastic Deformation on Residual Stress Measurements," Adv. In X-Ray Anal., 12 (1968), pp 269-300.

67. R.H. Marion, "Anomalies in Measurement of Residual Stress by X-ray Diffraction," Proceedings of a Workshop on NDE of Residual Stress, Air Force Flight Materials Laboratory, Aug 1975.

68. R.I. Garrod and G.A. Hawkes, "X-Ray Analysis on Plastically Deformed Metals," Brit J. Appl. Phys., 14 (1963) pp 422-428.

69. A.L. Esquival and K.R. Evans, "X-Ray Diffraction Study of Residual Macrostresses in Shot-Peened and Fatigued 4130 Steel," Exp. Mech., November 1968, pp 496-503.

70. G. Dietrich and J.M. Potter, "Stress Measurements on Cold-Worked Fastener Holes," Adv. in X-Ray Anal., 20 (1976) pp 321 - 328.

71. R.L Chrenko, "X-Ray Residual Stress Measurements Using Parallel Beam Optics," Adv. in X-Ray Anal., 20 (1976) pp 393-402.

72. P.S. Prevey and M.S. Field, "Variation in Surface Stress Due to Metal Removal," Annals of CIRP, 24 (1975) pp 497-501.

73. F. Rotvel, "On Residual Stress Due to Random Load Fatigue," Symposium on Random Load Fatigue, AGARD-CP-118 (1972).

74. J.M. Potter and R.A. Millard, "The Effect of Temperature and Load Cycling on the Relaxation of Residual Stresses," Adv. in X-Ray Anal., 20 (1976) pp 309-320.

75. M. Nagao and V. Weiss, "X-Ray Diffraction Study of Low Cycle Fatigue Damage in Plain Carbon Steel," Journal of Engr'g and Mat'ls Tech., Trans. ASME (H), April 1977, pp 110-113.

76. H.J Latiere, "X-Ray Diffraction Study of the Plastic Zone," Engr'g Frac. Mech., 8 (1976), pp 691-700.

77. T. Yokobori and K. Sato, "X-Ray Study on the Substructure Near the Fatigue Crack," Rep. of Res. Int. for Strength and Fracture of Materials, Tohoku Univ., Sendai, Japan, 8 (1972).

78. R.E. Herfert, "Automated Residual Stress Analyzers using X-ray Diffraction," Proceedings of a Workshop on NDE of Residual Stress, Air Force Materials Laboratory, Aug 1975, pp 141-152.

79. S.B. Catalano, "Residual Stress Measurements on Tank Automotive Components,"Ibid, pp 53-61.

80. R.C. Larson, "X-Ray Diffraction Measurements of Residual Stresses in Aluminum Alloys," Adv. in X-Ray Anal., 7 (1964) p 33.

81. M.R. Jones and J.B. Cohen, "Study of the Precision of X-Ray Stress Analysis," Adv. in X-Ray Analysis, 20 (1976), pp 291-307.

APPENDIX I SPECIMEN DRAWINGS

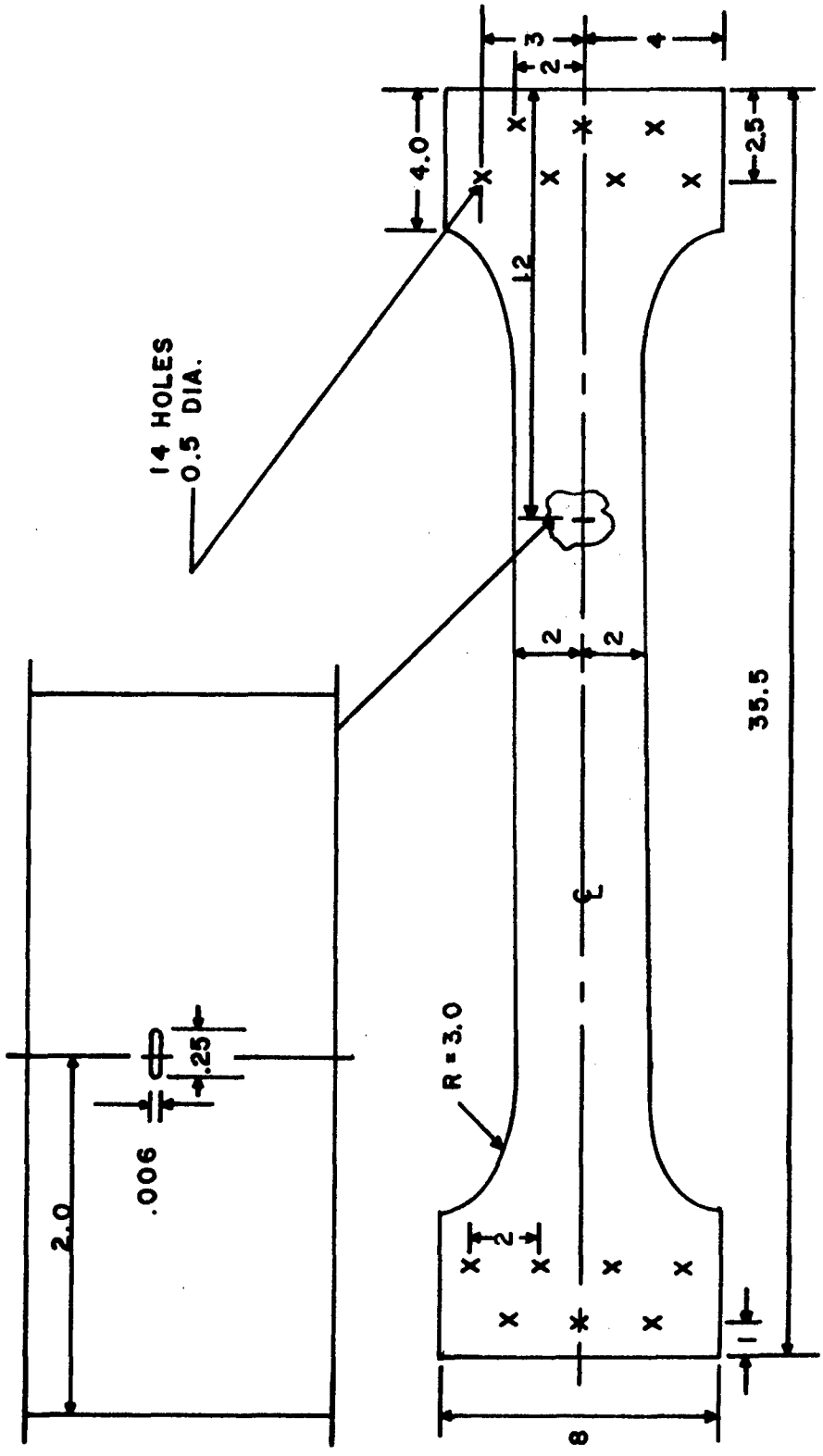


FIGURE AI-1 CENTER-CRACKED SPECIMEN

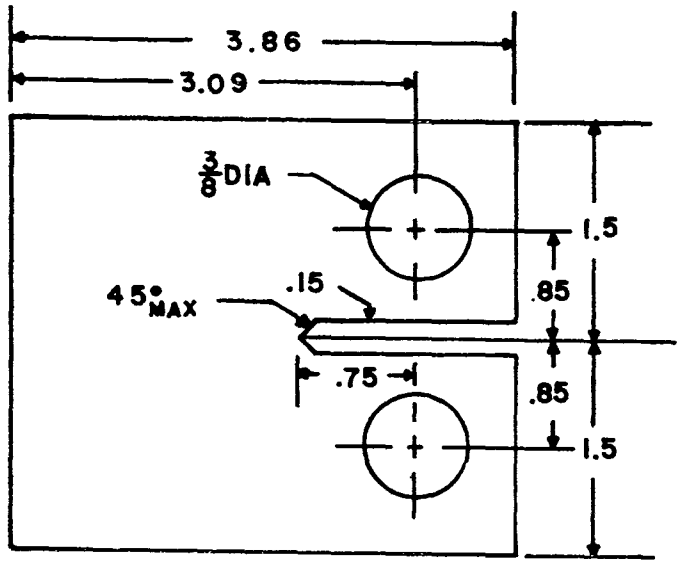


FIGURE AI-2 WEDGE OPENING LOAD SPECIMEN

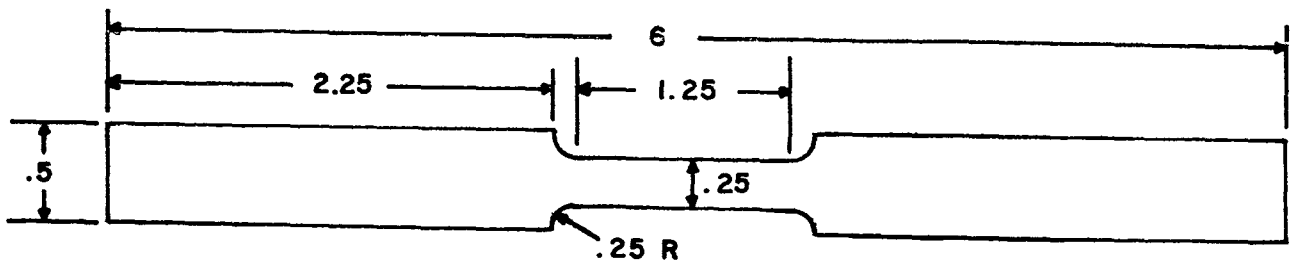


FIGURE AI-3 SUBSCALE TENSILE SPECIMEN

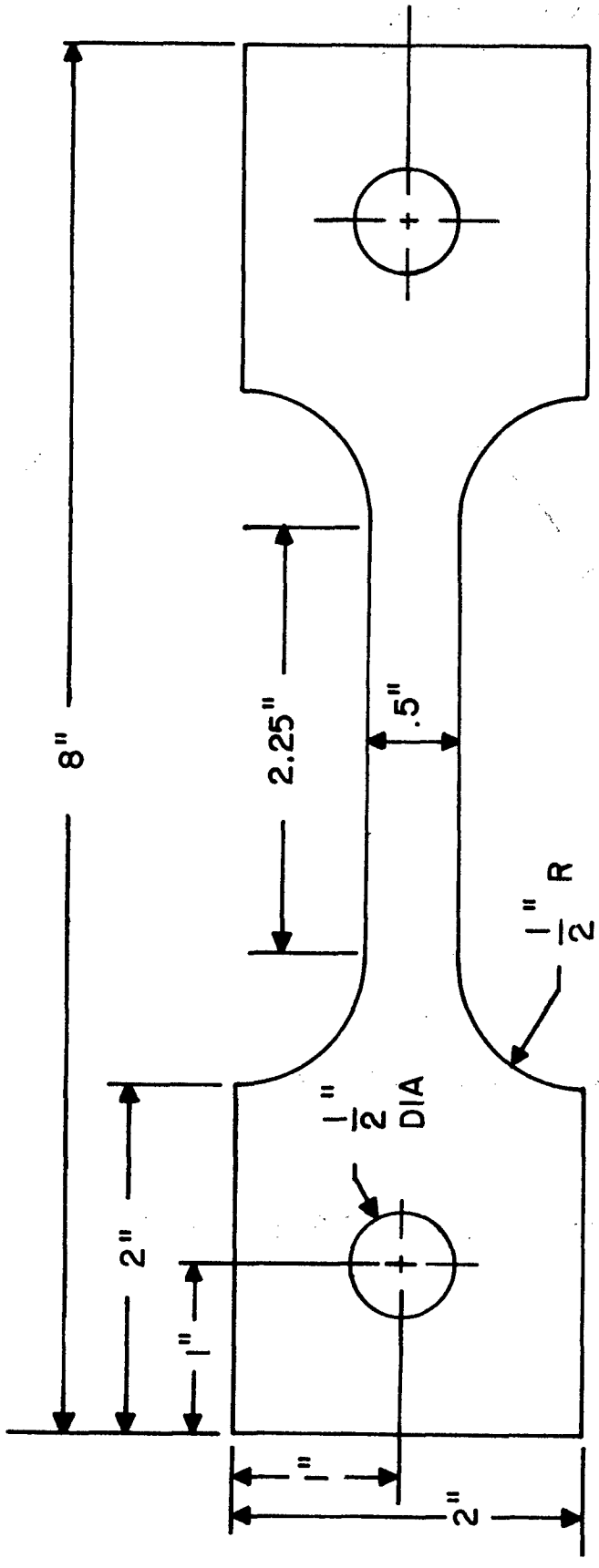


FIGURE AI-4 TENSILE SPECIMEN

APPENDIX II - TENSILE TESTS:
LOAD DISPLACEMENTS DIAGRAMS

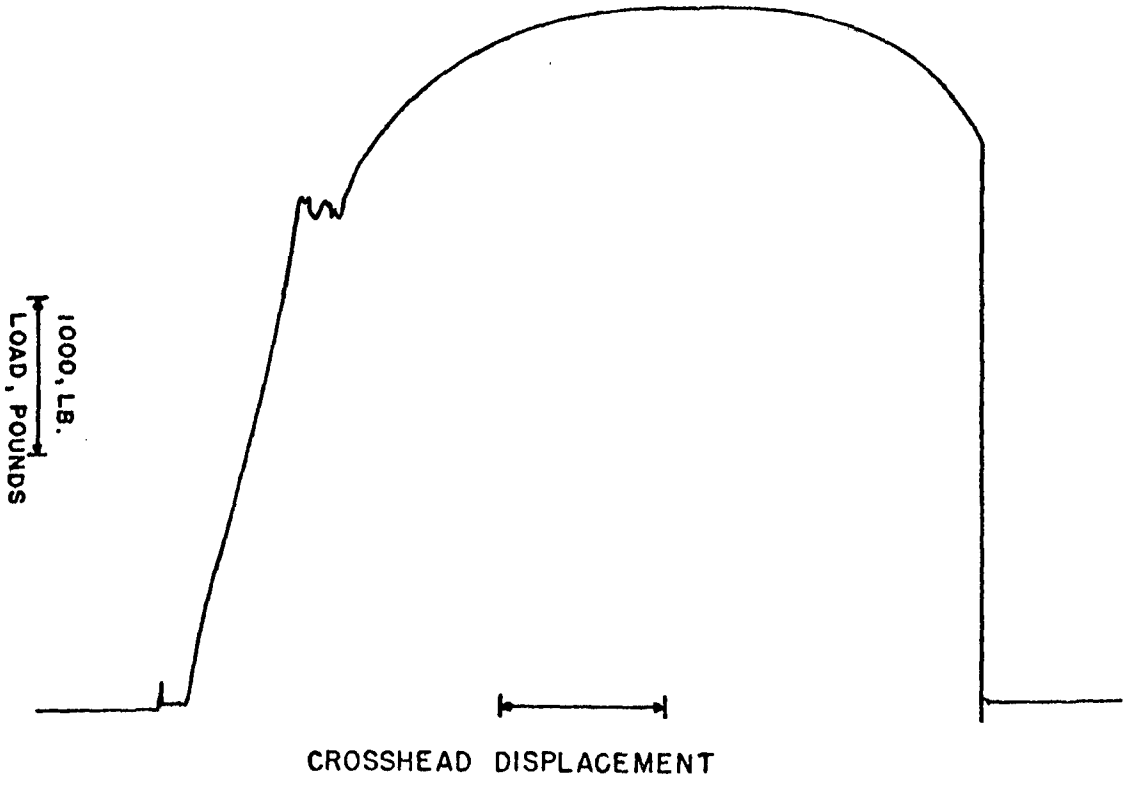


FIGURE AII-1 1020 STEEL SPECIMEN ST20-1

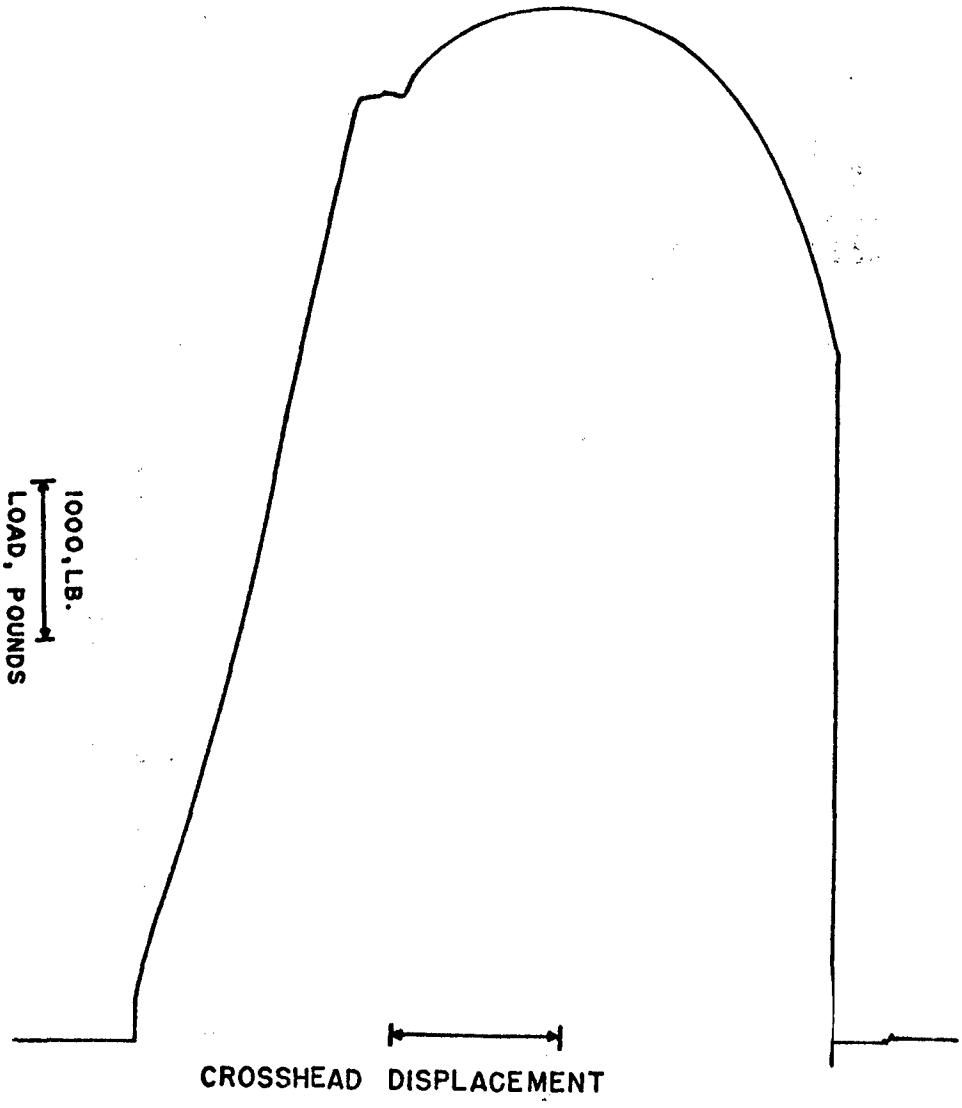


FIGURE AII-2 1045 STEEL SPECIMEN ST45-6

APPENDIX III - TEST DATA

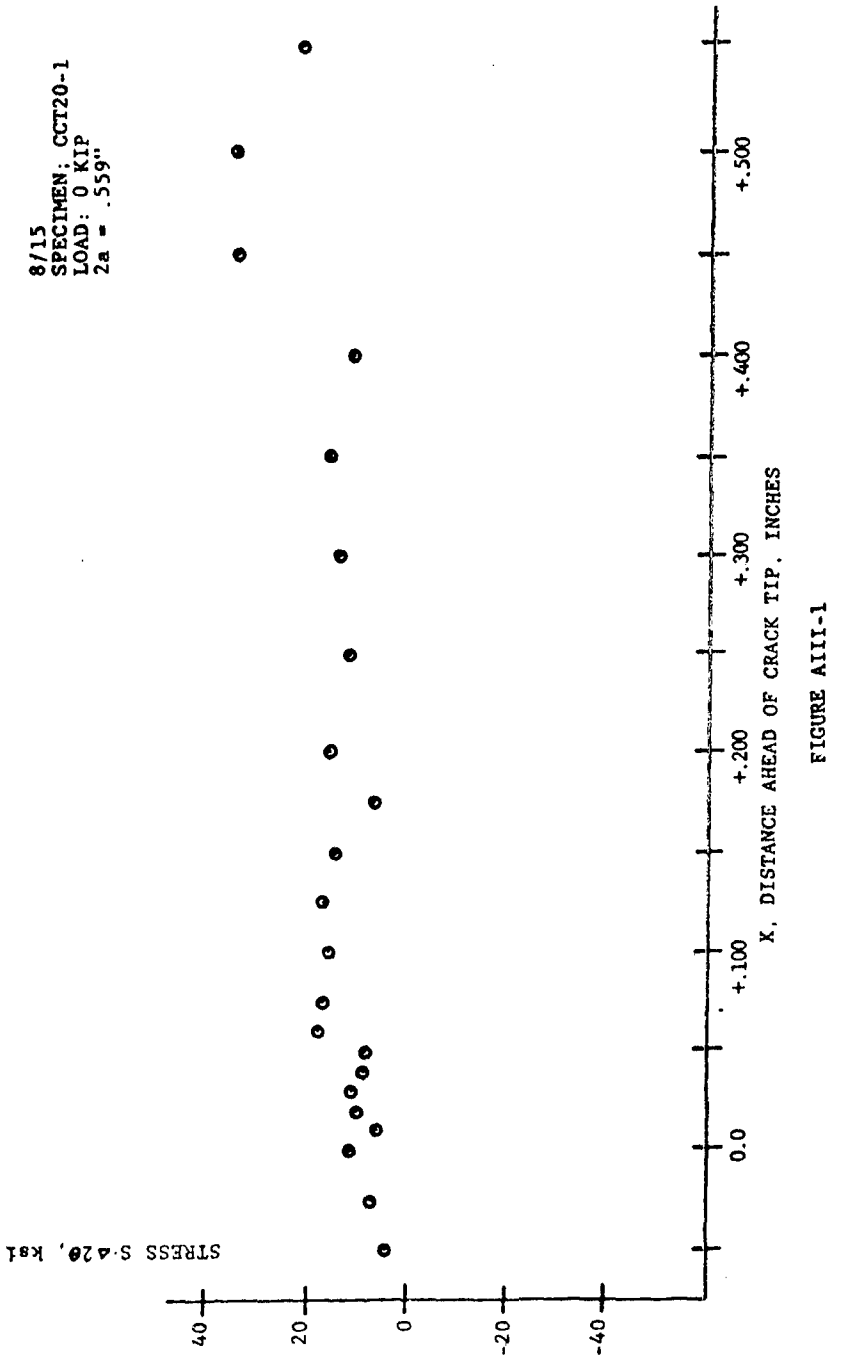


FIGURE AIII-1

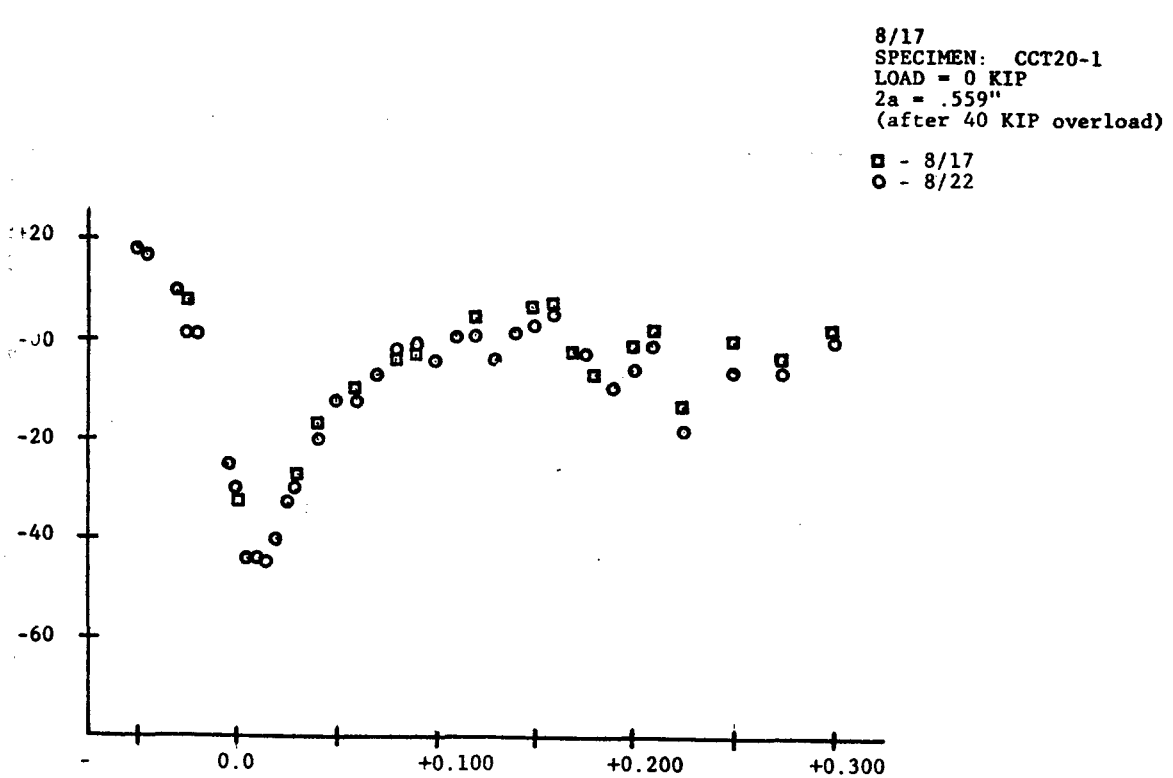


FIGURE AIII-2

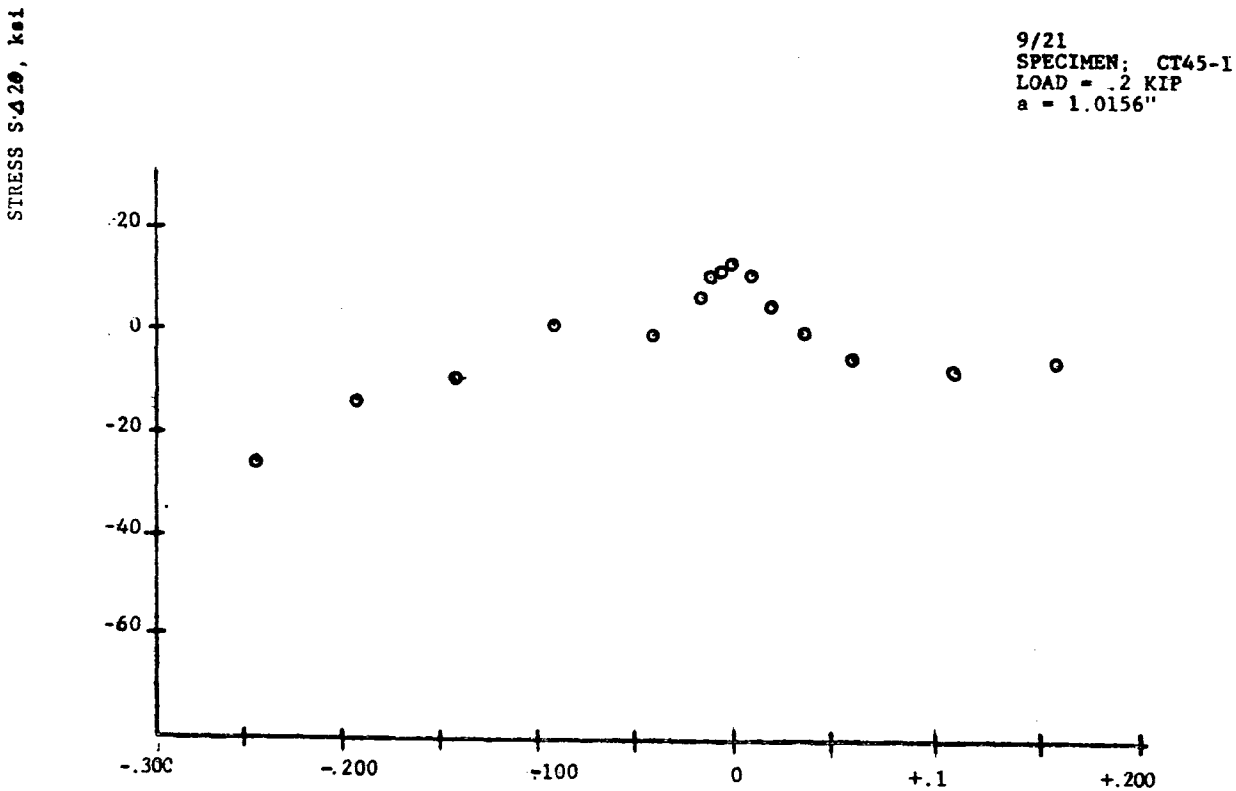


FIGURE AIII-3

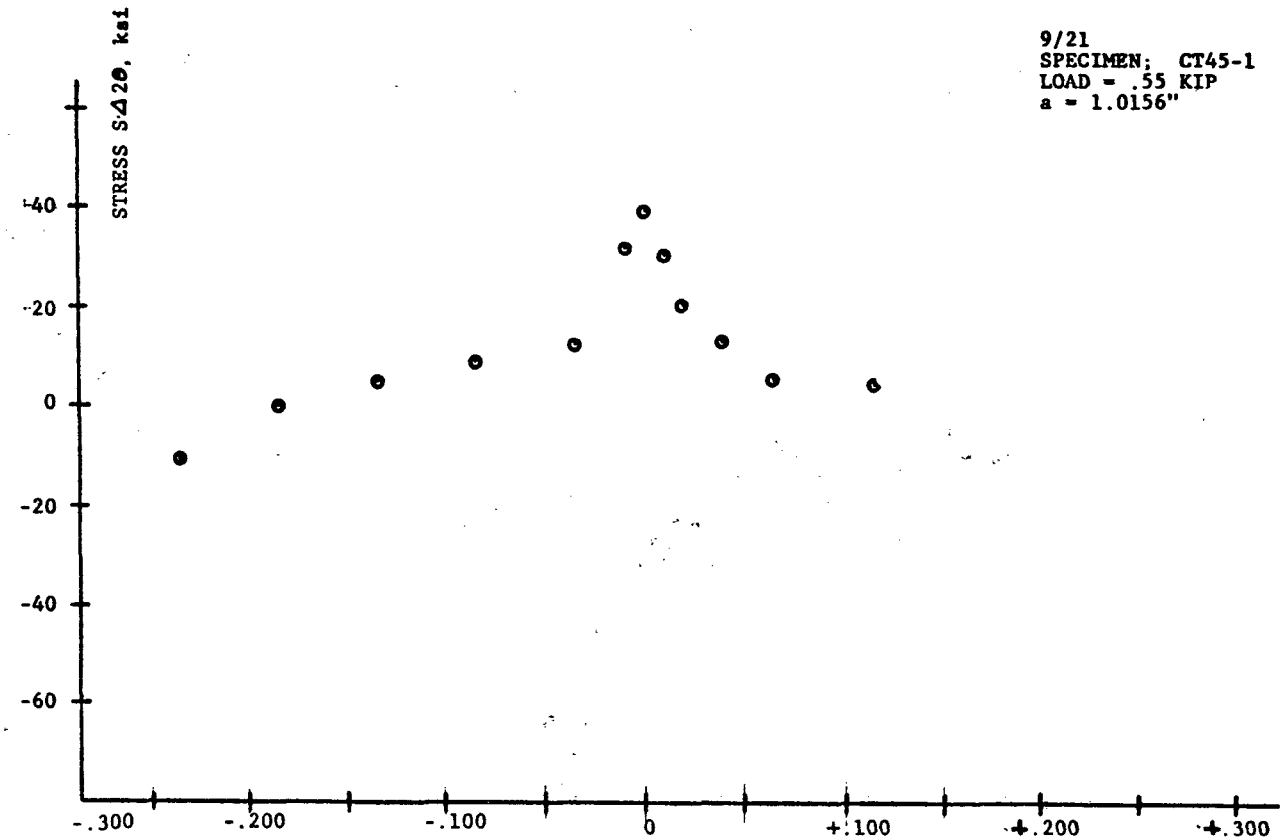


FIGURE AIII-4

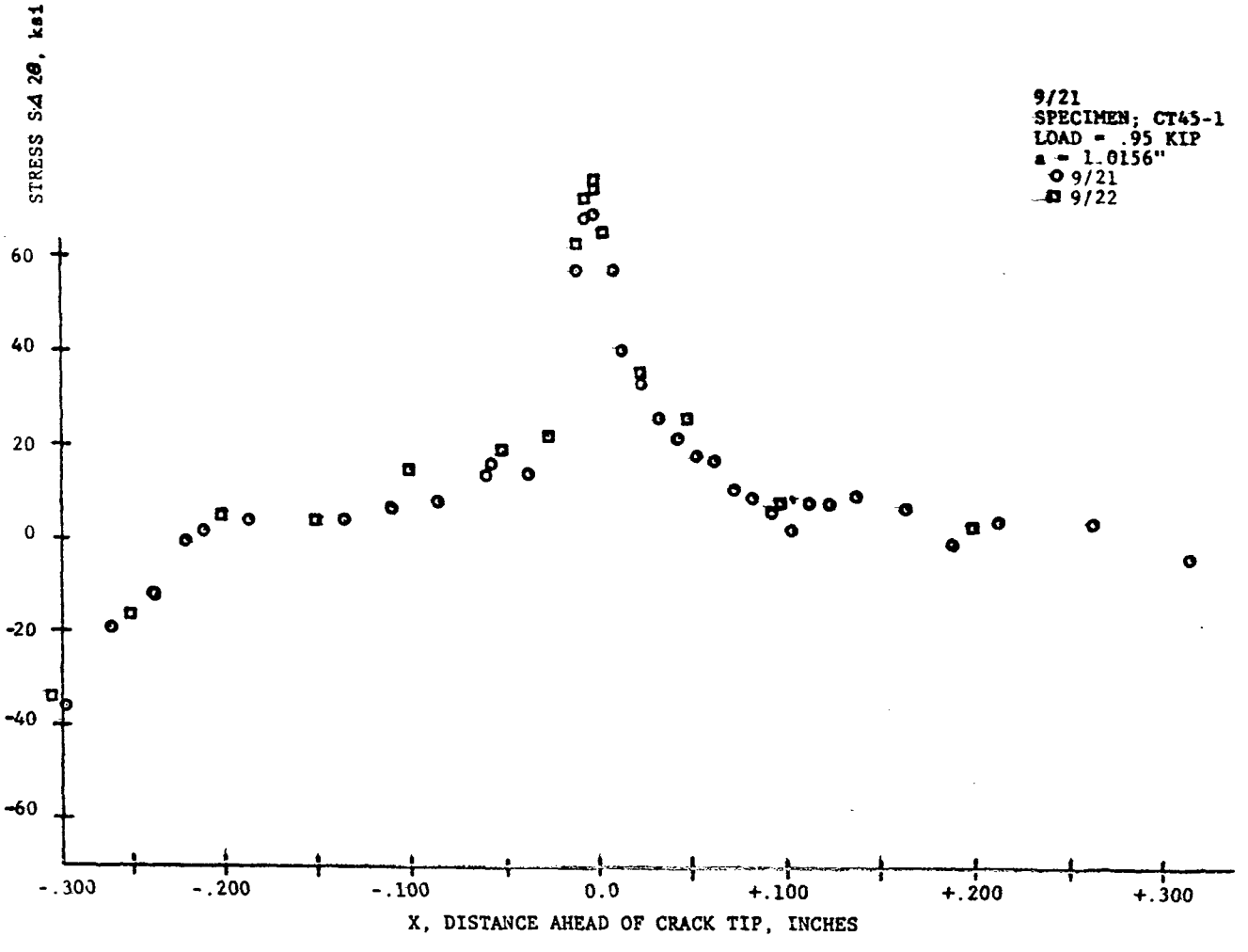


FIGURE AIII-5

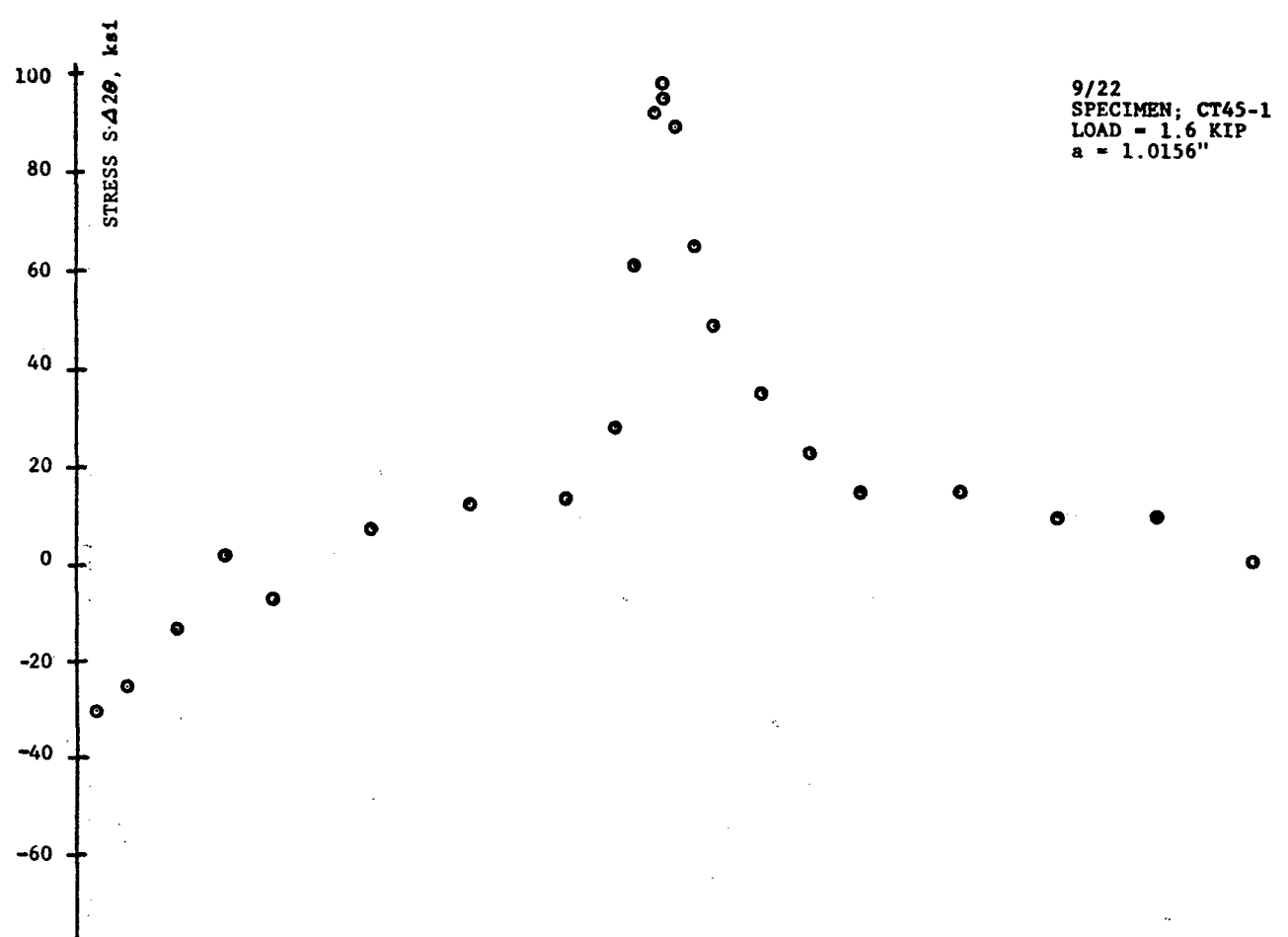

FIGURE AIII-6

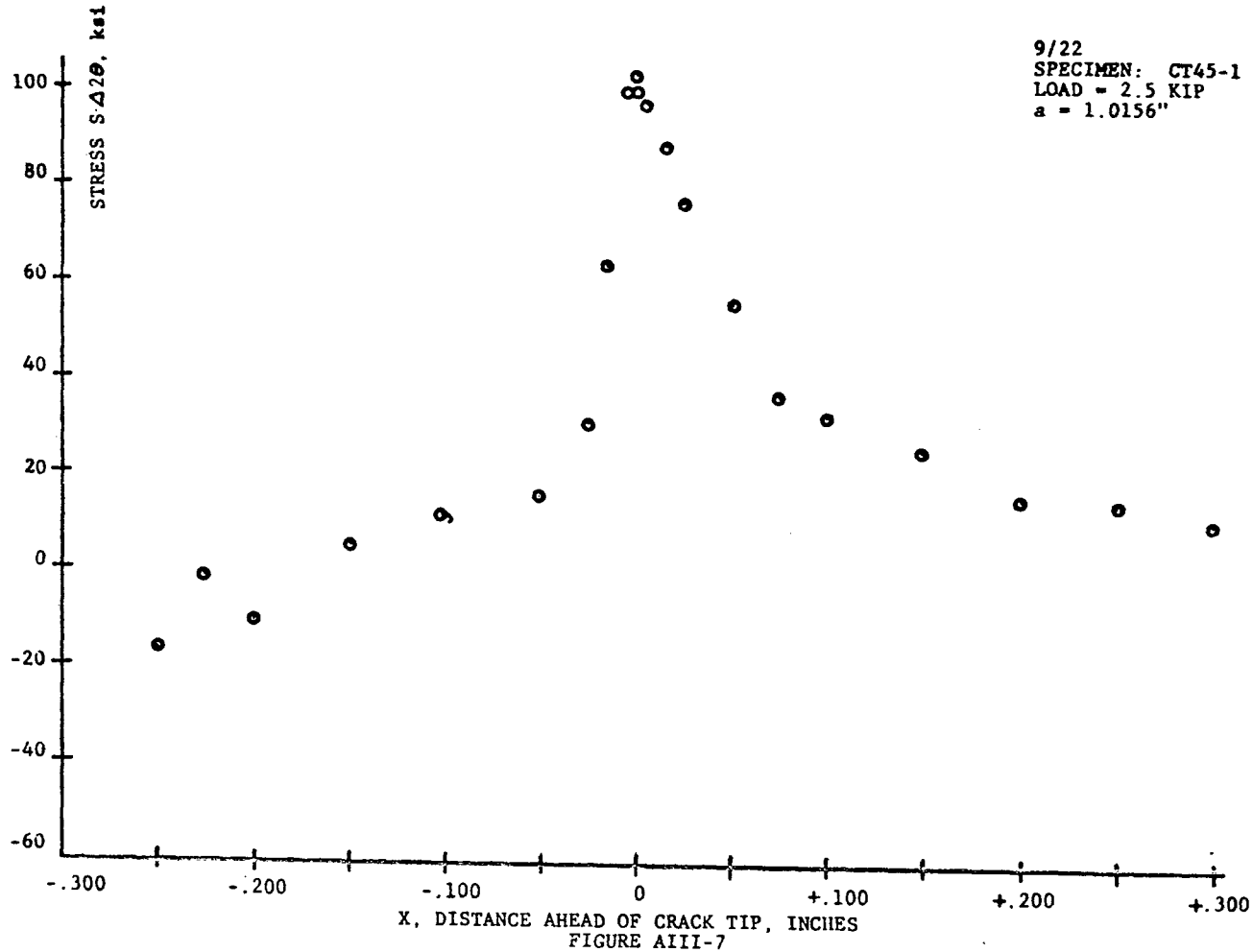

FIGURE AIII-7

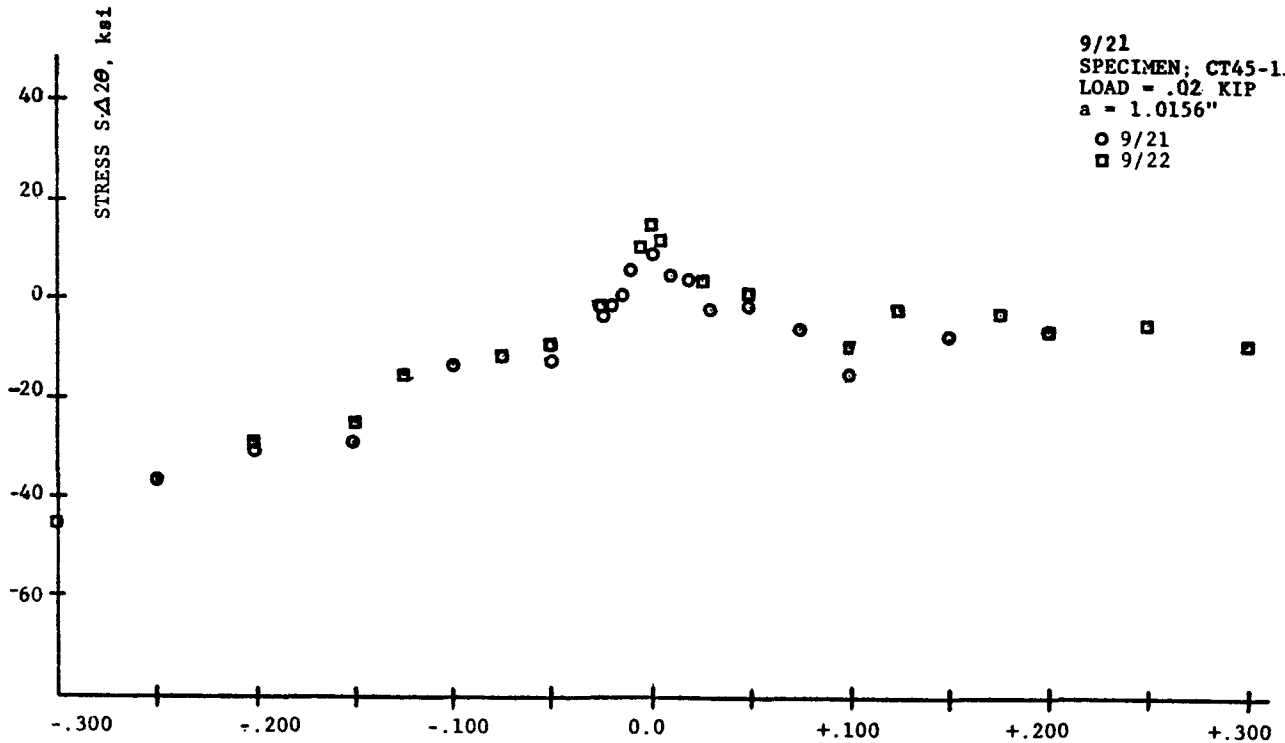


X, DISTANCE AHEAD OF CRACK TIP, INCHES

FIGURE AIII-8

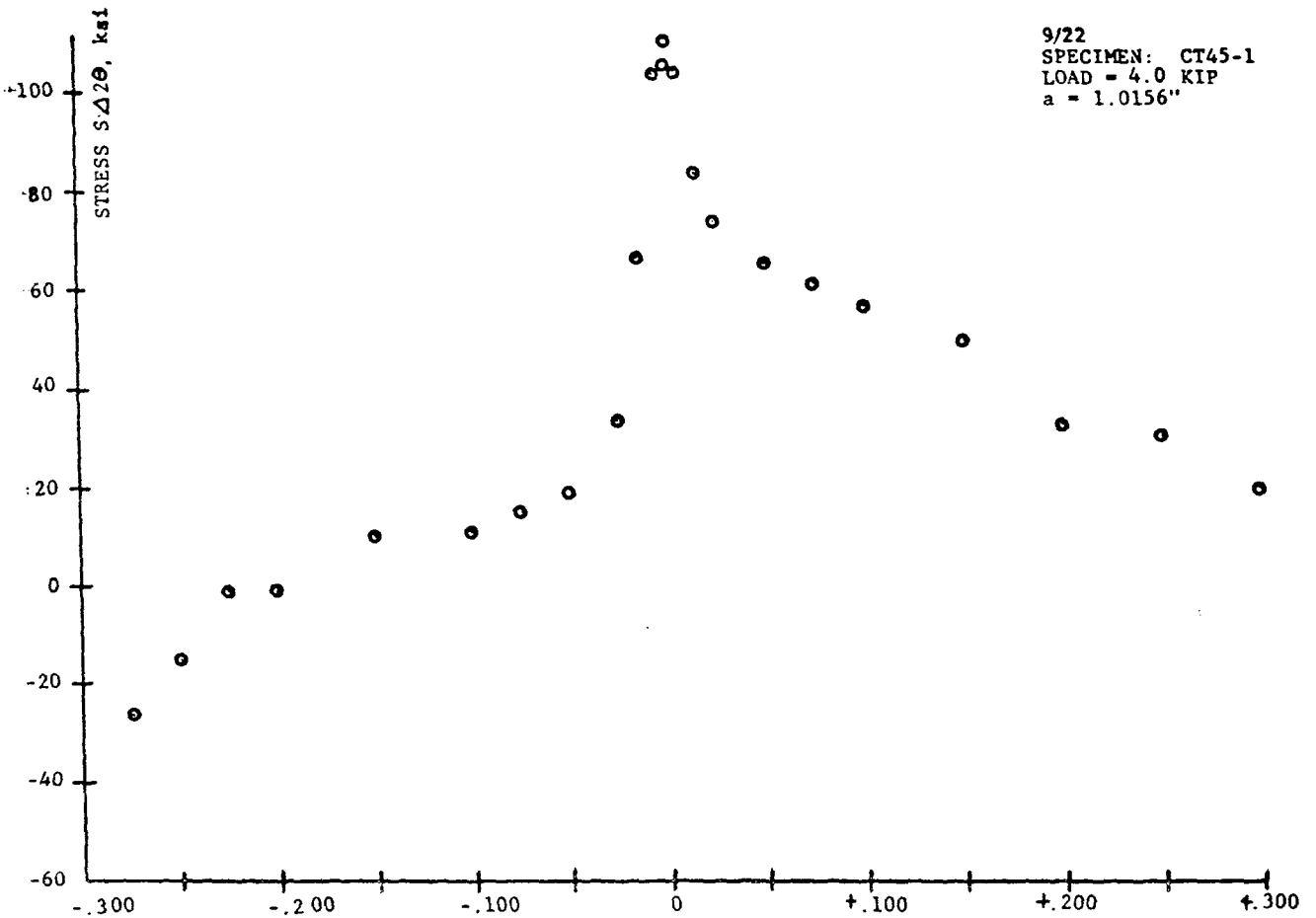

FIGURE AIII-9

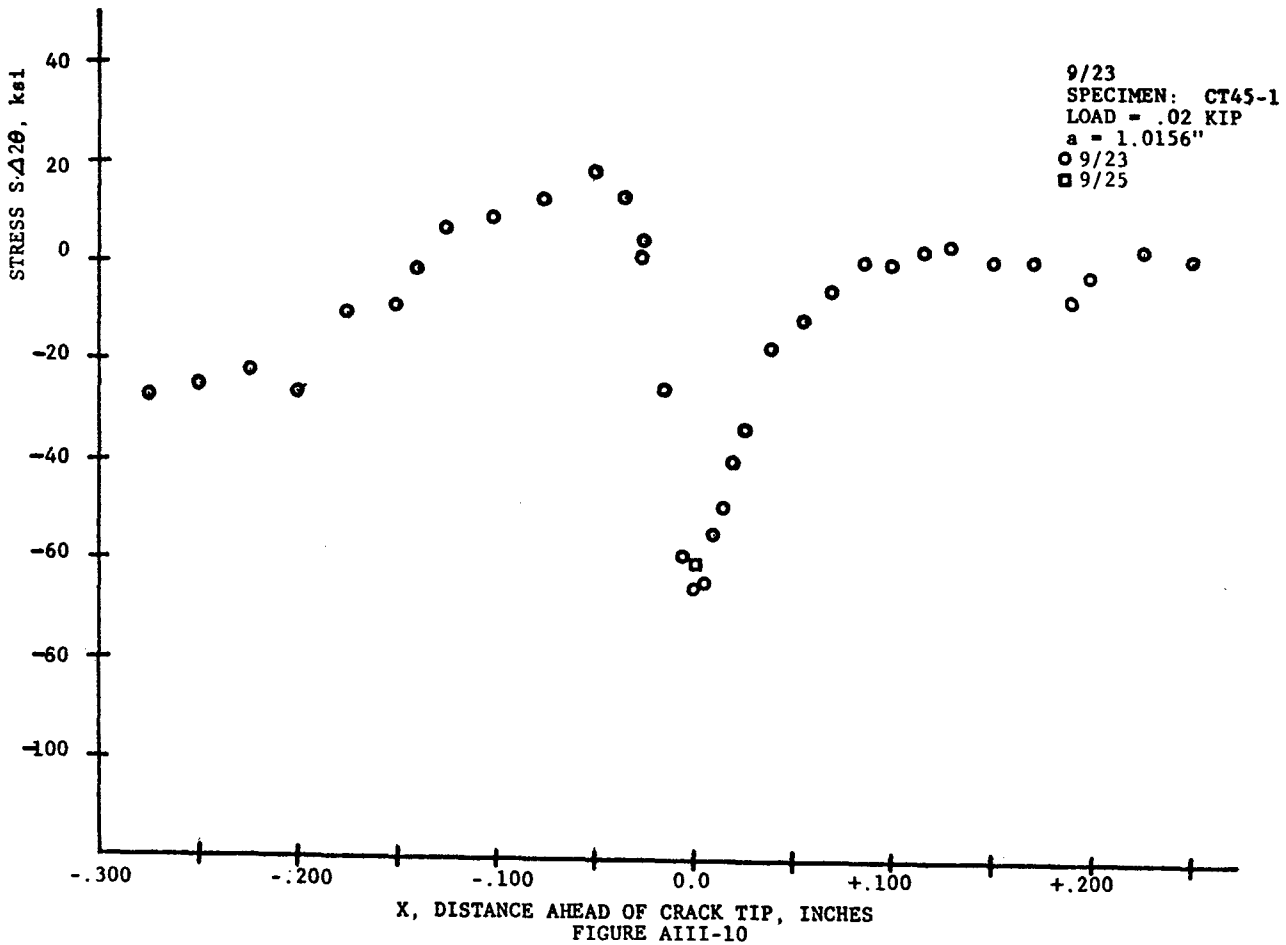

FIGURE AIII-10

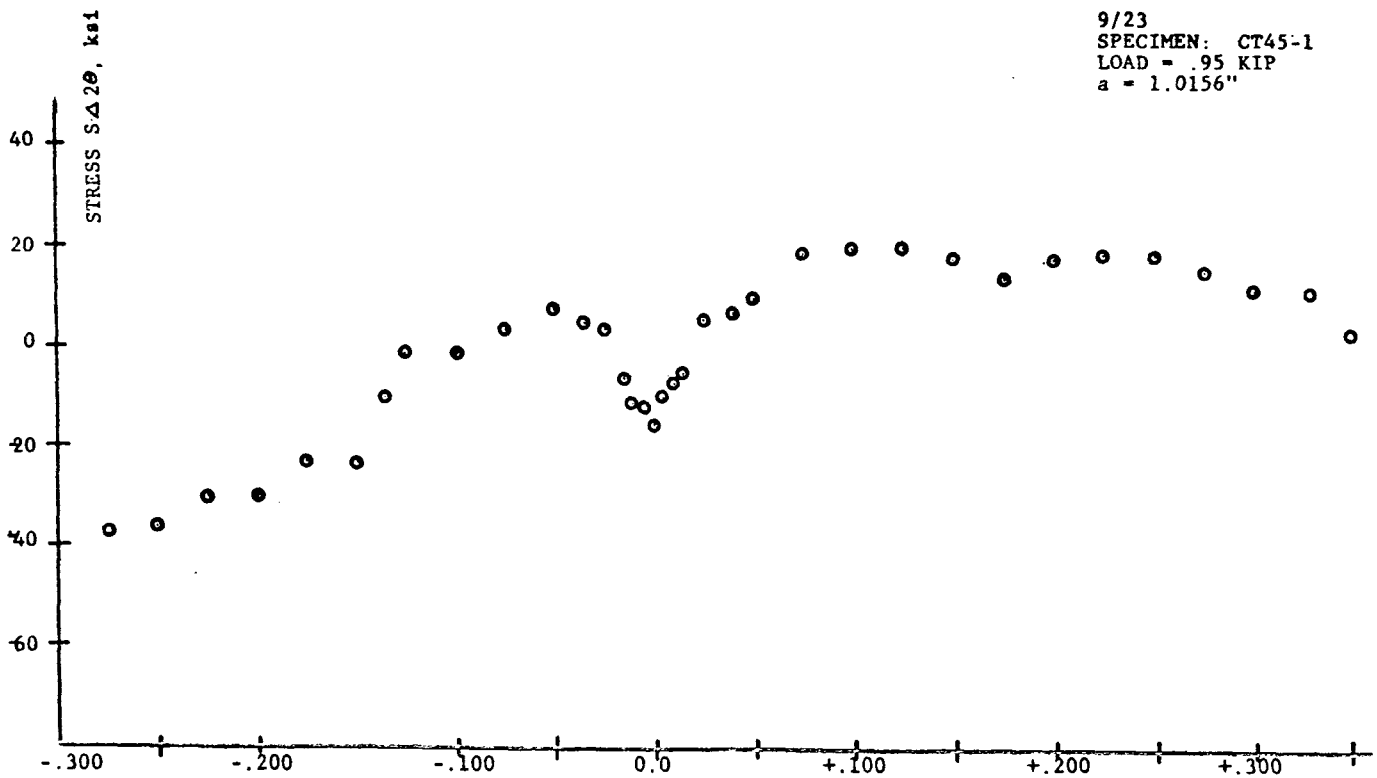


FIGURE AIII-11

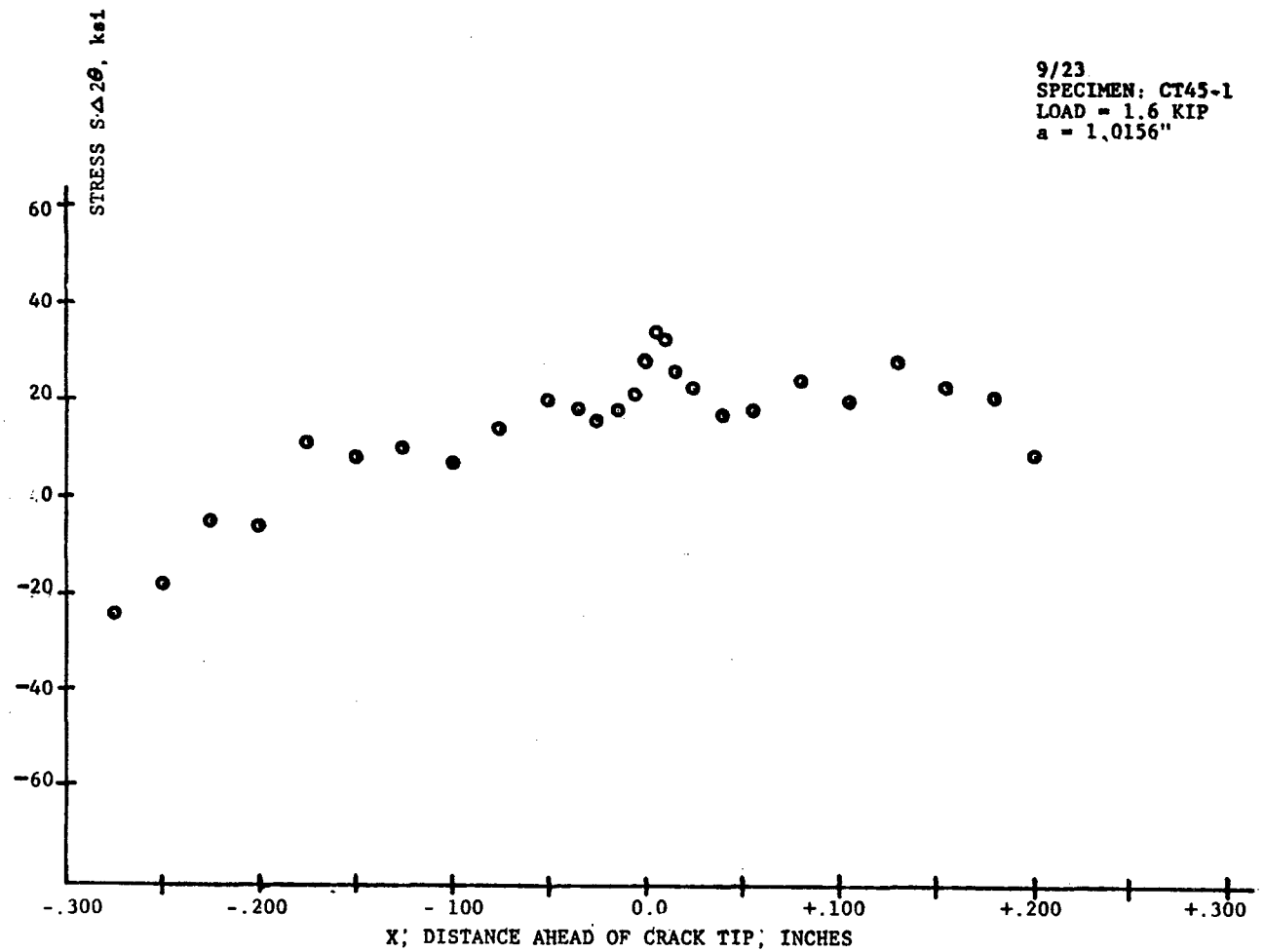


FIGURE AIII-12

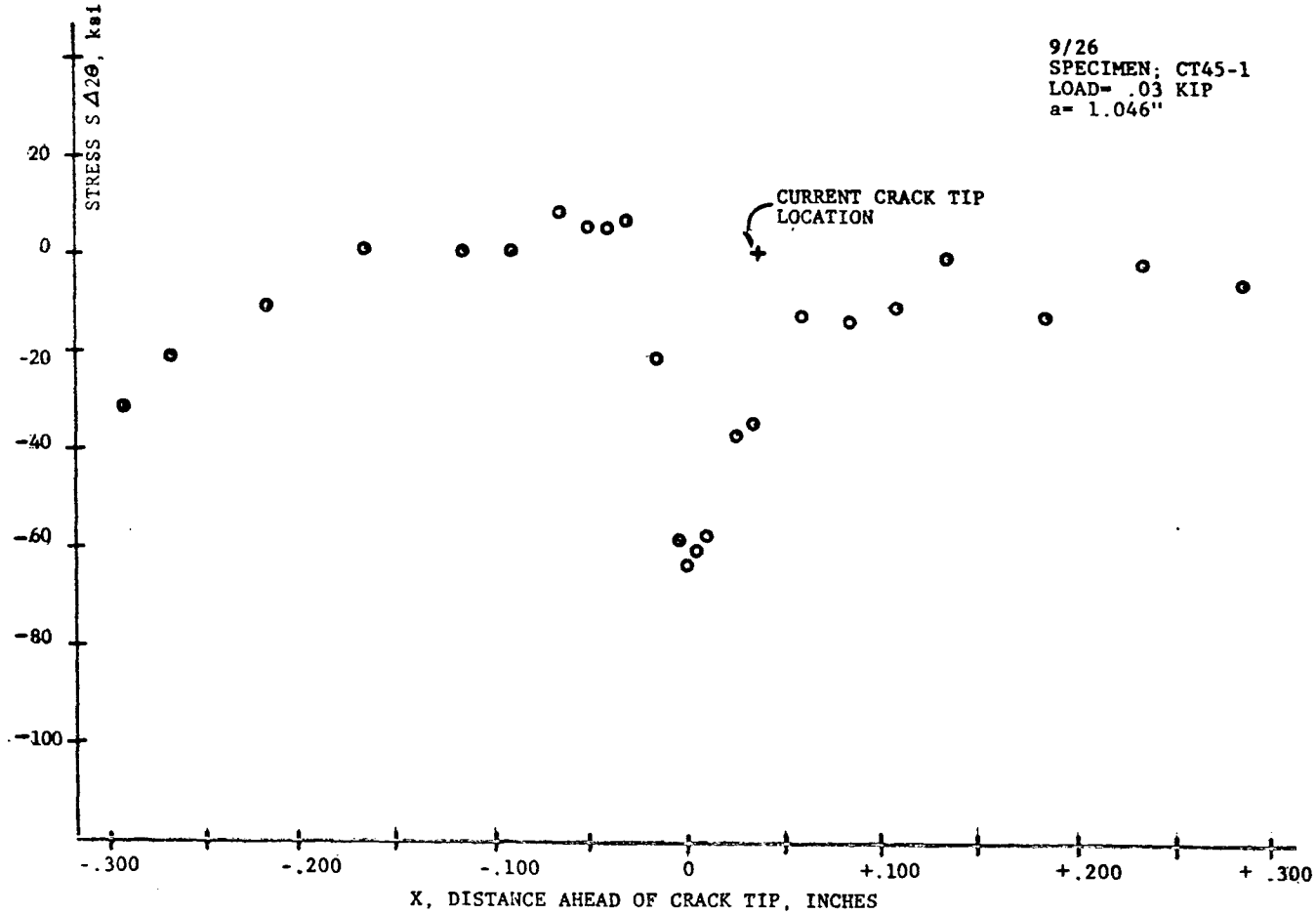


FIGURE AIII-13

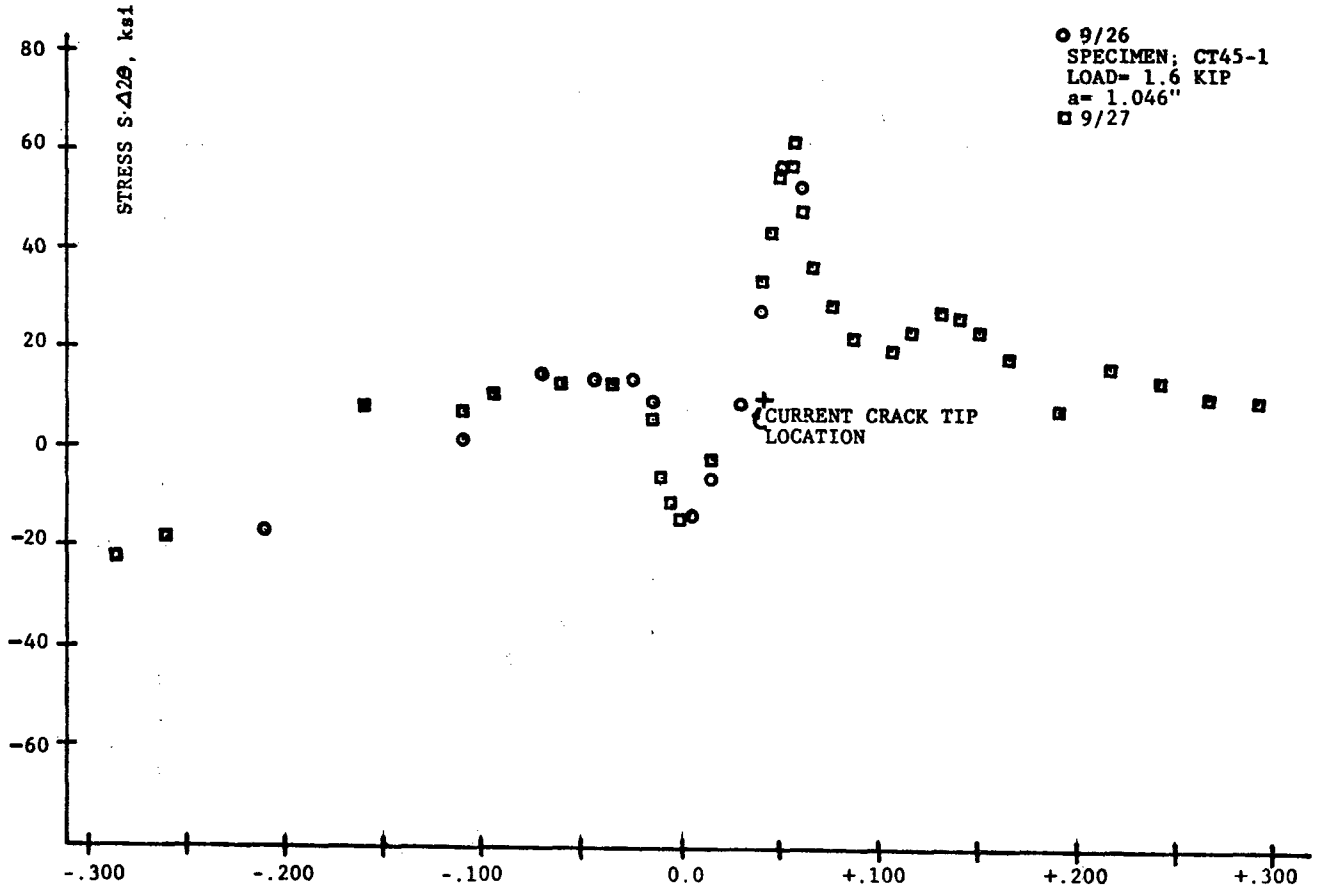

FIGURE AIII-14

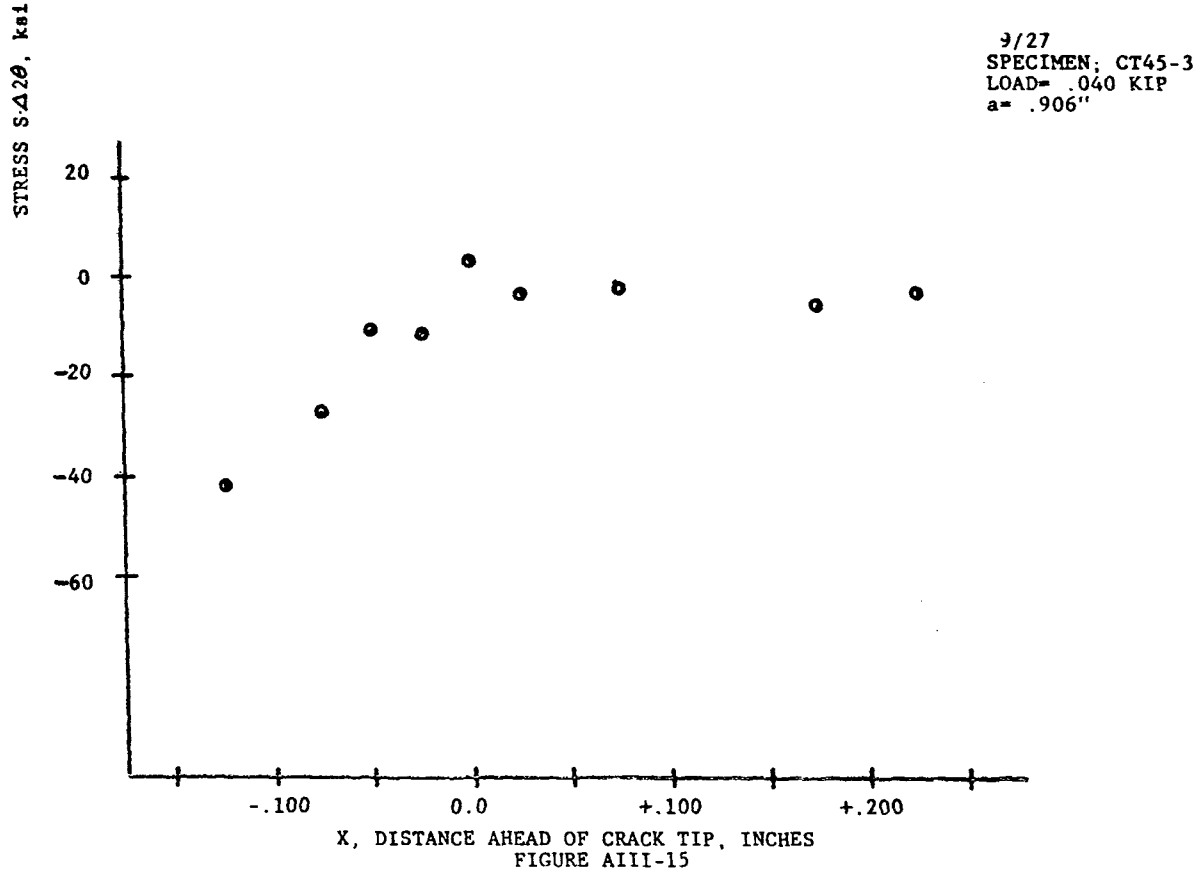


FIGURE AIII-15

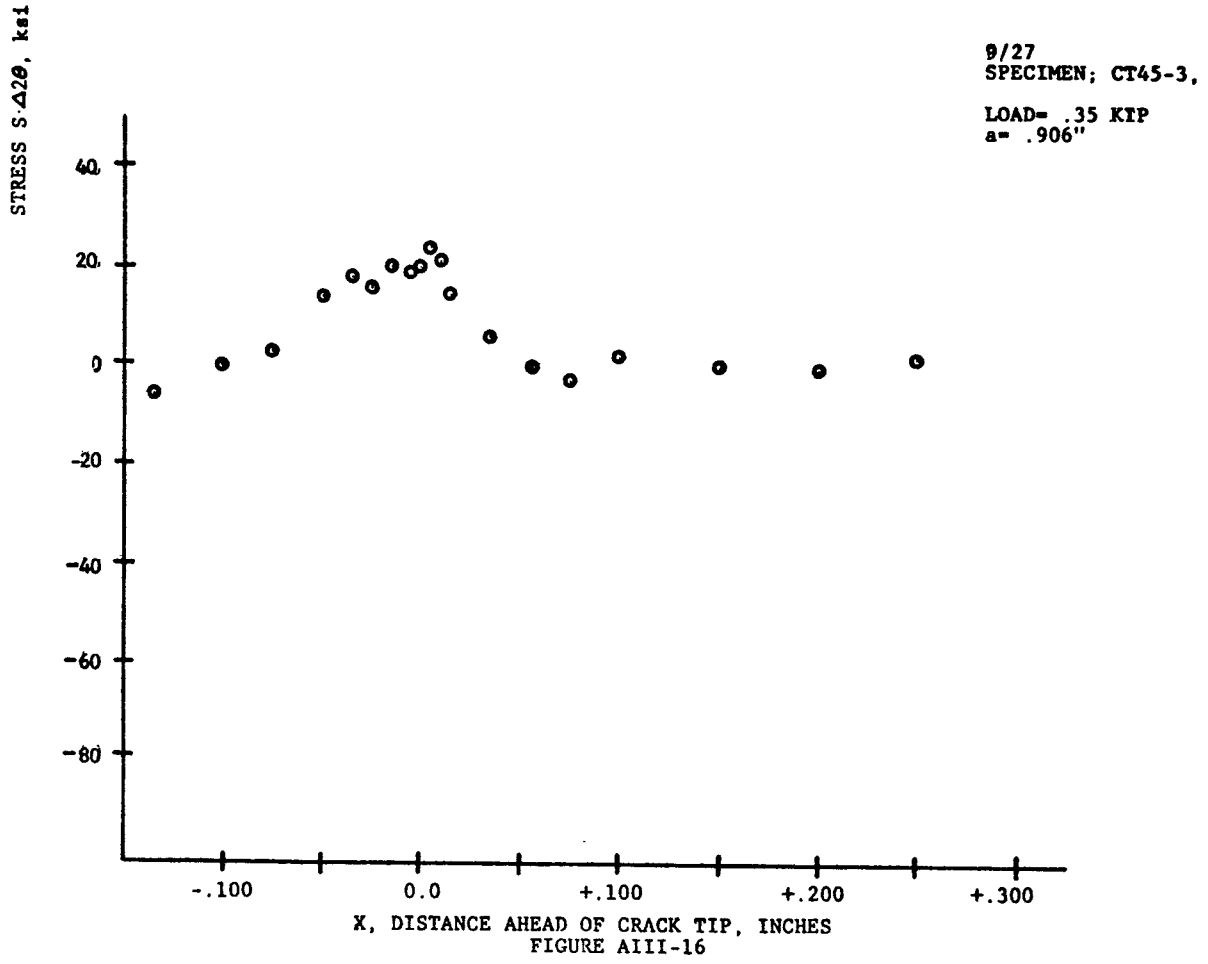

FIGURE AIII-16

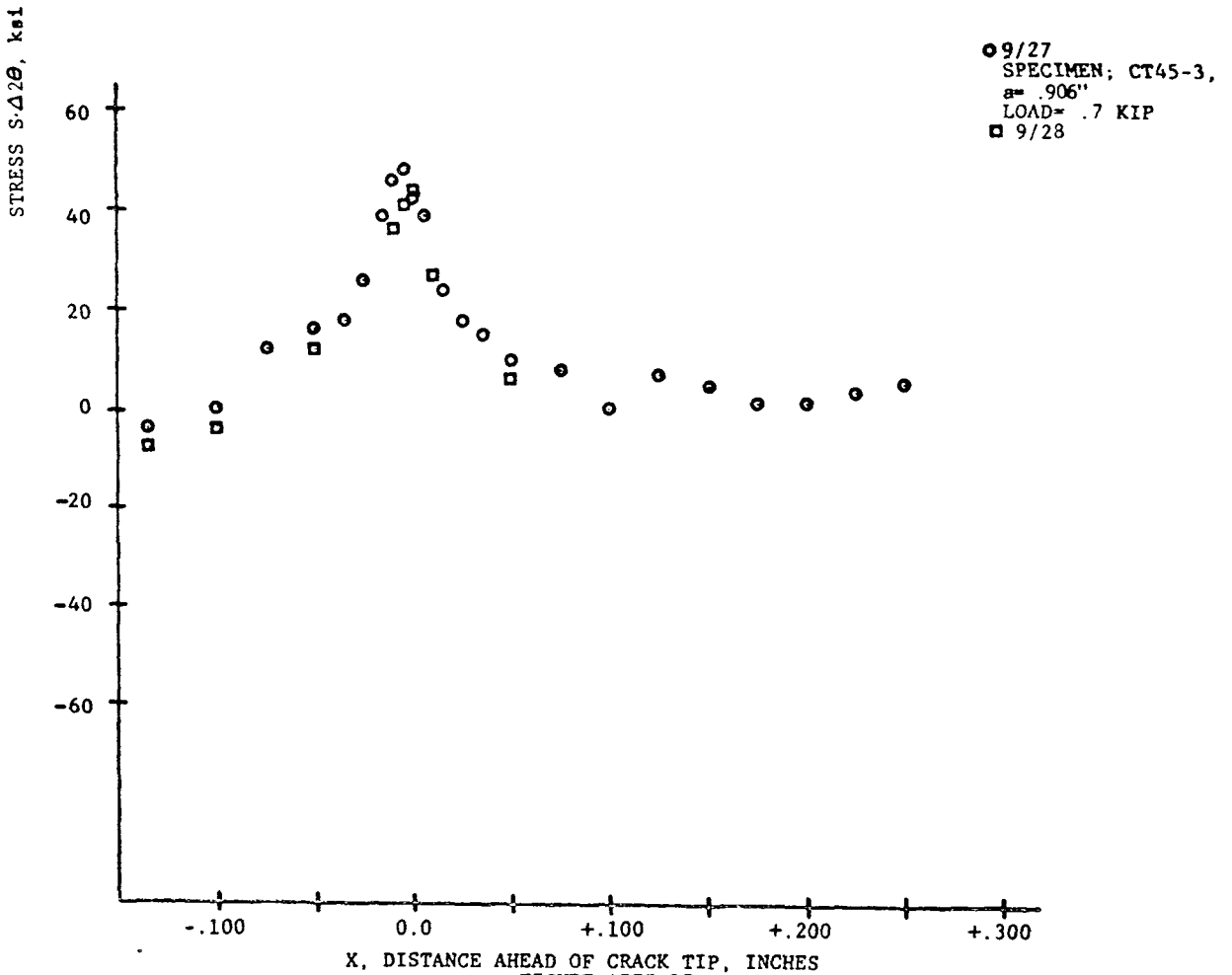

FIGURE AIII-17

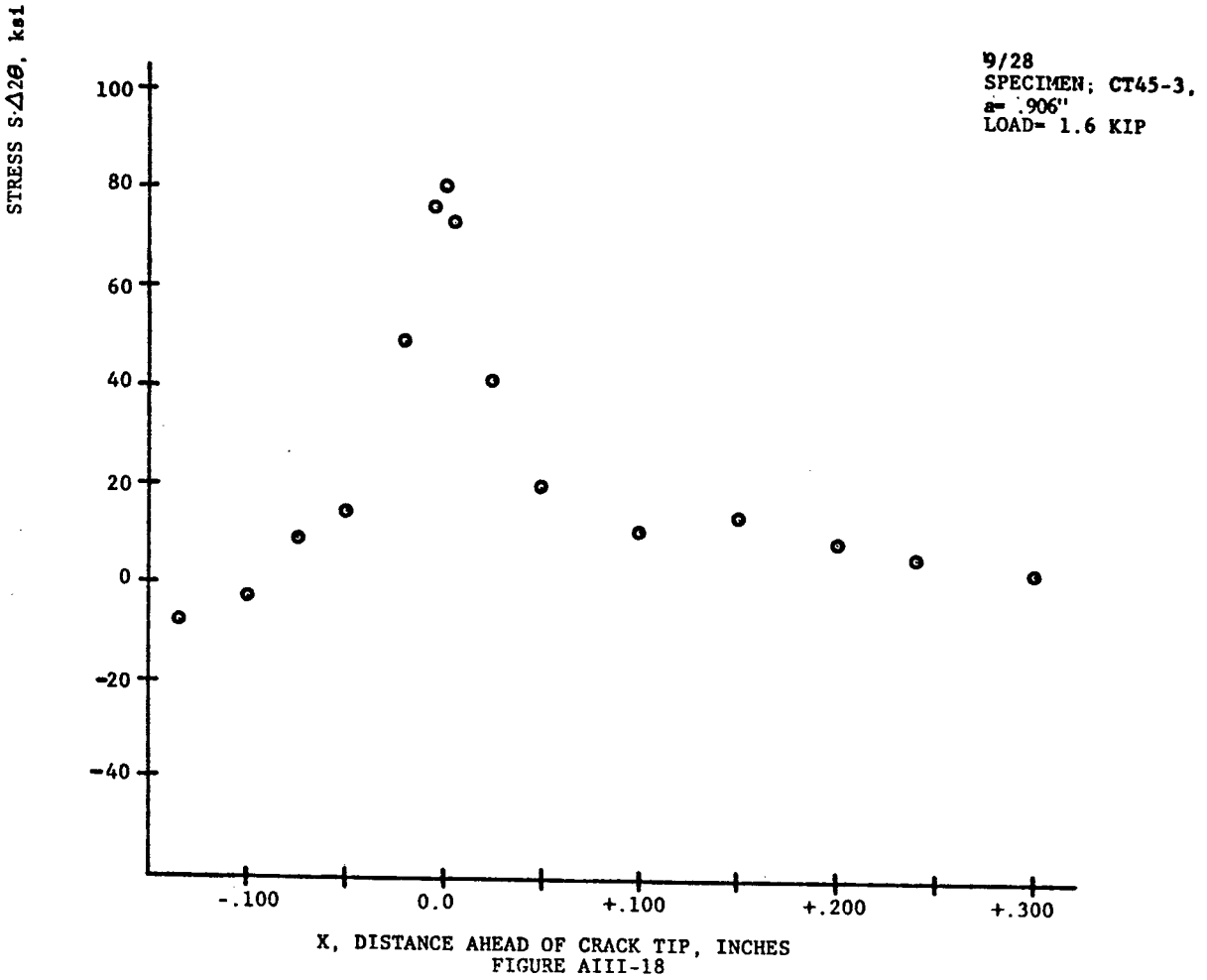

FIGURE AIII-18

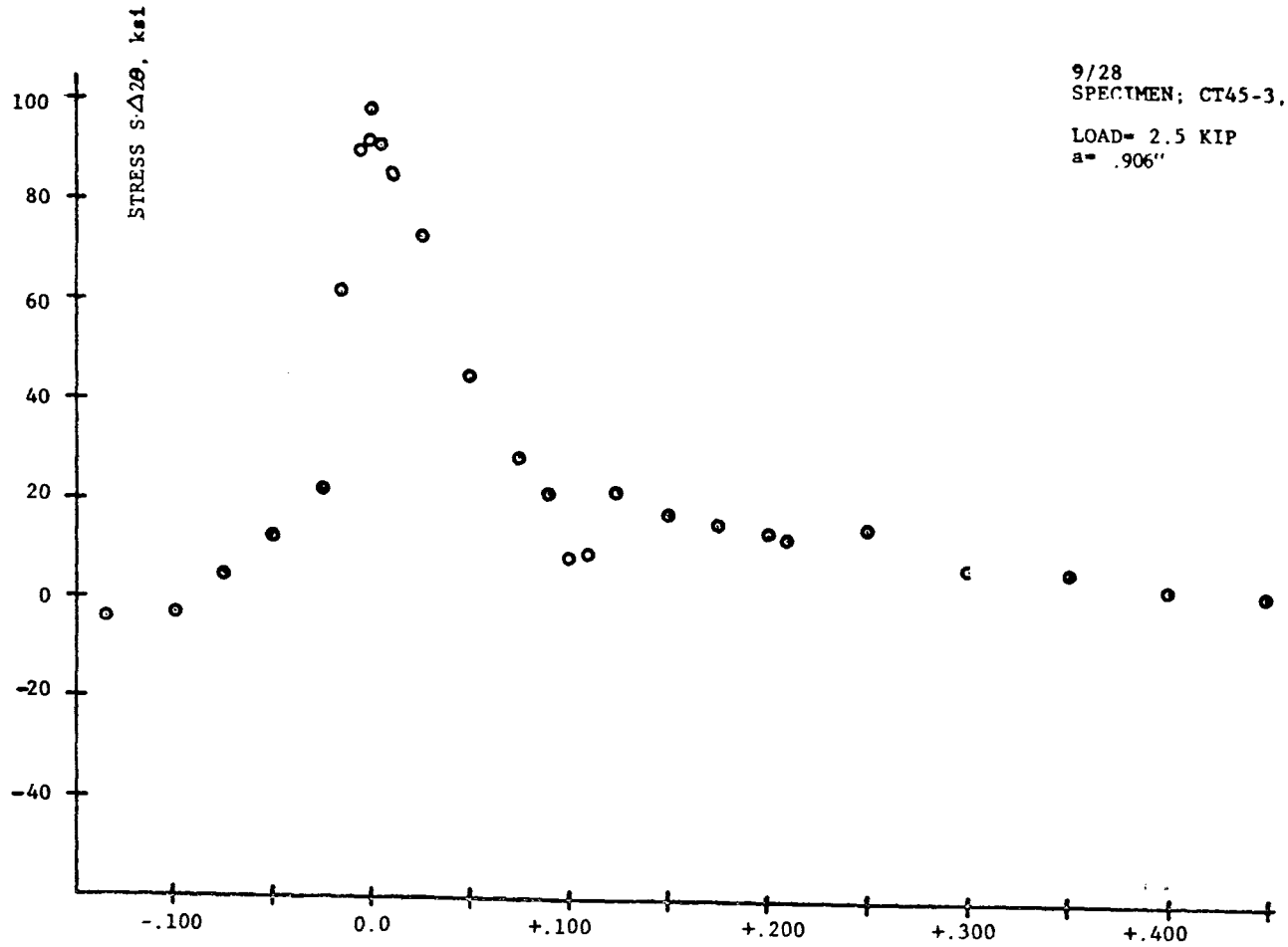


X, DISTANCE AHEAD OF CRACK TIP, INCHES
FIGURE AIII-19

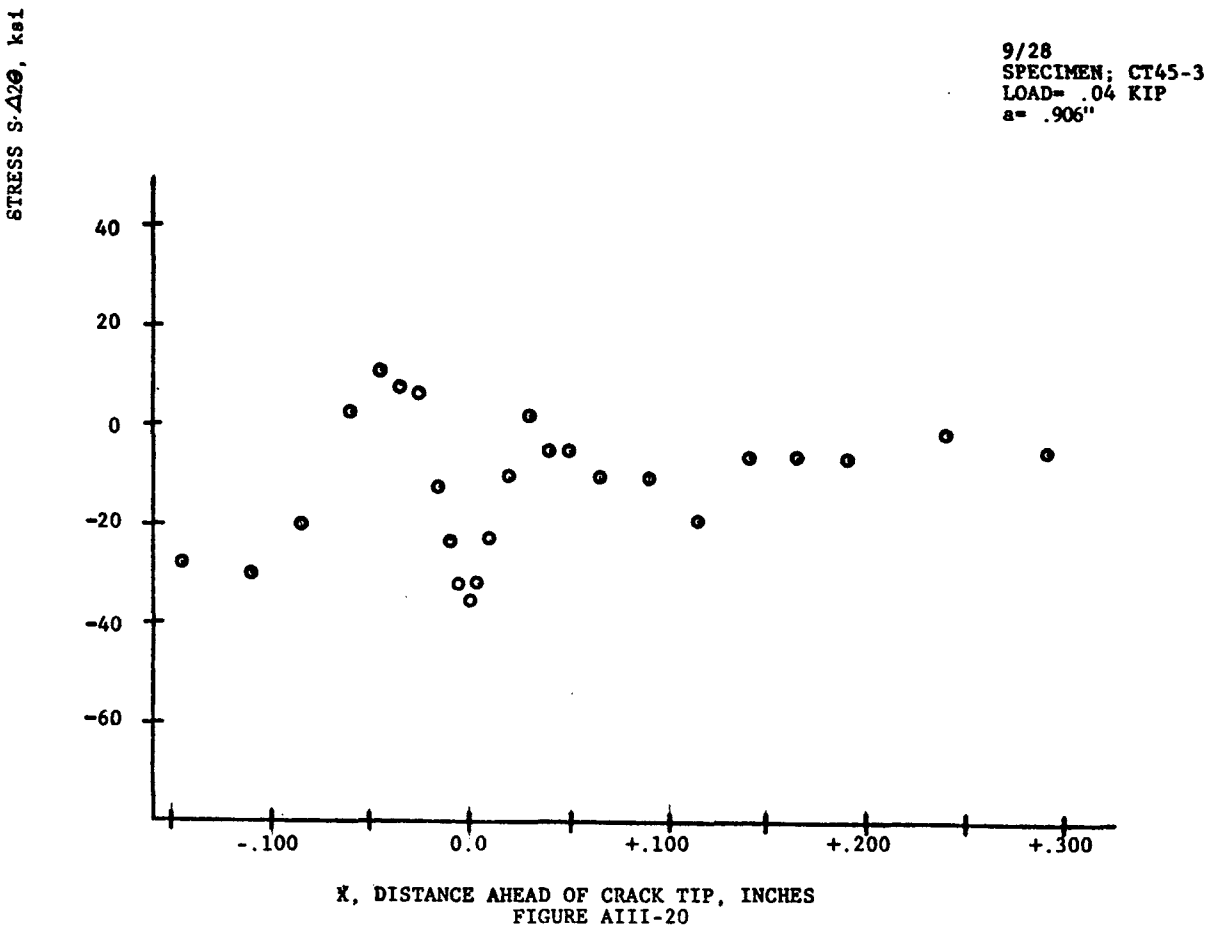


FIGURE AIII-20

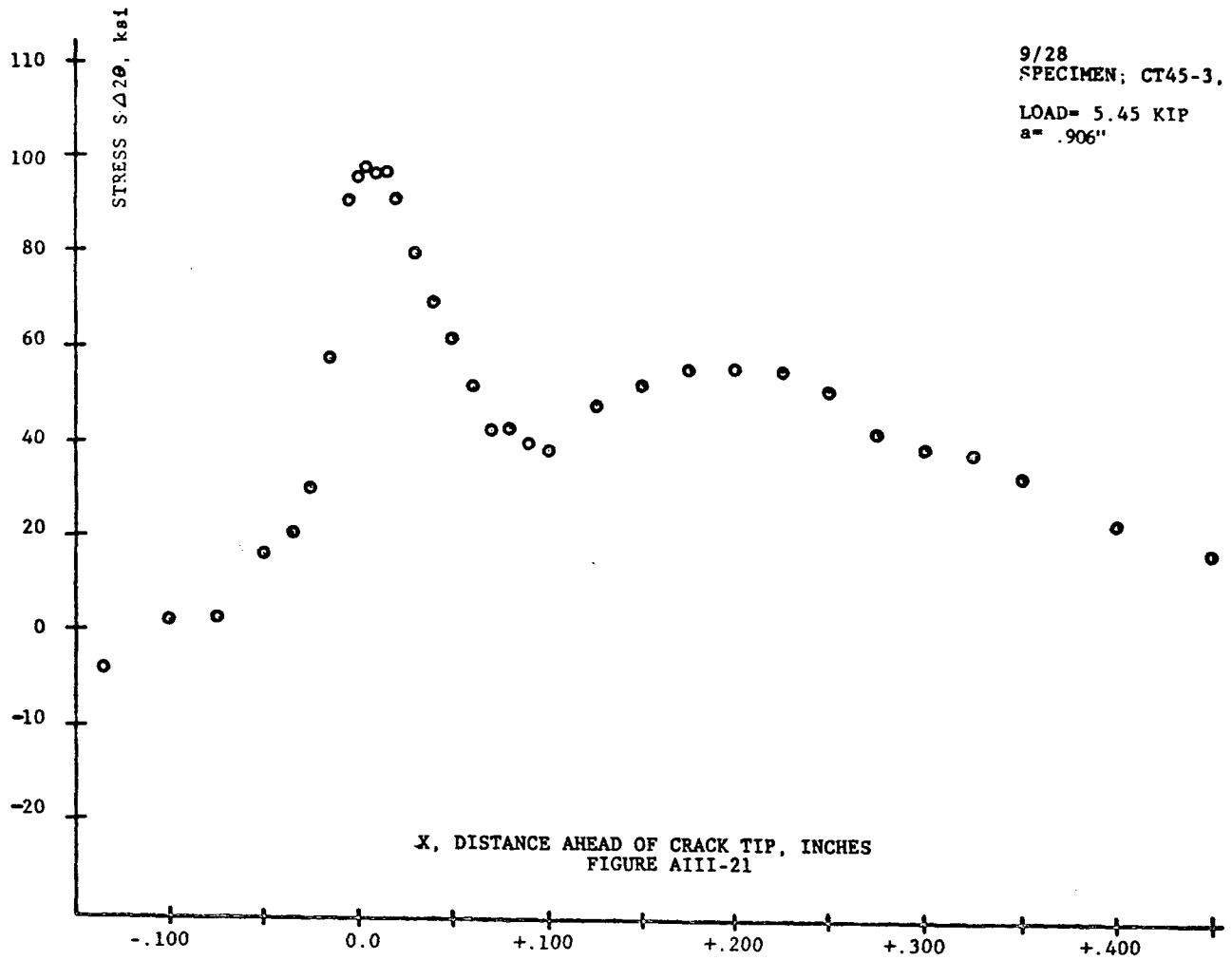


FIGURE AIII-21

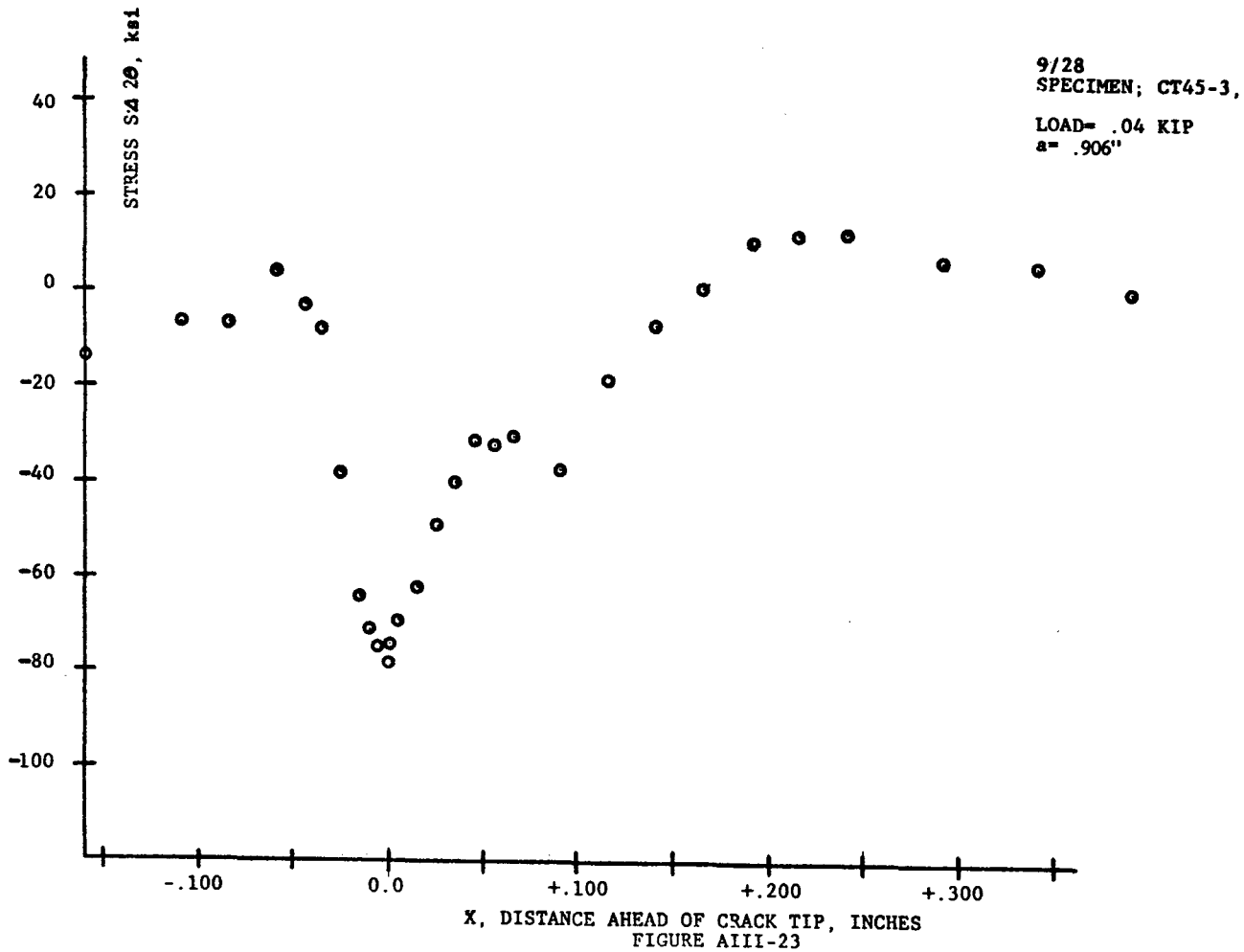

FIGURE AIII-23

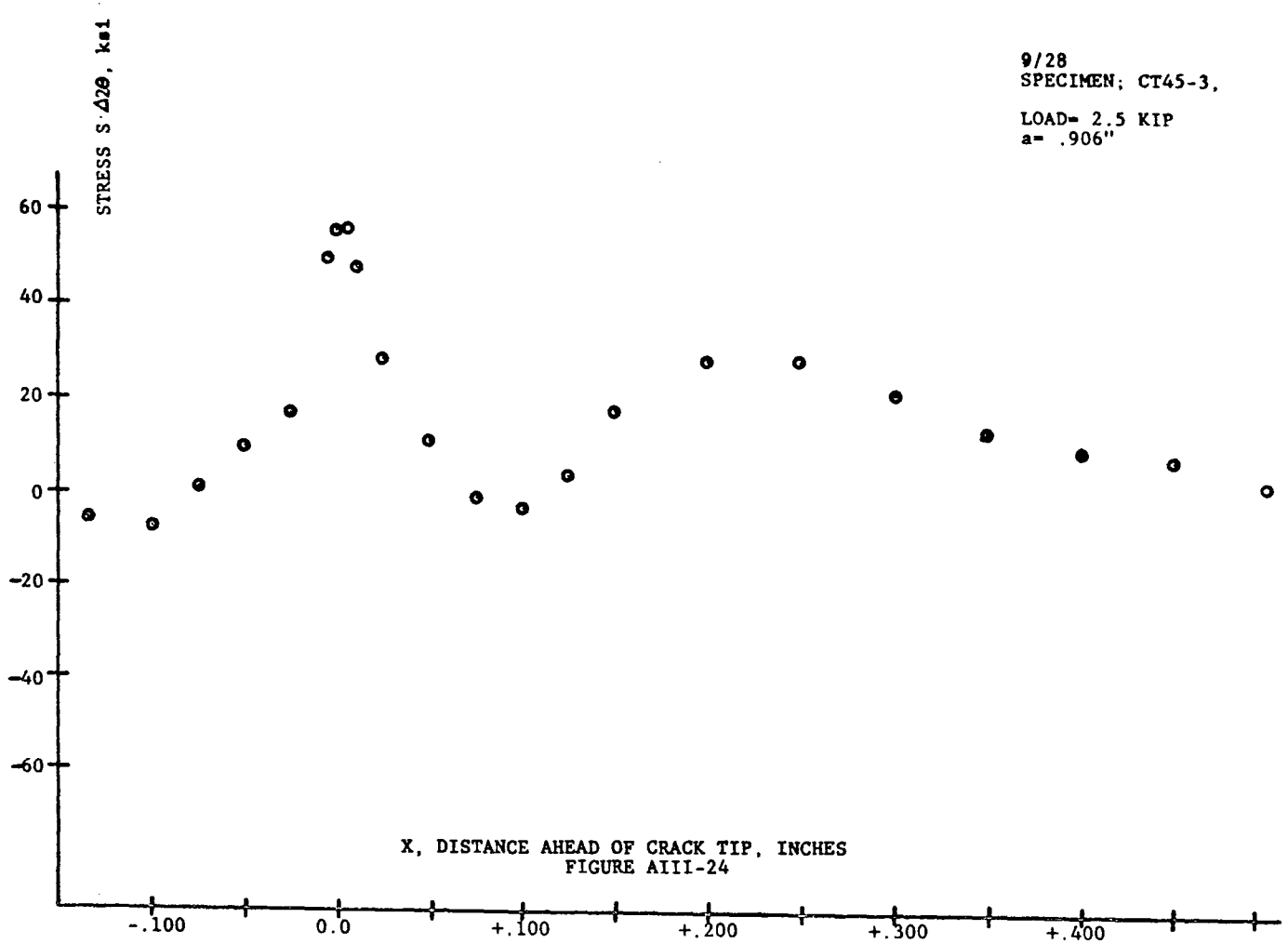


X, DISTANCE AHEAD OF CRACK TIP, INCHES
FIGURE AIII-24

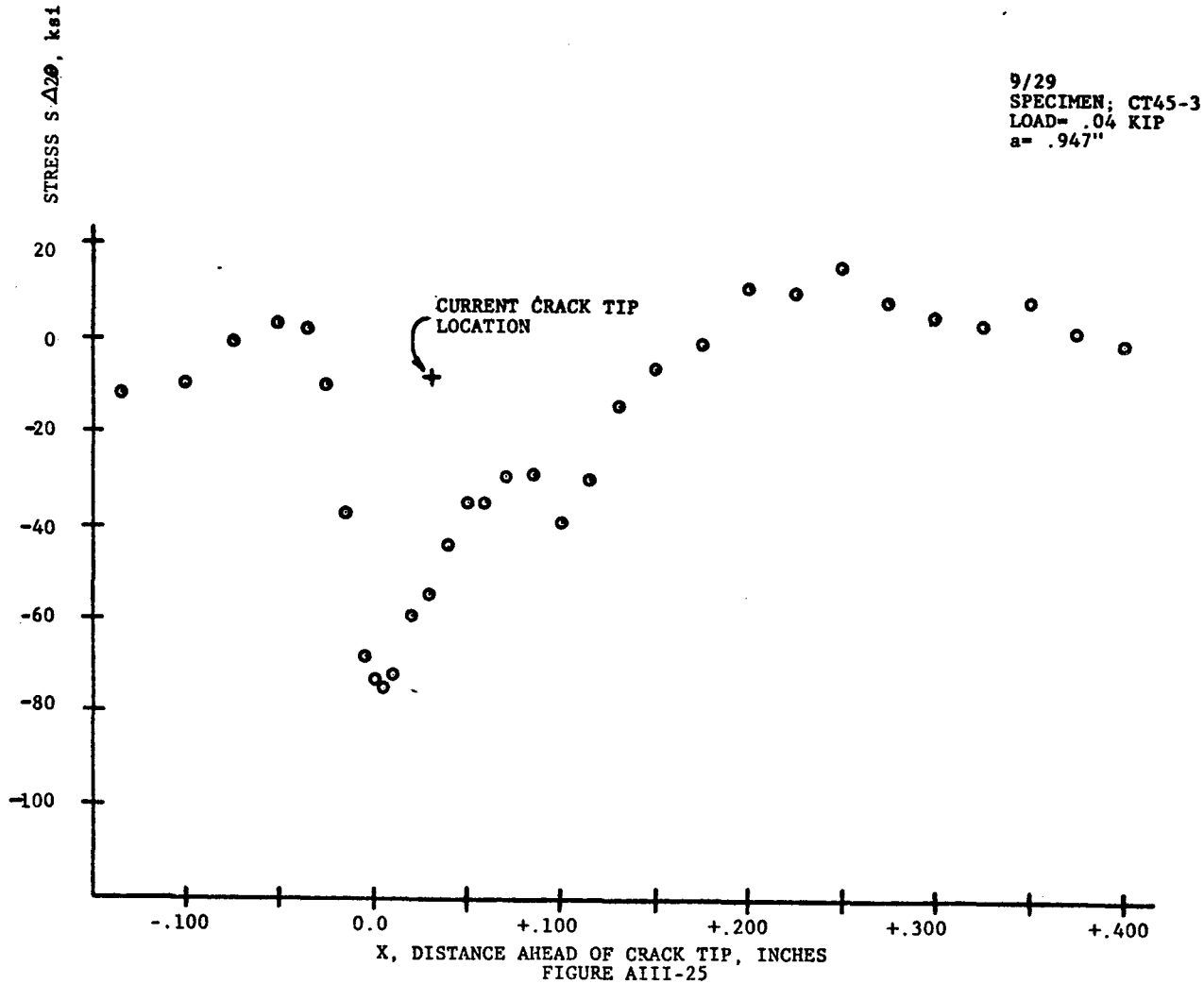

FIGURE AIII-25

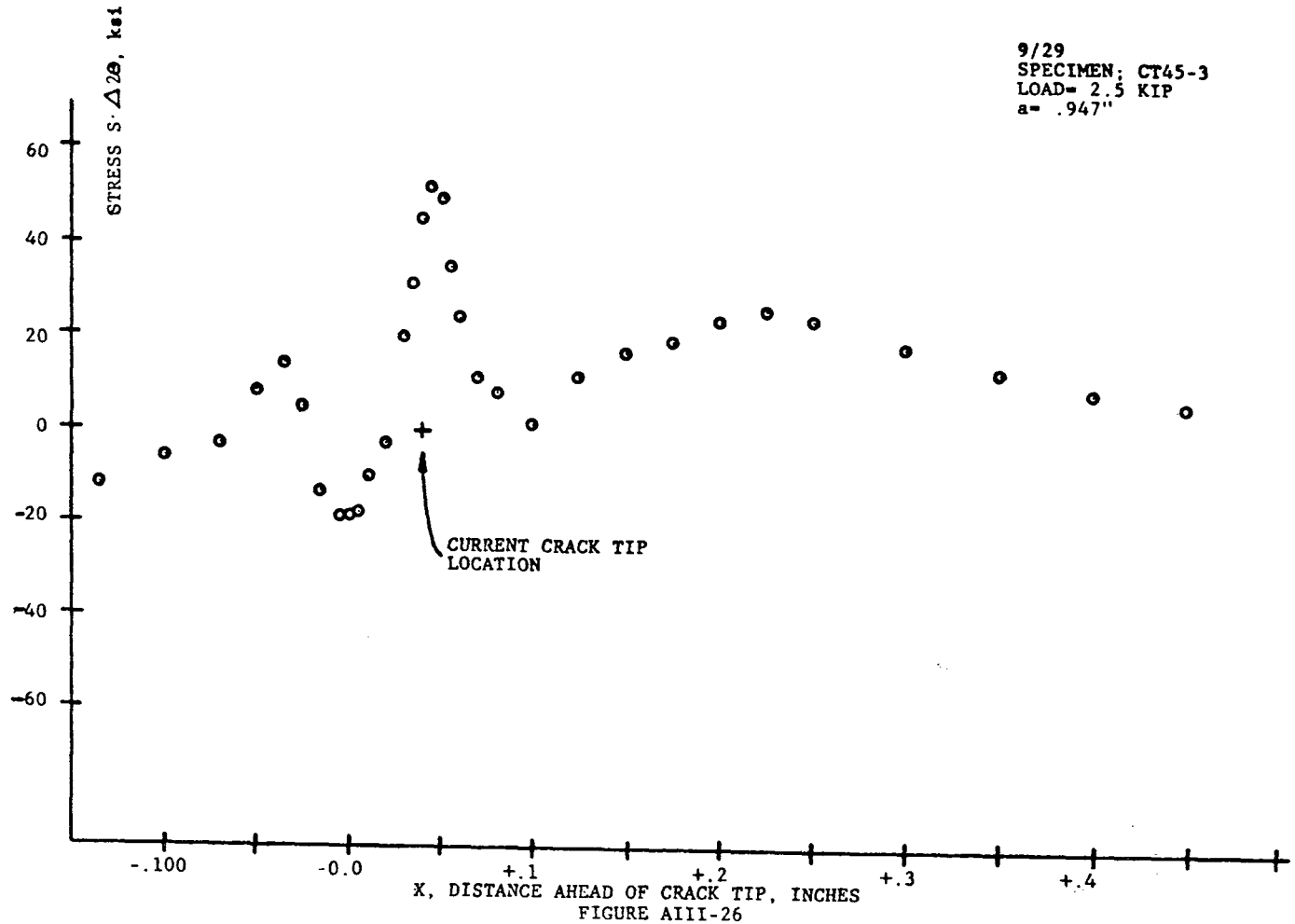

FIGURE AIII-26

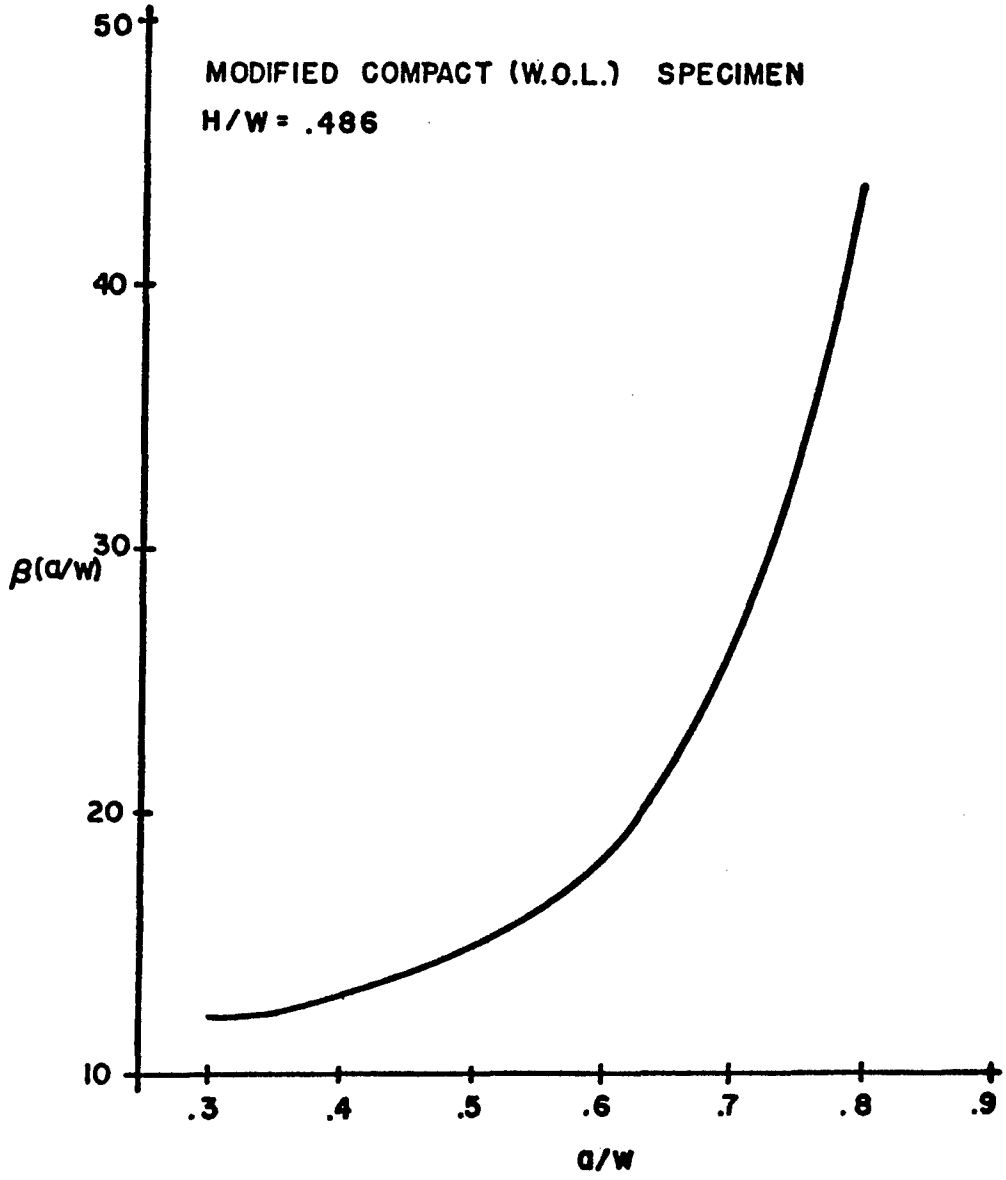


FIGURE AIV 1 , STRESS INTENSITY CALIBRATION CURVE

## APPENDIX IV - STRESS INTENSITY CALIBRATION AND CRACK GROWTH CALIBRATION

From equation 1

$$K = \frac{P}{BW}\sqrt{a} \cdot \beta(a/w) \qquad \text{(AIV-1)}$$

Where K is the opening mode stress intensity, P is the applied load, a is the measured crack length, B is the specimen thickness and W is the specimen width. For the modified compact specimen (H/W = .486, H = specimen height), Wilson (A1) determined the geometry correction factor, $\beta$ in equation AIV-1, to be given by

$$\beta(a/w) = 30.96 - 195.4(a/w) + 730.6(a/w)^2 - 1186.3(a/w)^3 + 754.6(a/w)^4 \qquad \text{(AIV-2)}$$

This equation is valid from $0.3 \leq a/w \leq 0.8$ and is shown graphically in Figure AIV-1.

Periodically, cyclic testing was interrupted to measure the crack length. Using the measured crack length, a, and the elapsed cycles, N, the secant method was used for computing the crack growth rate, $\Delta a/\Delta N$. It involves calculating the slope of a straight line connecting two adjacent data points on the a versus N curve. This can be expressed as

$$\frac{\Delta a}{\Delta N} = \frac{a_{i+1} - a_i}{N_{i+1} - N_i} \qquad \text{(AIV-3)}$$

The computed $\Delta a/\Delta N$ is an average rate over the $a_{i+1} - a_i$ increment and, therefore, the average crack length, $\bar{a} = 1/2(a_{i+1} + a_i)$, was used to calculate K in equation AIV-1 or $\Delta K$ in equation 1b.

REFERENCE

A1. E.T. Wessel, "State-of-the-Art of the WOL Specimen for $K_{1_c}$ Fracture Toughness Testing," Engr'g Frac. Mech., (1968).



☆U.S.Government Printing Office: 1978 — 757-080/560